TRANSPARENT PHOTOCATALYTIC ANTIMICROBIAL COATINGS

By

WEI BAI

A DISSERTATION PRESENTED TO THE GRADUATE SCHOOL
OF THE UNIVERSITY OF FLORIDA IN PARTIAL FULFILLMENT
OF THE REQUIREMENTS FOR THE DEGREE OF
DOCTOR OF PHILOSOPHY

UNIVERSITY OF FLORIDA

2012

To my family

ACKNOWLEDGMENTS

I would like to express my greatest gratitude to my advisor, Dr. Ben Koopman, for his support, guidance, encouragement over the past five years. I am also very grateful to my co-chair, Dr. Brij Moudgil, for bringing me into the fascinating discipline of interfacial phenomena and providing me with many opportunities to present my research in conferences. Most achievements during my Ph.D. study would not be possible without their excellent guidance and supports. I like to extend my appreciation to my Ph.D. committee members, Dr. Chang-Yu Wu, Dr. Jean-Claude Bonzongo and Dr. Spyros Svoronos for their generous help and support during my graduate study at the University of Florida, and to Dr. Myoseon Jang for attending my Ph.D. defense as a substitute for Dr. Wu.

I am grateful to Dr. Vijay Krishna, who always provided me with valuable feedback and insightful suggestions for my research. I am thankful to Dr. Jie Wang and Dr. Angelina Georgieva, for their hard work on synthesizing polyhydroxy fullerenes for my research. I am thankful to the MAIC faculty members, Dr. Luisa Amelia Dempere, Dr. Valentin Craciun and Dr. Eric Lambers, for training me on electron microscopy and X-ray analysis. I am thankful to Dr. Gill Brubaker and Mr. Gary Scheiffele for training me on the particle sizing and surface characterization instruments in PERC. I would like to acknowledge the contributions of all the former and current group members of “PHFers” that are not yet mentioned: Dr. Jie Gao, Dr. Hideya Nakamura, Ailin Qin, Matt Shore, Jonathan Solomon, Kyle Fischer, Wilton Mui, Gayathri Mohan and Abhinav Thakur.

I would like to acknowledge financial support from the Center for Nano Bio Sensors (University of Florida) , NSF-I/UCRC for Particulate and Surfactant Systems, NSF-AIR (Award number: 1127830) and University of Florida Alumni Fellowship. I

would also like to acknowledge my industrial collaborator, Mr. Joseph Navarro (CEO of NanoHygienix LLC), for his support on my research.

A special thanks of mine goes to my wife, Fan Li, who is always by my side and encourages me whenever I feel exhausted. Without her, my life would be less colorful. I wish to thank my parents and parents-in-law for their unconditional love and unwavering support. They sacrificed their personal time to help take care of my children, enabling my wife and I to focus on our Ph.D. studies. I arrived in Gainesville alone five years ago. Right now I have a growing family with two adorable kids, Roger and Chloe. I cherish every moment in this lovely neighborhood and value all the friendships I have made throughout the journey.

TABLE OF CONTENTS

page

LIST OF TABLES

LIST OF FIGURES

LIST OF ABBREVIATIONS

CFU	COLONY FORMING UNIT
PHF	POLYHYDROXY FULLERENE
TiO_2	TITANIUM DIOXIDE
UVA	ULTRAVIOLET A

Abstract of Dissertation Presented to the Graduate School
of the University of Florida in Partial Fulfillment of the
Requirements for the Degree of Doctor of Philosophy

TRANSPARENT PHOTOCATALYTIC ANTIMICROBIAL COATINGS

By

Wei Bai

August 2012

Chair: Ben Koopman
Cochair: Brij Moudgil
Major: Environmental Engineering Sciences

A study was carried out to develop and evaluate thin, transparent, photocatalytic coatings for inactivating microbes on outdoor and indoor surfaces under UVA and visible light. The photocatalysts investigated were P25, anatase with crystallite sizes of 7 and 15 nm, rutile with crystallite sizes of 22 and 99 nm and a commercial photocatalyst. The photocatalysts were characterized by XPS, XRD, BET surface area, SEM, dynamic light scattering, adsorption and zeta potential. Coating structure was characterized by SEM and coating performance was characterized by dye degradation and microbe inactivation. The TiO_2 particles with small crystallite size exhibited much higher activity than commercial photocatalyst. Photocatalysis with the smaller sizes of rutile and anatase was found to utilize different portions of the visible light spectrum. Polyhydroxy fullerene (PHF) was tested as an enhancer of photocatalysis. Nanocomposites of PHF and anatase self-assemble by adsorption of PHF onto anatase. PHF was found to enhance the UVA-photocatalytic performance by a factor of 2 to 3. This was achieved with a PHF/anatase weight ratio of 0.01, at which the anatase surface was found to be nearly saturated with PHF. Photocatalytic performance of anatase coating under visible light was also enhanced by PHF. The degree of

enhancement was up to 3-fold relative to anatase alone with a PHF/anatase ratio of 0.1. Sodium dodecyl sulfate (SDS), Tween 20 and NaOH were evaluated as dispersant for aqueous TiO_2 suspension. Addition of any of these chemicals at the appropriate concentrations stabilized TiO_2 suspensions. However, SDS and Tween 20 impaired the photocatalytic activity of TiO_2. The coating performance of TiO_2 was found to be related to the pH of the TiO_2 suspension used to make the coating. At either high (13) or low (7.5) pH, TiO_2 particles aggregated in suspension, reducing the surface coverage of the coating and decreasing photocatalytic activity. At TiO_2 suspension pH in the range of 9 to 12, the TiO_2 aggregate size was minimized and coating performance was maximized. The performances of three photocatalyst systems using commercial photocatalyst, a rutile/anatase mixture and the PHF/anatase nanocomposite as the top coats were evaluated in beta facilities in southern Florida. The commercial photocatalyst and the rutile/anatase were marginally effective in reducing microbe counts. Preliminary data indicate that the PHF/anatase nanocomposite is highly effective in reducing microbe counts at a beta facility.

CHAPTER 1
INTRODUCTION

1.1 Problem Statement

Surfaces of windows, walls, furniture, carpets etc. in buildings are repositories of viruses, bacteria and fungi that cause infections, allergies and respiratory problems.[1–5] Viral infections such as influenza lead to $12 billion/year medical costs and productivity loss in the US alone.[6] Pandemics with emerging pathogens such as H1N1 virus could cost $3 trillion globally.[7] The Norovirus (Norwalk) virus, notable for infecting cruise ship passengers with incapacitating gastrointestinal illness, can live on surfaces for up to four weeks. Hospital-acquired (nosocomial) infections cause or contribute to 99,000 deaths in the U.S. each year.[8] These infections can involve antibiotic resistant bacteria, such as methicillin resistant *Staphylococcus aureus* (MRSA). Asthma affects nine million U.S. children under the age of 18, and causes an estimated $20 billion per year in medical expenses and productivity loss in the U.S.[9] Control of environmental asthma triggers such as allergens and air pollutants could substantially reduce asthma in children.[10–12] Common alcohol or hypochlorite disinfectants are ineffective against bacteria, viruses and fungal spores.[12]

Prevention of surface-transmitted infections within the indoor environment can be accomplished by reduction of microbial survival using disinfecting chemicals, heat, radiation or antimicrobial surfaces. Desirable features of an antimicrobial agent are:

- easy to apply and long-lasting
- does not involve harmful chemicals
- destroys pathogenic microbes
- retains the appearance and texture of the underlying surface
- activating agents such as light, if necessary, are present in the normal indoor environment
- low cost

1.2 Conventional Disinfection Technology

Conventional technologies for microbe inactivation are heat, radiation and chemical based inactivating agents.[13] These techniques and their limitations are briefly outlined below.

- Heat: Heat is not a feasible method for disinfecting surfaces as the high temperature application is expensive and could damage the surfaces. Furthermore, thermal techniques cannot be applied for inactivation of all microorganisms present on surfaces.[14]

- Radiation: Germicidal ultraviolet (UVC) and gamma rays are the two major types of radiation utilized for inactivation. The major disadvantage associated with this technique is cost. High intensity radiation is required to ensure complete inactivation of microorganisms.[14] Inactivation with gamma rays requires special facilities, whereas UVC radiation requires, at a minimum, eye and skin protection

- Chemical agents: Alcohols, aldehydes and surfactants are commonly employed for cleaning surfaces. However, they are effective against only against certain bacteria. Strong chemical agents, such as chlorine bleach, are not recommended for treating surfaces as they can easily oxidize and damage them. A major disadvantage of chemical agents is that they generate toxic byproducts, including mutagens and carcinogens.[14]

As can be seen from the above discussion, conventional disinfectants suffer disadvantages which prevent them from being effective at stopping surface-mediated transmission of disease. Need for frequent re-application and the potential for damage to surfaces are two of their most notable limitations.

Antimicrobial surfaces break the cycle of infection in healthcare and other facilities that are prone to surface-mediated infectious diseases (Fig. 1-1). Two sets of approaches can be delineated from research on control of microbial populations on walls, ceilings, and other surfaces.[15] The first approach is to prevent microbial adhesion to the surfaces. The prominent methodologies for coating large areas are super-hydrophilic (e.g., TiO_2 based self-cleaning coatings from Saint Gobain and Pilkington) or

superhydrophobic coatings. Antiadhesive products intended only for small area applications, such as poly (ethylene glycol) coatings, diamond-like carbon coatings and Sharklet™ are not included in this discussion.

Although, super-hydrophilic and super-hydrophobic coatings may be effective in preventing adhesion of microbes on surfaces, they do not destroy the microbes. The second approach–antimicrobial surfaces–are discussed next.

1.3 Antimicrobial Surfaces

The second approach is destruction of microbes with passive or active coatings, which are discussed below.

1.3.1 Microbioside-releasing Coatings

Antimicrobial agents, such as antibiotics or inorganic antimicrobials, are incorporated in a polymer matrix for slow release by diffusion. Commercial microbioside-releasing coatings are Microban®, which contain Triclosan as broad spectrum antimicrobial, and AgION™ and SilvaGard™, which release Ag^+ ions for destroying microbes. These coatings can induce microbial resistance and, thus, are not desirable in healthcare settings. The coatings have a finite lifetime that is related to the rate of release of the antimicrobial agents. Furthermore, silver ions and dioxins produced by Triclosan under UV light are toxic to humans.

1.3.2 Polycationic Coatings

Cationic polymers destroy microbes by electrostatic interactions with the negatively charged parts of microbes. Polyethyleneimine (e.g., Aegis Microbe Shield™) containing surface coatings have been shown to be effective against some bacteria and viruses, but not against bacterial spores.

1.3.3 Light-activated Coatings

Light-activated release of potent reactive oxygen species, such as hydroxyl radicals, is another way of destroying microbes. Light-activated coatings act against all microbes, and because they attack the microbial surface, there is no potential for inducing resistance. Furthermore, these coatings tend to be longer lasting. The two categories of light-activated coatings are discussed below:

Photosensitizers: Organic dye molecules with absorption in visible light, such as Rose Bengal and Toluidine blue, have antimicrobial properties. The photosensitizer is usually incorporated in a polymer matrix for producing antimicrobial coatings. The polymer matrix is susceptible to degradation by the reactive oxygen species produced by the photosensitizer.

Photocatalysts: Materials such as titanium dioxide (TiO_2) and zinc oxide can convert light energy to chemical energy. The chemical energy produced is usually in form of free radicals (hydroxyl and superoxide radicals). Photocatalytic technology is an attractive approach for destroying environmental pollutants and pathogenic microbes because of the following characteristics:[13]

- The TiO_2 coating is easy to apply and is long-lasting
- Preparation of coatings from TiO_2 powders require no harmful chemicals (disinfectants) and does not release toxic byproducts
- Microbes are not only killed, but are completely mineralized
- Coatings can be made thin enough so that the appearance and texture of the underlying surface are retained
- TiO_2 formulations are low in cost

The chief disadvantage of TiO_2 is low quantum efficiency, which typically necessitate thick, white coatings to achieve antimicrobial action over feasible time

scales. Recently, technologies for enhancing TiO_2 photocatalysis have shown promise for increasing microbial inactivation rates under visible light.

1.4 Methods to Enhance TiO_2 Photocatalysis

The quantum yield[1] of TiO_2 is low, normally less than 1%.[16] In addition to quantum yield, two major phenomena affect the efficiency of TiO_2 photocatalysis, including light adsorption and the fate of charge-carriers (electrons, holes) at the photocatalyst surface. Accordingly, two major strategies to enhance TiO_2 photocatalysis are to extend the range of wavelengths over which TiO_2 can absorb light and to enhance the surface reactivity of the photocatalyst.

1.4.1 Extend Visible Light Adsorption

Pure anatase absorbs electromagnetic radiation with wavelength less than 380 nm (UVA, UVB), which constitutes only 3% of the solar spectrum.[17] Extending the absorption spectrum of anatase to the visible region significantly improves the overall capture of incident photons. It also makes it possible to apply TiO_2 photocatalysis for indoor applications.

Doping with non-metal and transition metal. Numerous studies have indicated that doping with non-metal elements, such as boron, carbon, nitrogen, sulfur or phosphorous, significantly enhances the capability of visible light adsorption of TiO_2.[18–21] Nitrogen is the most frequently used dopant because its atomic size is close to that of oxygen, it has a low ionization energy and it is highly stable. As a consequence, nitrogen can readily substitute for oxygen within the TiO_2 crystal lattice. Through

[1] Quantum yield is defined as the number of events occurring per photon absorbed per photon absorbed.[112] In TiO_2 photocatalysis, quantum yield can be specified as the number of charges transferred to adsorbed species per photon absorbed.

nitrogen doping, the band gap energy of TiO_2 can be reduced from 3.2 eV to 2.7–2.9 eV.[18]

Transition metals, such as Cr, Co, V and Fe,[22–25] are also able to extend the optical response of TiO_2 to the visible region. Doping with a transition metal in the crystal lattice of TiO_2 gives rise to a decrease in the band gap energy of TiO_2.

Dopant free method. Although dopants can improve the solar spectrum usage, they can also act as charge carrier recombination centers, adversely affecting the efficiency of TiO_2 photocatalysis.[26] Band gap engineering techniques have recently been applied to create dopant-free, pure TiO_2 phases that are visible light active.[27–30] Chen *et al.*[27] introduced disorder in the surface layers of nanophase TiO_2 through hydrogenation, obtaining black TiO_2 nanoparticles with band gap of 1.0 eV. Tao *et al.*[28] synthesized a new, dopant-free, low-band-gap phase of TiO_2 on the surface of rutile TiO_2 by oxidation of bulk titanium interstitials. The band gap of the resulting phase was 2.1 eV. Zuo *et al.*[29] synthesized partially reduced TiO_2 with Ti^{3+} present in the bulk material. The TiO_2 containing Ti^{3+} exhibited high visible light activity. The literature cited above shows the crucial role of defects and surface disorder in engineering the band gap of TiO_2.

Dye photosensitization. Dye photosensitization has been reported to be an effective way enhancing visible light photocatalysis.[31–34] Various dyes, such as coumarin,[35] $Ru(bpy)_3^{2+}$,[36] Eosin Y,[37] merocyanine[38] *etc.*, have been employed to increase the efficiency of solar cells, photocatalytic pollutant degradation and hydrogen production under visible light. The dye photosensitization process starts with electron excitation from the highest occupied molecular orbital of the dye to the lowest

unoccupied molecular orbital upon absorption of visible light. The photoexcited dye subsequently transfers an electron into the conduction band of TiO_2. This conduction band electron of TiO_2 subsequently migrates to the surface and reacts with electron acceptors, generating a free radical ($O_2^{\bullet-}$, $^{\bullet}OOH$ or $^{\bullet}OH$).[39–41]

1.4.2 Enhance Surface Reactivity

Effect of particle size. The amount of TiO_2 surface available for reaction directly relates to the particle size of TiO_2, which affects specific surface area, the band gap and charge-carrier recombination. As the particle size decreases, the specific surface area increases, giving more reactive surface area for organic pollutant degradation and microbe inactivation.[42]

As the particle size of TiO_2 is decreased to its critical size, typically 10 nm or less,[43, 44] the TiO_2 particle behaves as a “giant atom”. Due to spatial confinement, the photogenerated charge-carrier, upon illumination, cannot fit into such a small particle. In other words, the band of TiO_2 spilts into discrete electronic states within the conduction band and valence band.[45] As a result, the band gap increases and the band gap edges shift to yield large redox potentials.[16] Kormann *et al.*[46] synthesized a 2–4 nm anatase and rutile nanoparticles. The blue shift of band gap for anatase and rutile with respect to their bulk phases were 0.15 and 0.1 eV, respectively. The quantum size effect of TiO_2 does increase the redox potential of TiO_2, but it requires incident light with higher energy to activate the photocatalyst.

Influences of particle size on the charge-carrier recombination were also reported.[47, 48] Recombination of electrons and holes can take place within the interior or at the surface of the photocatalyst. In larger particles of TiO_2, recombination of the charge-carriers within the interior of the particle is dominant. As particle size decreases,

the diffusion distance is also decreased, so that eventually surface recombination becomes dominant.[48] Thus, methods to inhibit surface recombination would be effective only for smaller particles.

Methods to synthesize small particles of TiO_2 with narrow size distribution were reported. Satoh *et al.*[49] used a dendrimer template to synthesize TiO_2 nanoparticles with a diameter of 1–2 nm with a standard deviation of 0.3–0.6 nm. The highly branched macromolecules have well-defined structures that enable them to bind metal ions to generate precursors that can be converted into nanoparticles. Yan et al.[50] reported a microemulsion-mediated hydrothermal method to synthesize TiO_2 nanocrystalline (size range from 9 to 18 nm) under low temperature condition.

Doping with noble metals. Deposition of noble metals such as Pt, Au or Ag within the crystal lattice enhances the photocatalytic activity of TiO_2.[51–53] The noble metals serve as electron scavengers, decreasing the rate of recombination of electron and holes, thus increasing the interfacial transfer rate of the charge-carriers.

Semiconductor coupling. Research on the coupling of semiconductor photocatalysts into nanocomposite alloys such as CdS/TiO_2,[54] ZnO/TiO_2[55] and Bi_2S_3/TiO_2[56] were reported. These coupled semiconductors decreased the recombination rate of charge-carriers, enhancing the overall photocatalytic efficiency.

1.5 Goal and Objectives of the Study

Most of the methods described above, such as doping or nanocomposite formation, require a sol-gel process, which is energy-intensive, requires toxic chemicals and is expensive. These drawbacks have hindered large scale applications of TiO_2 photocatalysis. Thus, engineering a highly active, TiO_2 photocatalyst formulation that utilizes a facile synthesis procedure is highly desirable.

Fullerene, a new class of carbon allotrope,[57] exhibits strong electron affinity, which is beneficial for charge-carrier separation in the TiO_2 photocatalytic process. However, the interaction of fullerene and TiO_2 is weak due to poor aqueous solubility of fullerene. Chemically modified fullerene with multiple hydroxyl groups (polyhydroxy fullerene, fullerol or fullerenol) significantly increases the aqueous solubility of fullerene, while retaining its electron affinity. Krishna *et al.*[58] demonstrated that polyhydroxy fullerene (PHF) enhances TiO_2 photocatalysis in aqueous systems. Nanocomposites of PHF and TiO_2 form through physical mixing. Other advantages of using PHF as an enhancer of photocatalysis include the small amount required[2] and its biocompatibility[3].

The goal of this study was to develop stable formulations of polyhydroxy fullerene/TiO_2 nanocomposites for application as transparent, antimicrobial coatings for use under UVA or visible light. The specific objectives of this research were:

- Optimize the PHF/TiO_2 nanocomposite composition to maximize the microbe inactivation rate under UVA or visible light;
- Select and optimize a system for dispersing TiO_2 particles in aqueous suspension
- Evaluate the performance of prototype TiO_2 formulations in beta facilities

1.6 Overview of the Dissertation

The dissertation is organized into a total of six chapters. In Chapter 2, a study to develop a single layer coating of the PHF/TiO_2, with anatase phase of TiO_2, nanocomposite is described. The nanocomposite was optimized for application under low-irradiance UVA light. Dye degradation was used as initial indicator for performance for optimization. The optimized nanocomposite coating was tested for inactivation of

[2] The concentration of PHF required for enhanced photocatalysis is10 times lower than other enhancers, such as metals or dyes

[3] The concentration of PHF used in this study is a magnitude lower than the LC_{50} for mammalian cells.

Aspergillus niger spores. In Chapter 3, a study to develop a two-layer TiO_2 coating for indoor applications is described. The two-coat system mimics current commercial practice in application of photocatalytic coatings. A nanocomposite of PHF and anatase was found to be superior to rutile or anatase alone. The coating system was optimized using dye degradation as performance measure, and then tested for its ability to inactivate *Staphylococcus aureus*, a surrogate for MRSA. In Chapter 4, a study to select and optimize a dispersion system is described. Three dispersant systems were tested: NaOH for pH adjustment, Tween 20 and sodium dodecyl sulfate. Two model photocatalysts were employed: P25 and a 1:1 mixture of rutile and anatase. Settling rate and visual opacity were used as indicators of the degree of dispersion, while dye degradation was used as the indicator of performance. In Chapter 5, a study to evaluate prototype photocatalyst formulations in three different Florida beta facilities was carried out. Performance of photocatalytic coatings was monitored for up to 8 months after coating application. Finally, in Chapter 6, the overall conclusions from this work and suggestions for future work are given.

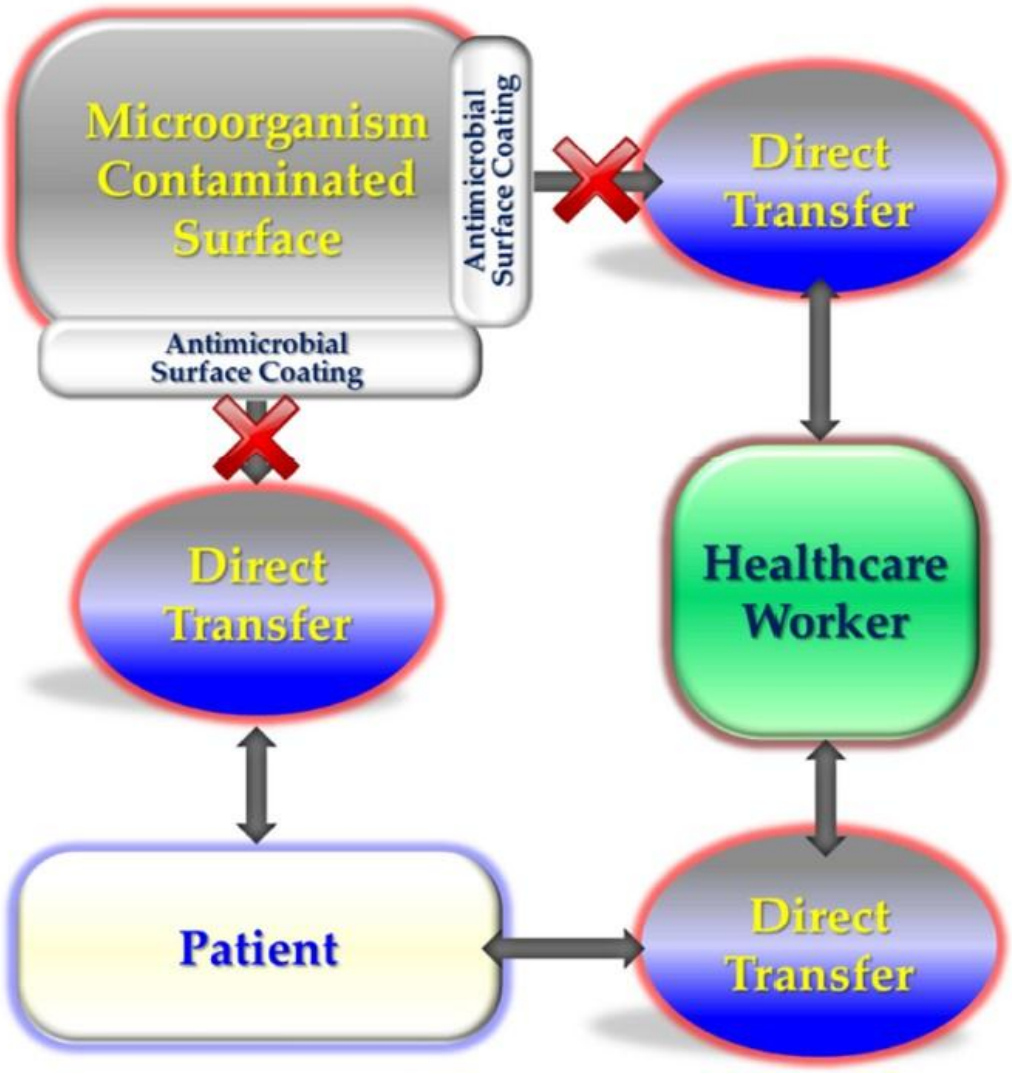

Figure 1-1. The role of surfaces and antimicrobial coatings in the transmission of hospital-acquired infections. Redrawn from Page *et al*.[15]

CHAPTER 2
ENHANCEMENT OF NANO TITANIUM DIOXIDE PHOTOCATALYSIS IN TRANSPARENT COATINGS BY POLYHYDROXY FULLERENE

Microbe transmission via surfaces is a common mode for the spreading of infectious diseases.[15] A simple way to combat disease transmission via surfaces is to apply antimicrobial coatings. The ideal antimicrobial coating has the following properties:

1) effective in killing pathogenic microorganisms;

2) requires no toxic or hazardous chemicals for synthesis;

3) does not alter the appearance or texture of underlying materials (*i.e.*, transparent)

4) activated by agents that are readily available, such as light

5) inexpensive

Ultraviolet-A (UVA) active, photocatalytic coatings based on titanium dioxide (TiO_2) have the potential to satisfy all of these criteria. Furthermore, they also destroy organic pollutants such as volatile organic compounds and are self-cleaning. To achieve thin, transparent coatings that are also antimicrobial, it is important to maximize the efficiency of the photocatalyst in converting light energy to chemical energy.

A number of approaches have been devised to improve the efficiency of TiO_2 photocatalysis under UVA illumination. Doping or forming nanocomposites with noble metals (Pt, Au and Ag),[51–53] metal ions,[59] metal oxide,[60] carbon nanotubes,[61, 62] graphene oxide,[63] fullerene[64, 65] and polyhydroxy fullerene[58, 66] enhances photocatalytic efficiency. However, doping or nanocomposite formation typically requires a sol-gel process, which is energy-intensive, requires toxic chemicals and is expensive. In contrast, nanocomposites of polyhydroxy fullerene (PHF) and TiO_2 form spontaneously through self-assembly when the two components are mixed. Krishna *et al.*[58, 66]

demonstrated that PHF/TiO_2 nanocomposite in aqueous suspension photocatalytically degraded organic dye 2.6 times faster and inactivated *Escherichia coli* 1.9 times faster than TiO_2 alone. They showed that PHF physically adsorbs on TiO_2, and postulated that the adsorbed PHF serves as an electron scavenger, which facilitates electron-hole pair separation, and leads to greater production of hydroxyl radicals. Electron paramagnetic resonance spectroscopy confirmed that photocatalytic production of hydroxyl radicals was increased in the presence of PHF. Polyhydroxyfullerene is water-soluble, biocompatible and biodegradable and has been shown to possess antioxidant properties, inhibit allergic response and inhibit tumor growth.[67–71] The concentrations of PHF utilized in the PHF/TiO_2 nanocomposite are four orders of magnitude lower than the LC10 reported for human dermal fibroblasts.[72]

Until now, the capability of PHF to enhance the photocatalytic activity of TiO_2 in a coating has not been evaluated. The objective of this study was therefore to test the effectiveness of thin, transparent coatings made of PHF/TiO_2 nanocomposite. The optimal ratio of PHF to TiO_2 for use in formulating the nanocomposite was determined using dye degradation as the performance measure. The optimized nanocomposite was then tested for inactivation of *Aspergillus niger*, a fungal species commonly occurring in both indoor and outdoor environments and frequently cited as a contributor to respiratory diseases, such as asthma.[73] *A. niger* spores are highly resistant to photocatalysis, in comparison to viruses and bacteria.[74]

2.1 Experimental

2.1.1 Chemicals and Reagents

Chemicals were obtained from Fisher Scientific, except as noted. Titanium dioxide (anatase, 5 nm) was obtained from Alfa Aesar (Ward Hill, MA). Polyhydroxy fullerene

(PHF) was obtained from BuckyUSA (Houston, TX) or synthesized in our laboratory according to the protocol of Gao *et al.*[75] Procion red MX-5B dye was obtained from Sigma-Aldrich Inc. (St. Louis, MO). Phosphate-buffered saline (PBS) solution was prepared by dissolving 12.36 g Na_2HPO_4, 1.80 g NaH_2PO_4 and 85.00 g NaCl in 1000 mL of deionized water and then diluting 10x immediately before use. PBS/SDS solution was prepared by adding 0.576 g sodium dodecyl sulfate (SDS) to 1000 mL of PBS and then autoclaving at 120°C and 16 bar for 15 minutes.

2.1.2 Culturing and Enumeration of *Aspergillus niger* Spores

Asperigillus niger (ATCC 16888) were grown on potato dextrose agar for 7 days at 37ºC and then fungal spores were scraped from the agar plate with an inoculation loop and suspended in sterile deionized water. A series of 10-fold dilutions (10^{-1} to 10^{-5}) was prepared from the suspension by adding 0.333 mL of sample to 3.0 mL sterile PBS/SDS in a dilution tube, followed by vortexing for 10 seconds.

To enumerate the spores in a dilution, a volume of 0.1 mL was spread over sterile dichloran rose bengal chloramphenicol agar in 100×15mm Petri dishes. The plates were inverted and then incubated at 37ºC for 24 hours. Where possible, results were taken from plates that contained between 30 and 300 colonies.

2.1.3 Coating Preparation and Testing

The steps of each experiment are described below (Fig. 2-1).

Step 1–Ten mg of TiO_2 was added to a volume of 9 mL of deionized water in a 20 mL scintillation vial. The TiO_2 suspension was sonicated (Misonix Sonicator 3000, Farmingdale, NY) at the highest power level (providing 180–200 W) for 30 minutes total (10 min on/2 min off × 3). A volume of 1 mL of PHF solution, containing 200, 100, 50 or

0 mg/L PHF, was then added and the suspension was mixed with magnetic stirrer for 10 minutes.

Step 2–Grout was chosen as a test substrate because it is prone to fungal colonization. Grout surface was prepared by mixing grout powder (Mapei KeracolorTM U, Deerfield Beach, FL) with deionized water at a 2:1 mass ratio using a spatula for 5 minutes, allowed to stand unmixed for 10 minutes, and then mixed for another 2 minutes. The grout-water mixture (0.15 g wet weight) was spread over a glass slide (2.5 cm × 1.8 cm) and dried overnight at room temperature. Thickness of TiO_2 coatings on grout surfaces was calculated from

$$d = \frac{cV}{\rho A f_d} \quad (2\text{-}1)$$

where d = calculated thickness of TiO_2 coating, c = aqueous concentration of TiO_2, V = volume of TiO_2 suspension applied to surface, ρ = density of TiO_2, A = area of surface and f_d = maximum volume fraction of randomly close packed spheres = 0.634[76] Ceramic tiles were used to test photocatalytic inactivation of A. niger spores, because commercial grout formulation contains antimicrobial agents. Tiles (2.5 cm × 2.5 cm) were obtained from American Olean Inc. (Dallas,TX). The tile surfaces were almond-colored with a matte finish. PHF/TiO_2 nanocomposite suspension was pipetted onto the grout or tile surface to give a surface loading of 64 µg/cm^2. The coated surfaces were dried overnight at room temperature. Additional tiles were coated with Stöber silica (SiO_2; Geltech) to serve as an inert control surface. SiO_2 suspension was prepared by adding 10 mg of SiO_2 to a volume of 10 mL deionized water, giving a concentration of 0.1 wt%. The suspension was sonicated as described previously. A volume of 0.4 mL of

SiO_2 suspension was pipetted onto the tile surface to give a surface loading of 64 $\mu g/cm^2$.

Step 3–Organic dye or A. niger spores were applied to the test surfaces. A volume of 0.1 mL of Procion red MX-5B solution (100 mg/L) was pipetted onto coated or bare grout and allowed to spread. The dye was air dried for 1 hour before testing. A volume of 0.2 mL of A. niger suspension ($2–3\times10^5$ spores/mL) was pipetted onto each coated tile surface and allowed to spread, giving a surface loading of 6400–9600 spores/cm^2. The tiles with spores were dried in the dark in a biosafety cabinet for 24 hours.

Step 4–The photocatalytic experiments were carried out in a chamber with 16 solar UVA lamps (320 to 400 nm with peak intensity at 350 nm). The UVA lamps (RPR 3500A) were purchased from Southern New England Ultra Violet Company (Branford, CT). Air was circulated in the chamber to maintain uniform temperature of 30–32 ºC. Grout or tile surfaces were placed on a platform in a plastic bin (42 cm × 28 cm × 15 cm) filled to a depth of 4 cm with deionized water. The bin was covered by a plastic film in order to maintain relative humidity of 80-85%. No condensate formed on the film during the experiments. A Thermo-Hydro probe was utilized to monitor the temperature and relative humidity. The distance between samples and UVA lamps was 49.5 cm, giving an intensity of 15–17 W/m^2 under the film, which is typical of the UVA irradiance under indirect sunlight. The UVA intensity was measured by a PMA2110 detector (Solar Light Co., Glenside, PA).

Step 5–Performance of the photocatalytic coatings was measured by dye degradation or spore inactivation. Dye degradation was based on UV/VIS reflectance after 0, 6, 12 and 24 hours of exposure to UVA. Reflectance was measured with a

Perkin-Elmer Lambda 800 with PELA-1000 Reflectance Spectroscopy Accessory at a wavelength of 538 nm, at which absorbance of MX-5B Procion Red dye is highest. Dye degradation was calculated according to:

$$\% \text{ dye degradation} = \frac{A_0 - A_t}{A_0} \times 100 \quad (2\text{-}2)$$

where A_0 is the calculated absorbance of dye coated on photocatalytic or bare grout surface before exposure to UVA and A_t is the absorbance of dye coated on photocatalytic or grout surface after exposure to UVA at a given time. Absorbance was calculated as the negative $\log_{10}$ of reflectance expressed as fraction. Because the color of bare grout varied somewhat, it was necessary to subtract this background color. Therefore, A_0 and A_t were calculated from

$$A_0 = A_{0'} - A_b \quad (2\text{-}3)$$

$$A_t = A_{t'} - A_b \quad (2\text{-}4)$$

where A_0' and A_t' are the measured absorbance of dye on grout at time zero and time t, respectively, and A_b is the measured absorbance of the bare or photocatalytically coated grout surface without dye at a given time.

Photocatalytic inactivation of *A. niger* spores was based on viable spore counts after exposure of spores on test surfaces to UVA. Spores were recovered by immersing a tile in 20 mL PBS/SDS within a polypropylene centrifuge tube and vortexing for 15 seconds. The tube was then sonicated at highest power for 3 minutes. During sonication, the tube was immersed in a flowing water bath at 28 ºC. After sonication, the tube was vortexed for 15 seconds and the tile was removed from the centrifuge tube using a sterile forceps. The tube was then vortexed again for 15 seconds. The viable

spores in a volume of 0.1 mL suspension from the centrifuge tube were enumerated as described previously. Inactivation was calculated from

$$\%Inactivation = \frac{CFU_0 - CFU_t}{CFU_0} \times 100\% \quad (2\text{-}5)$$

where CFU_t is the number of colonies after time t and CFU_0 is the number of colonies at time zero.

Step 6–Morphological changes to *A. niger* on photocatalytic coating exposed to UVA were observed using scanning electron microscopy (JOEL 6335F FEG-SEM) at 10 kV accelerating voltage and 15 mm working distance. Because of the potentially detrimental effects of vacuum and the electron beam on spores, each tile was observed once under SEM. Hence, three different tiles with spores were prepared and then observed, one at each exposure time.

2.1.4 Aqueous Aggregate Size, Zeta Potential and BET Surface Area

Aggregate size of the nanocomposite and of TiO_2 in aqueous suspension was measured by dynamic light scattering (Nanotrac ULTRA, Microtrac, Inc. York, PA). Zeta potential was measured by doppler shift analysis (ZetaPlus, Brookhaven Instruments Corporation, Holtsville NY). Specific surface area of TiO_2 powder was measured under nitrogen using a NOVA 1200 with multipoint BET (Quantachrome Instruments, Boynton Beach, FL). TiO_2 was degassed and dried under vacuum at 110ºC for 12 hours prior to measurement.

2.1.5 Adsorption

PHF was combined with TiO_2 as described previously in the section on coating preparation and testing. A 2 mL volume of the mixture was transferred to a centrifuge tube, followed by 30-minute centrifugation at 20,800×g. The supernatant was carefully

removed by pipette and the procedure was repeated two more times. The concentration of free PHF in the final supernatant was measured by UV/Vis spectroscopy at 330 nm.[77, 78] The extent of adsorption was found to follow the Langmuir relationship:

$$\Gamma = \Gamma_{max} \frac{Kc}{1+Kc} \quad (2\text{-}6)$$

where Γ is the mass PHF adsorbed per mass TiO_2 , c is the concentration of free PHF in equilibrium with TiO_2, Γ_{max} is the maximum mass PHF adsorbed per mass TiO_2 and K is the Langmuir equilibrium constant. The Langmuir parameters Γ_{max} and K were estimated by least squares non-linear regression.

The fraction of surface coverage of TiO_2 by PHF was calculated from

$$\text{Surface coverage} = \frac{\Gamma N_A A_P}{m_P A_S} \quad (2\text{-}7)$$

where N_A is Avogadro's constant, A_P is the projected area of a PHF molecule (1.33 nm^2,[58] m_P is the molecular weight of PHF (1094 g/mol from the empirical formula $C_{60}(OH)_{22}$) and A_S is the specific surface area of TiO_2 (109.2 m^2/g as measured in the present study).

2.1.6 Data Analysis

First-order fits between the extent of dye degradation or spore inactivation and UVA exposure time were based on the equation

$$\ln \frac{c_t}{c_0} = kt + b \quad (2\text{-}8)$$

and second order fits were based on the equation

$$\frac{1}{c_t/c_0} = k't + b' \quad (2\text{-}9)$$

where c_t and c_0 represent absorbance or colony forming units at times t and t_0, respectively, k and k' are the reaction rate coefficients for the first and second order fits, respectively, and b and b' are arbitrary constants.

The parameter values (k, b, k', b') for the fits were determined by least squares linear regression.

One-way ANOVA and post-hoc testing were carried out using the Dunnett's two-sided tests through NCSS statistical analysis and graphics software (NCSS, Kaysville, UT). The significance of differences between R^2 values of least square fits to experimental data was determined using the Fisher r-to-z transformation.[79]

2.2 Results

2.2.1 Characterization

The isotherm for adsorption of PHF on TiO_2 is given in Fig. 2-2. The theoretical maximum adsorption of PHF on TiO_2 was found to be 7.2 mg/g. This level was reached at a formulation ratio (g PHF added/g TiO_2) of 0.02. A decrease of the formulation ratio to 0.01 had almost no effect on the amount of PHF adsorbed, whereas dropping the formulation ratio still further to 0.005 decreased the amount of PHF adsorbed to 4.7 mg/g. The mean aggregate size of TiO_2 based on number distribution was 104 nm. This dropped to 94 nm for the nanocomposite at a formulation ratio of 0.005, and further dropped to the range of 83–86 nm at formulation ratios of 0.01 and 0.02. (Fig. 2-3). Zeta potential of TiO_2 was -41 mV at pH 6, compared to -48 to -49 mV for the nanocomposite (Fig. 2-3).

2.2.2 Dye Degradation

TiO_2 coatings with calculated thickness ranging from 2.5 to 12.5 μm changed the color of grout surfaces from almond to white, whereas a coating with a calculated

thickness of 0.25 μm had no effect on surface appearance of the grout (Fig. 2-4A–D). A scanning electron micrograph of the 0.25 μm thick coating shows its uniform, particulate make up. (Fig. 2-4E). Accordingly, a TiO_2 coating thickness of 0.25 μm was chosen for subsequent experiments. Another consideration in coating design is the effect of PHF on appearance. PHF is dark brown in color, giving PHF/TiO_2 suspensions a brown tint at higher PHF/TiO_2 ratios. To ensure that coatings remained colorless under all experimental conditions, a maximum PHF/TiO_2 weight ratio of 0.02 was established for performance testing.

Time-dependent degradation of Procion red dye on coated and bare grout is shown in Figure 2-5. Under UVA exposure with photocatalyst, degradation ranged from 66% to 74% in 24 hours. Without photocatalyst, degradation was 43%, which can be attributed to UVA photolysis. Almost no (4%) dye degradation was observed in the dark. PHF/TiO_2 ratios of 0.01 and 0.02 significantly (α=0.05) increased the extent of dye degradation at all sampling times, whereas a PHF/TiO_2 ratio of 0.005 significantly enhanced degradation only in the first 6 hours. The extent of dye degradation with the nanocomposite at 6 hours was almost doubled in comparison to TiO_2 alone. Based on these results, a PHF/TiO_2 ratio of 0.01 was selected for the spore inactivation study.

2.2.3 Spore Inactivation

A surface loading of 6400–9600 spores/cm^2 on the photocatalytic surface was chosen to give a sparse distribution of spores (Fig. 2-6), which limited spore agglomeration and thus allowed more precise enumeration of individual spores. The efficiency of spore recovery from test surfaces was evaluated by applying spores, allowing the surfaces to dry overnight in the dark, and then applying the recovery procedure. Complete recovery (within experimental error) was achieved from coatings

of the nanocomposite or TiO_2, whereas little more than half of applied spores were recovered from bare tile (Fig 2-7). This result is likely due to separation of particulate coatings from the tiles during the recovery procedure, carrying the spores with them. A particulate material without photocatalytic properties, SiO_2, was therefore used as a non-photocatalytic coating. As Figure 2-7 shows, complete recovery of spores was achieved from the SiO_2 coating.

The time dependent inactivation of A. niger spores on photocatalytic and non-photocatalytic surfaces under UVA exposure is shown in Fig. 2-8. A 12-hour inactivation of 60% was achieved with TiO_2 alone. This was increased to 78% with the nanocomposite at a PHF/TiO_2 ratio of 0.01. Decreases in the numbers of viable spores with time on the photocatalytic surfaces paralleled decomposition of spores as imaged by scanning electron microscopy (Fig. 2-9). The difference in performance levels between TiO_2 alone and the PHF/TiO_2 nanocomposite was highly significant (α=0.001). As Figure 2-8 shows, there was negligible inactivation of spores on the photocatalytic surfaces in the dark. Moderate (41% in 12 hours) inactivation was observed on SiO_2 coated surfaces.

2.2.4 Kinetics of Dye Degradation and Spore Inactivation

Time-dependent data for dye degradation and spore inactivation were modeled by first-order and second-order least square fits, as summarized in Table 2-1. Since the first-order and second-order equations at each contain two parameters, it was possible to test the significance of the differences between R^2 values obtained with the two different equations. In modeling photocatalytic dye degradation, second-order fits were significantly better than first-order fits ($P \leq 0.0006$). Conversely, in modeling photocatalytic spore inactivation by the PHF/TiO_2 nanocomposite, the first-order fit was

significantly better than the second-order fit ($P \leq 0.0009$). Kinetics of spore inactivation on TiO_2 were equally well described by first-order and second-order fits.

The enhancement of dye degradation and spore inactivation achieved by the nanocomposite are compared in Fig. 2-10. In the dye degradation tests, the PHF/TiO_2 ratios of 0.01 and 0.02 give equivalent results, which are significantly better than obtained with the 0.005 ratio. In the spore inactivation experiments, the degree of variability between replicates was greater, which is not unusual when testing biological materials. As a result, there was no statistical difference in the enhancement of photocatalysis achieved with nanocomposites with PHF/TiO_2 ratios of 0.005, 0.01 or 0.02.

2.3 Discussion

The findings of this research show that PHF enhances the performance of TiO_2 photocatalyst in thin, transparent coatings. As shown in Table 2-2, the 1.9 times enhancement of dye degradation achieved with the PHF/TiO_2 nanocomposite compares favorably with the enhancement ratios of 1.1 to 2.2 reported for other enhancers (Ag, Au, Cu, Fe, La, N, Sn, Sr). Given its comparable performance, the competitive advantage of PHF as an enhancer of photocatalysis lies in the fact that it is biocompatible, biodegradable, and the nanocomposite of PHF and TiO_2 requires no synthesis steps. The findings also raise three points for discussion: how the optimum PHF/TiO_2 ratio differs in a coating vs. the aqueous environment; how the kinetics of photocatalysis appear to change depending on the target component (dye vs. microbes); and how the observed enhancement of photocatalytic performance changes from the beginning to the end of the exposure period.

In the present study, the optimal ratio of PHF to TiO_2 was found to be 0.01, which is 10 times higher than reported by Krishna *et al.*[66] for aqueous suspensions of the PHF/TiO_2 nanocomposite. The adsorption isotherm developed in this study indicates that the maximum amount of PHF that can adsorb to TiO_2 is 7.2 mg/g. This corresponds to a maximum surface coverage of TiO_2 by PHF of 4.9%, which is nearly reached at a formulation ratio of 0.01 g PHF/g TiO_2 (Fig. 2-11). Increasing the ratio to 0.02 increases the surface coverage very slightly. Consequently, the photocatalytic activity of the nanocomposite is not significantly increased beyond a formulation ratio of 0.01. On the other hand, dropping the ratio to 0.005 significantly decreases the surface coverage to 3.2%, which results in lower photocatalytic activity. Unlike the aqueous system studied by Krishna et al., an excess of PHF in the coating does not impair activity, because the excess simply drains from the coating and does not shade the nanocomposite.

Assuming that hydroxyl radical is produced at a constant rate in a photocatalytic reaction, the reaction can be theoretically considered as pseudo first order, which is supported by various studies.[16, 80] However, our experimental data for photocatalytic dye degradation are better described by second-order reaction kinetics. This can be attributed to the production of colorless intermediates that accumulate during the experiment and consume hydroxyl radicals, decreasing the availability of hydroxyl radicals to unreacted dye. Hu *et al.*,[81] using ion mass spectra, identified more than 12 intermediate products in the photocatalytic degradation of Procion red dye, all of which are capable of reacting with hydroxyl radicals.

The degree to which dye degradation and spore inactivation are enhanced by the PHF/TiO_2 nanocomposite is time dependent. At 6 hours, the PHF/TiO_2 nanocomposite

surface degraded nearly 2 times as much dye as TiO_2 alone, compared to 1.1× at 24 hours. In the case of microbial inactivation, the nanocomposite surface inactivated 3 times as many spores as TiO_2 alone at 3 hours, compared to an enhancement of 1.3× at 12 hours. This relationship is expected as the remaining dye or viable spores on the surfaces approaches zero at longer exposure times.

2.4 Summary

The present study has shown that PHF enhances the UVA-photocatalytic performance of a thin, transparent TiO_2 coating by a factor of 2 to 3. This is achieved with a PHF/TiO_2 ratio of 0.01, at which the TiO_2 surface is nearly saturated with PHF. The enhanced performance of the PHF/TiO_2 nanocomposite was demonstrated by organic dye degradation and fungal spore inactivation. The self-assembled PHF/TiO_2 nanocomposite is very promising for use as thin, transparent, antimicrobial coatings.

Table 2-1. Comparison of first-order fits and second-order fits to photocatalytic dye degradation and spore inactivation data*

Contaminant	Treatment	First-Order Reaction Kinetics		Second-Order Reaction Kinetics		1st-order ≠ 2nd-order
		Equation	R2	Equation	R2	P
Dye	PHF/TiO_2=0.02	y=-0.053x-0.210	0.90	y=0.123x+1.153	0.99	0.0001
	PHF/TiO_2=0.01	y=-0.053x-0.181	0.92	y=0.123x+1.107	0.99	0.0006
	PHF/TiO_2=0.005	y=-0.042x-0.142	0.92	y=0.081x+1.099	0.99	0.0006
	PHF/TiO_2=0	y=-0.045x-0.058	0.98	y=0.083x+1.005	1.00	<0.0001
Microbes	PHF/TiO_2=0.01	y=-0.127x+0.048	0.99	y=0.300x+0.639	0.95	0.0009
	PHF/TiO_2=0	y=-0.079x-0.007	0.97	y=0.129x+0.836	0.95	0.29

* 1st-order: y is ln c/c_0; 2nd-order: y is c_0/c

Table 2-2. Effect of enhancers on UVA photocatalytic degradation of organic dyes by TiO_2 coatings

Study	Type of TiO_2	Enhancer	Mass ratio of enhancer to TiO_2	Model pollutant	UVA intensity (W/m2)	Time exposed to UVA (h)	Increase in rate
This study*	Anatase	PHF	0.01	Procion red MX-5B	15-17	6	1.9×
Arabatzis *et al.*[51]	Anatase and rutile (sol-gel)	Ag	0.013	Methyl orange	0.717	1	1.8×
Arabatzis *et al.*[52]	Anatase and rutile (sol-gel)	Au	0.051	Methyl orange	0.717	1	2.2×
Arpac *et al.*[82]	Anatase (sol-gel)	Sn	0.15	Malachite Green	N/A**	4	1.1×
Hermann *et al.*[83]	Anatase (sol-gel)	Ag		Malic acid	N/A	0.5	1.3×
Somekawa *et al.*[84]	Degussa P25	N		Methylene blue	N/A	N/A	1.2×
Wu *et al.*[85]	Anatase (sol-gel)	Fe and Au	Fe: 0.005 Au: 0.02	2,4-dichlorophenol	12.3	5	2.0×
Kumaresan *et a*l.[86]	Anatase (sol-gel)	Sr	0.001	2,4-dinitrophenol	N/A	5	1.8×
Okte and Yilmaz[87]	Anatase (sol-gel)	La	0.0028	Methyl orange	N/A	3	1.3×
Carvalho *et al.*[88]	Amorphous	Cu	0.007	Methylene blue	N/A	2	1.8×

*The TiO_2 film was exposed to air in this study, and to water in all other studies
**Not available in the reference

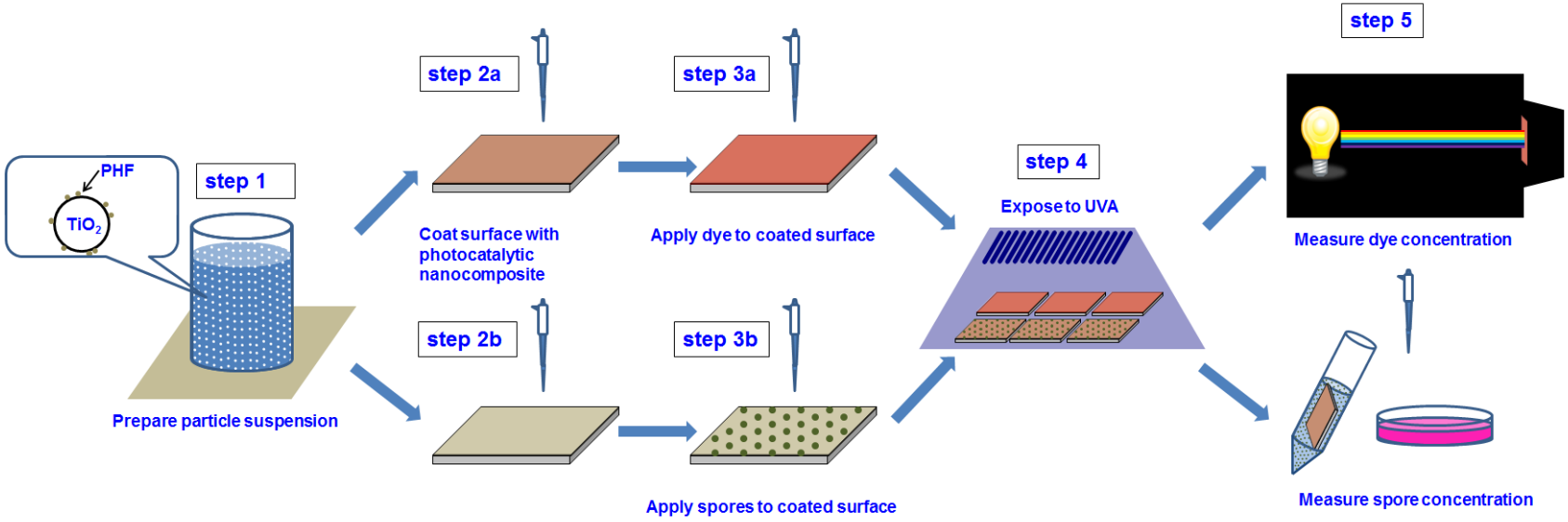

Figure 2-1. Procedure for testing performance of photocatalytic coatings

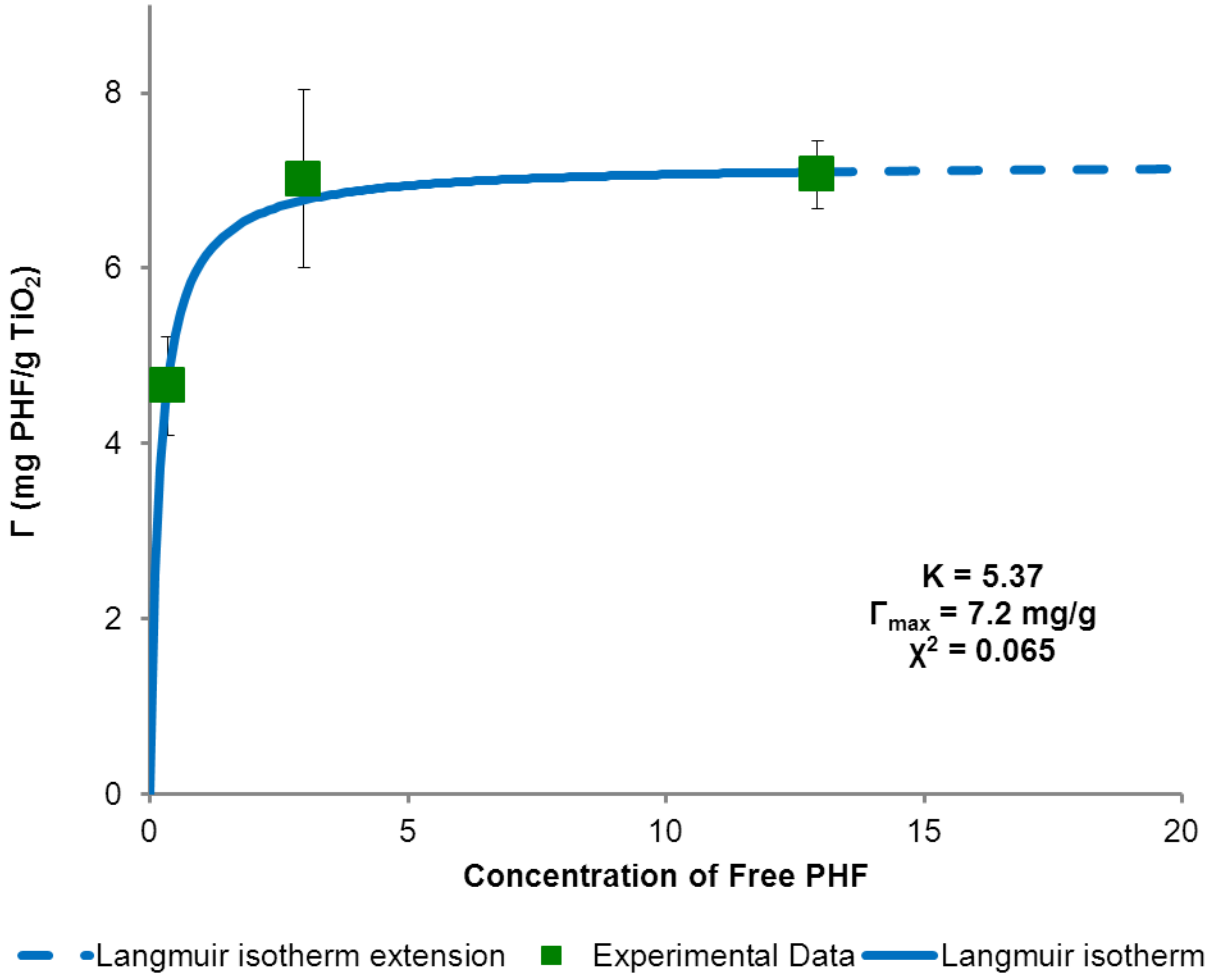

Figure 2-2. Langmuir isotherm for adsorption of PHF onto TiO_2 at pH 6 and 25°C

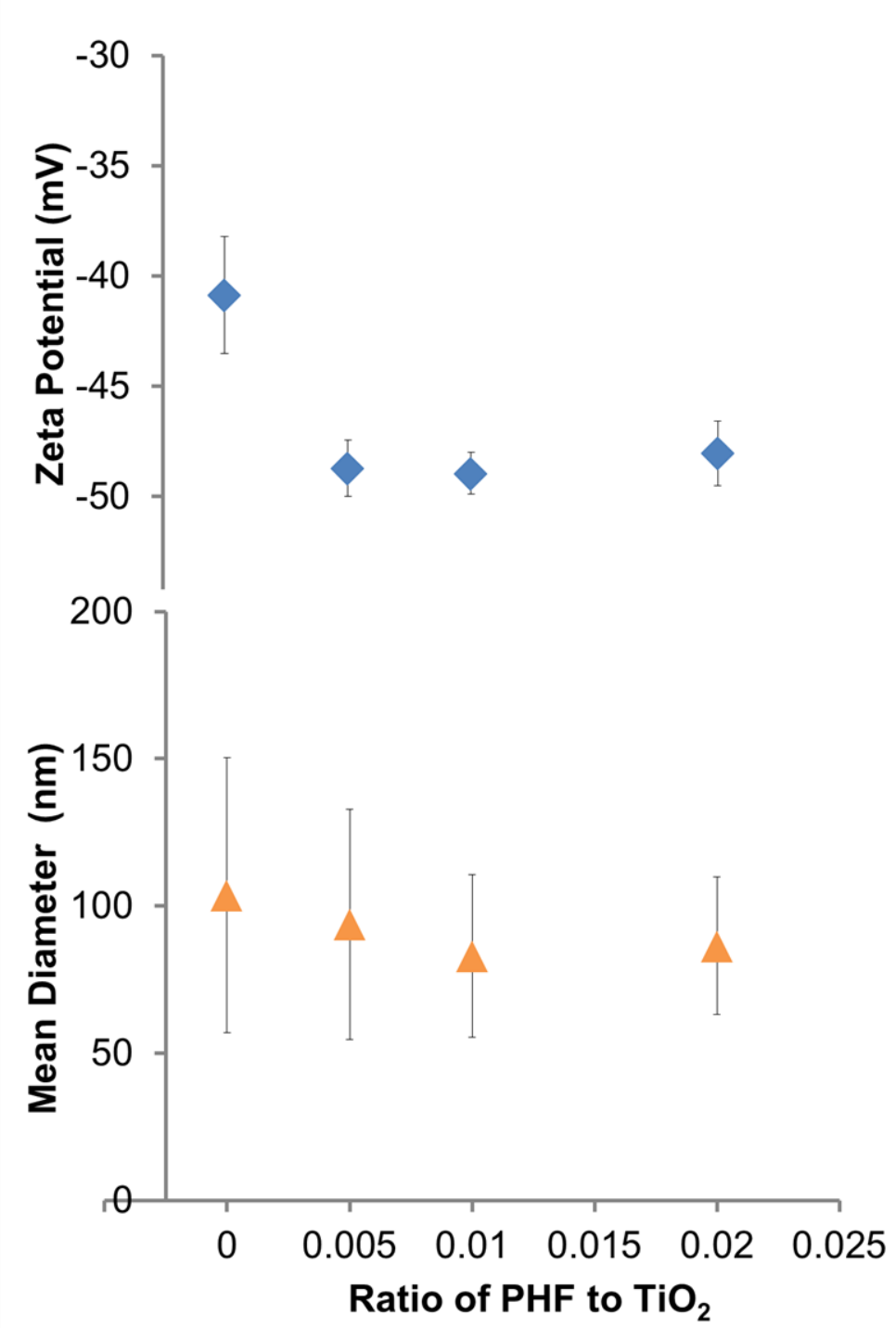

Figure 2-3. Aqueous aggregate size and zeta potential of TiO_2 and PHF/TiO_2

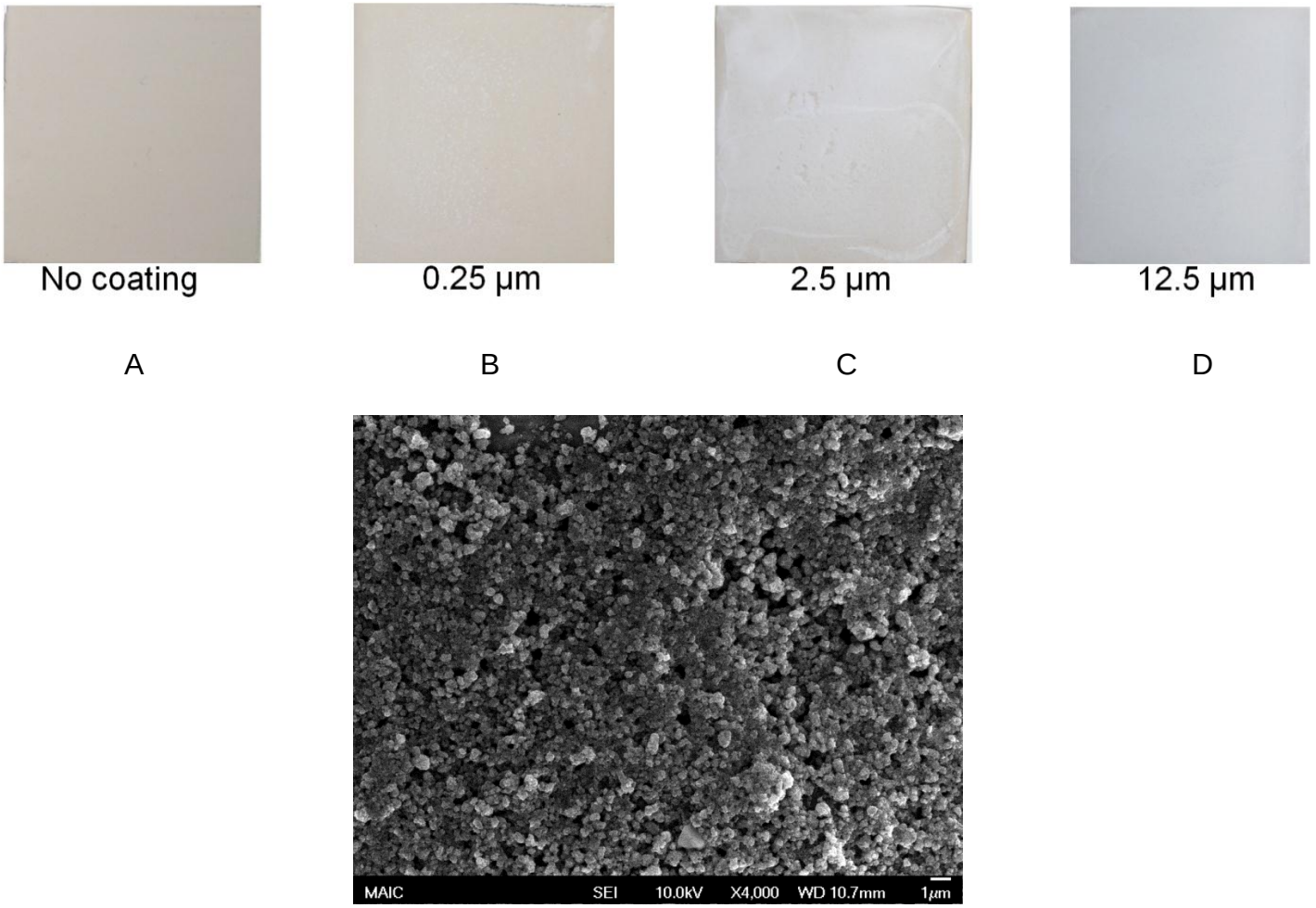

Figure 2-4. Coating appearance and structure. A) Effect of calculated TiO_2 thickness on appearance on grout surface. B) Effect of 0.25 µm thick TiO_2 coating on appearance on grout surface. C) Effect of 2.5 µm thick TiO_2 coating on appearance on grout surface. D) Effect of 12.5 µm thick TiO_2 on appearance on grout surface. E) Scanning electron micrograph of TiO_2 at the thickness of 0.25 µm

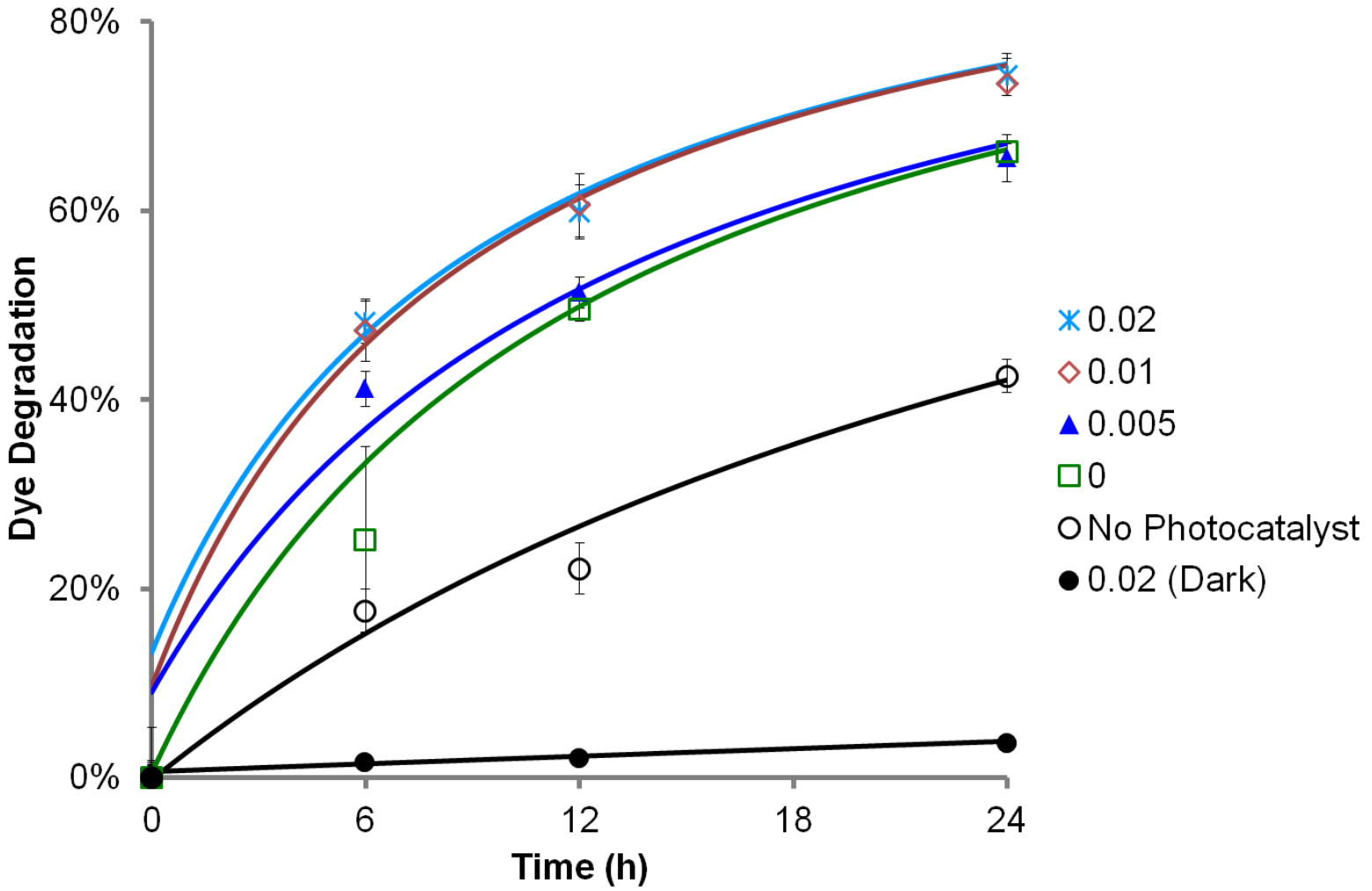

Figure 2-5. Optimization of PHF/TiO_2 mass ratio (0.02, 0.01, 0.005, 0) in photocatalytic nanocomposite. Error bars represent ± 1.0 SD. (Error bars for the dark control are too small to be seen.) Model lines represent second-order fits

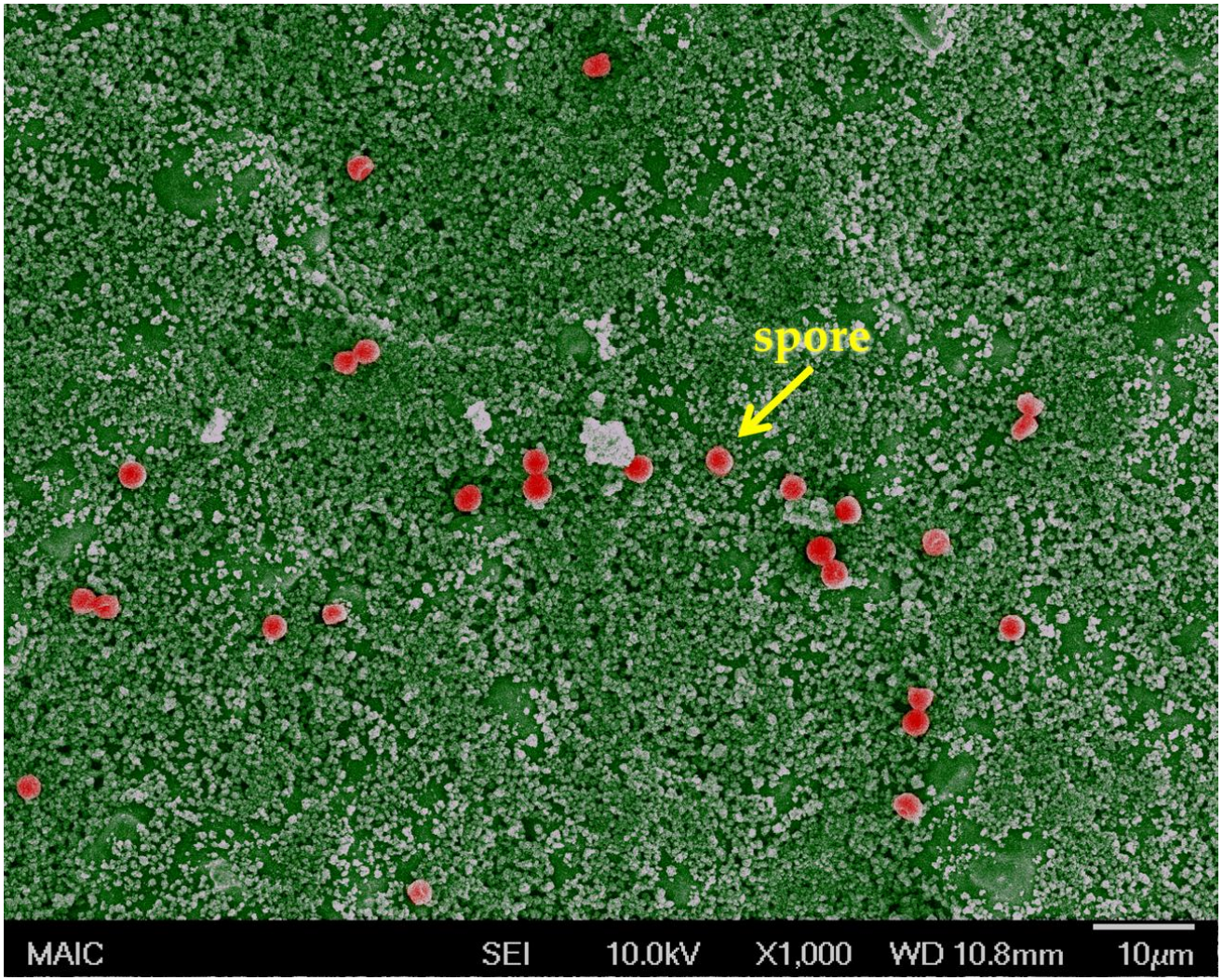

Figure 2-6. False-color image of *Aspergillus niger* spores on PHF/TiO_2 nanocomposite coating (Spores are red spheres; coating is green background; whitish coloring indicates charging of the coating during microscopy.)

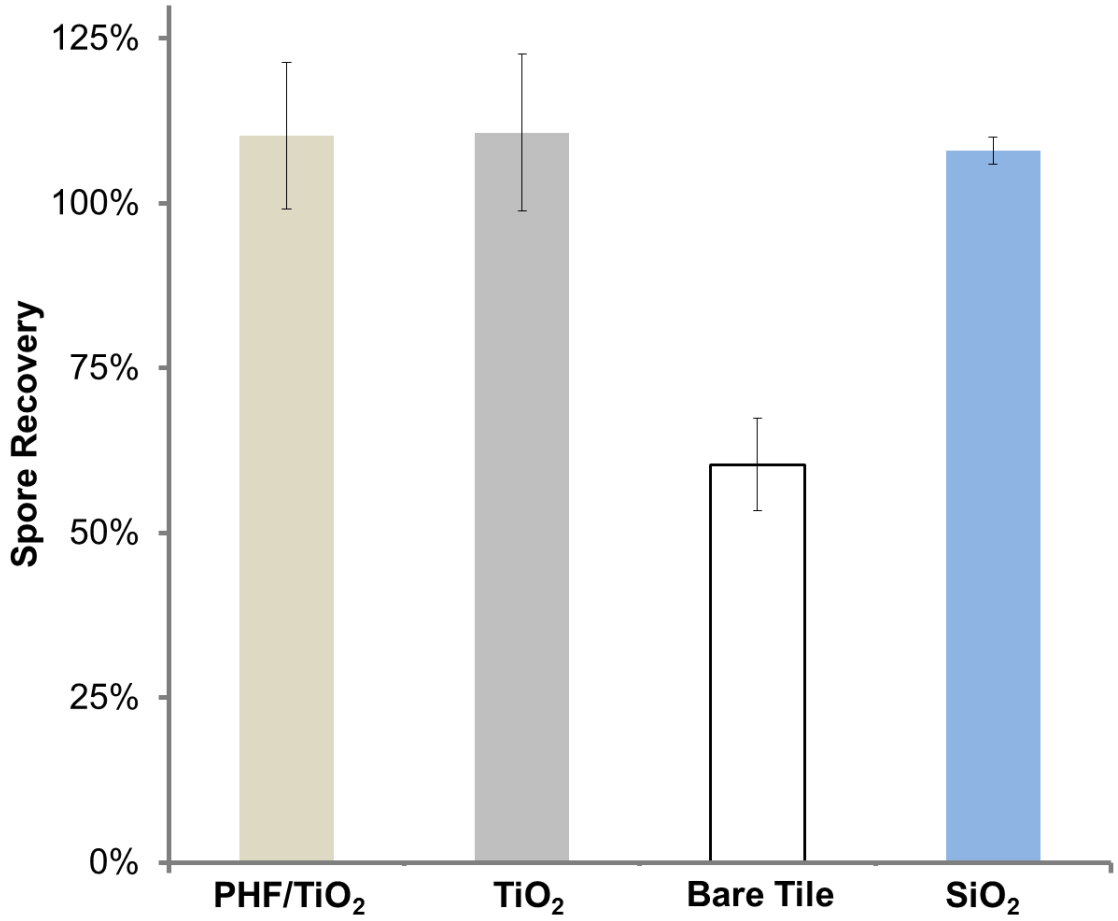

Figure 2-7. Recovery of *A. niger* from test surfaces. Error bars represent ± 1.0 SD

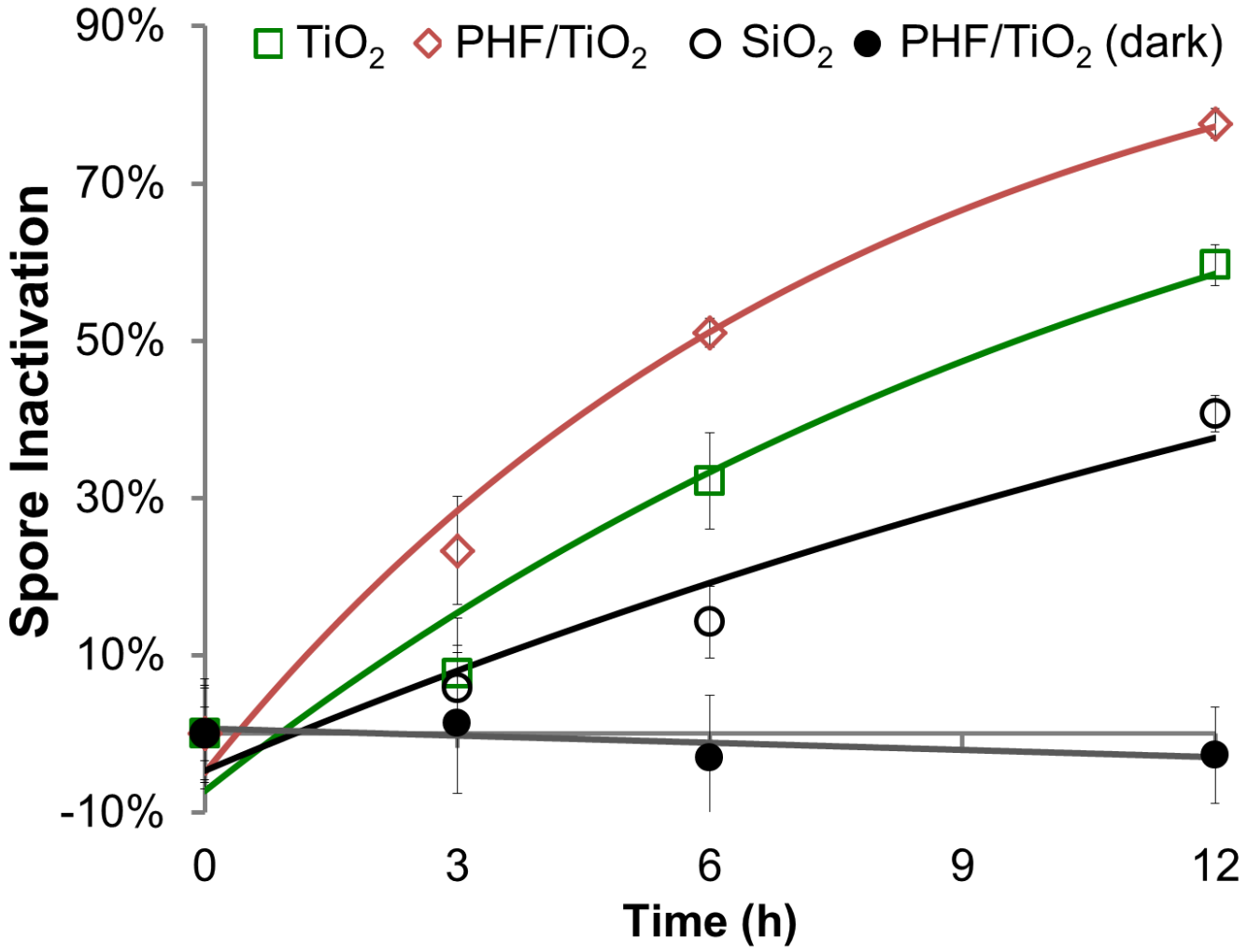

Figure 2-8. Inactivation of *A. niger* spores by test surfaces. Error bars represent ± 1.0 SD. Model lines represent first-order fits

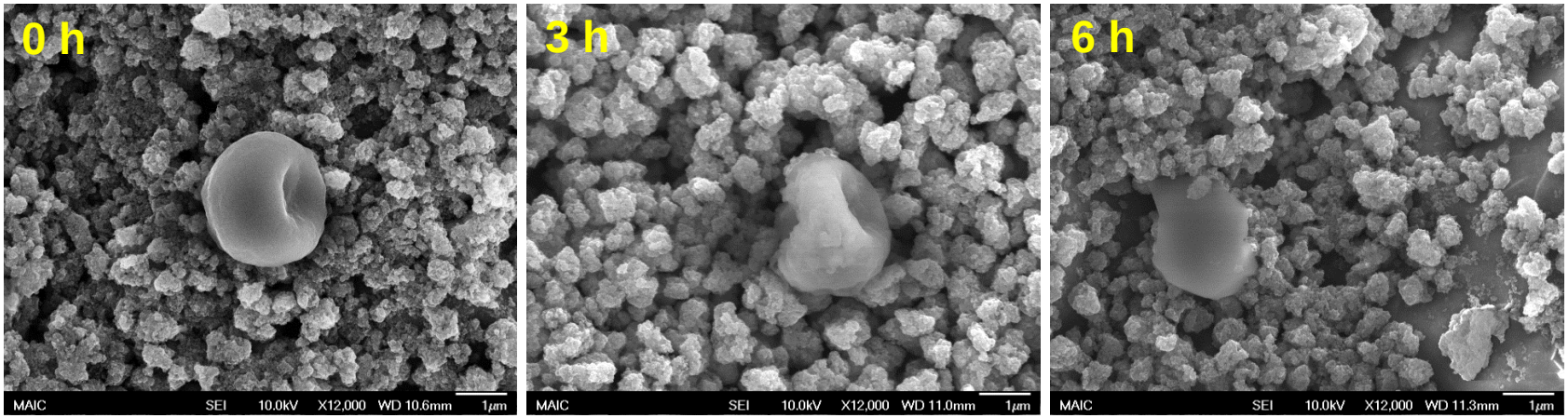

Figure 2-9. Temporal changes of spore morphology on photocatalytic coatings exposed to UVA

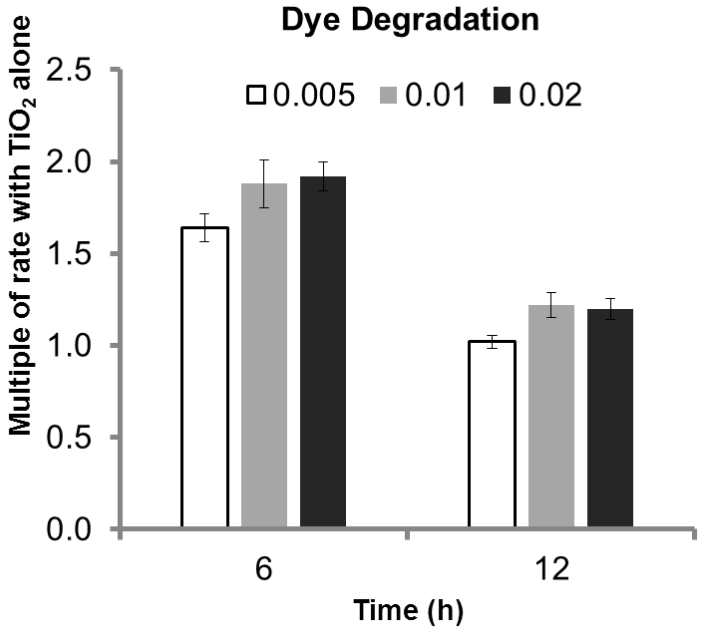

A

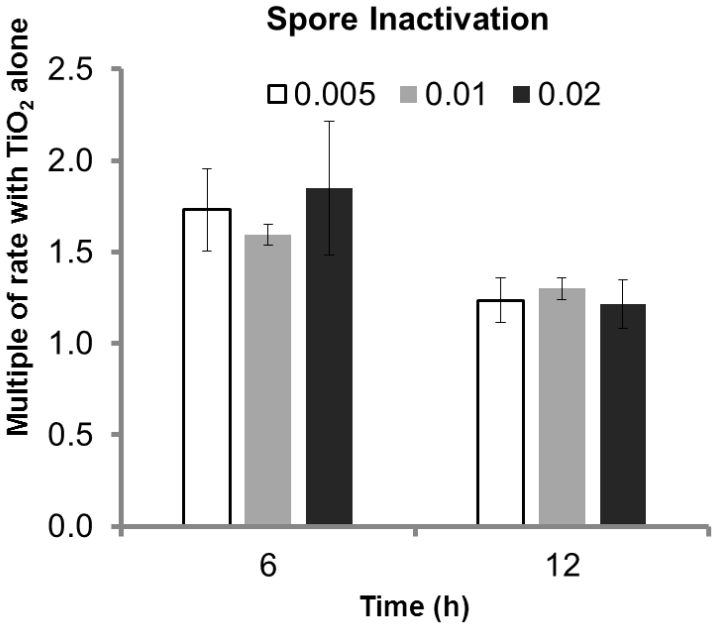

B

Figure 2-10. Photocatalytic enhancement by the nanocomposite at different PHF/TiO_2 ratios (0.005, 0.01 and 0.02) relative to TiO_2 alone. A) Dye degradation. B) spore inactivation

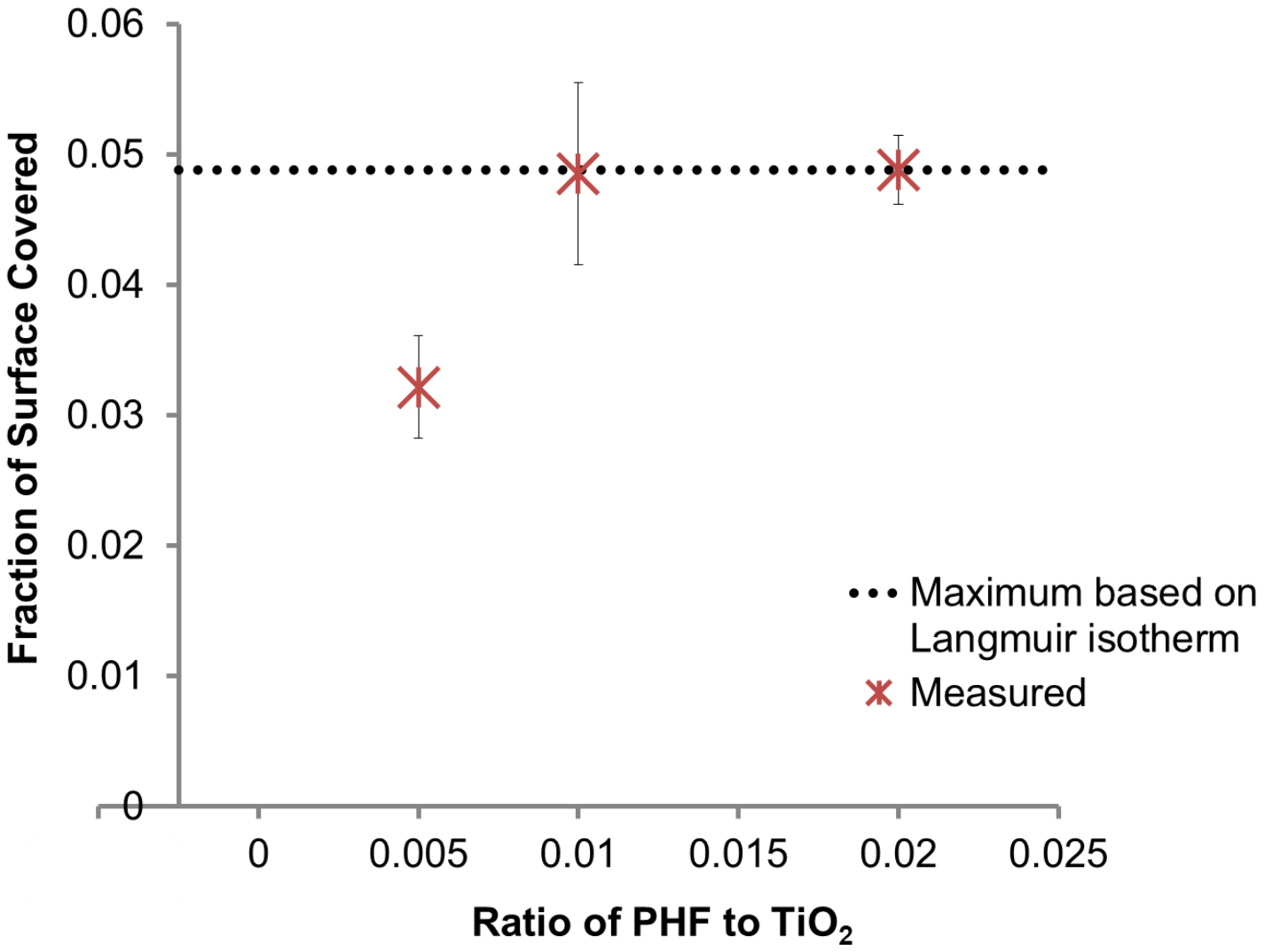

Figure 2-11. Surface coverage of PHF on TiO_2 as a function of the PHF/TiO_2 formulation ratio

CHAPTER 3
VISIBLE LIGHT ACTIVE, TRANSPARENT, ANTIMICROBIAL SURFACES

Chapter 2 demonstrated that PHF significantly enhances TiO_2 photocatalysis in transparent coating under UVA irradiance. The novel PHF/TiO_2 nanocomposite coating is very promising as it can be used for antimicrobial coating applications, reducing surface acquired infections. However, surface acquired infections occur more frequently in indoor environment, such as hospitals, assisted living facilities and other public buildings, where UVA (315–400 nm) is not available. Visible light (fluorescent lamp with wavelength above 400 nm) is readily available in indoor environments. The photocatalytic activity of PHF/TiO_2 under visible light is not yet identified. Hence, the objective of this study is to evaluate and optimize the visible light activity of PHF/TiO_2 nanocomposite and test its efficacy against model microbes (fungal and bacteria).

The first task was to select a coating system that is active under visible light. TiO_2 nanoparticles with different crystallite sizes and phases from four manufacturers were selected. They were characterized by XPS, XRD, BET surface area measurement, light adsorption and photocatalytic performance.

The second task was to combine the selected visible light active TiO_2 with PHF. The PHF/TiO_2 nanocomposite coating was optimized by varying the weight ratio of PHF to TiO_2. The photocatalytic performance was determined by organic dye degradation. The optimized PHF/TiO_2 nanocomposite was used to inactivate *Staphylococcus aureus*, a surrogate for MRSA and spores of *Aspergillus niger*, a common household allergen.

3.1 Experimental

3.1.1 Chemicals and Reagents

Five model photocatalysts were used: the mixed-phase P25, rutile (rutile22[4] and rutile99) and anatase (anatase7 and anatase15). The properties of these photocatalysts as given by the manufacturers are collected in Table 3-1. Commercial TiO_2 formulations (NuTiO^{TM} Primer and NuTiO^{TM} TiO_2) were obtained from Bioshield, Inc. (Fort Lauderdale, FL). A solution of Procion red MX-5B dye (Sigma-Aldrich Inc., St. Louis, Missouri) was prepared at a concentration of 2000 mg/L by dissolving 0.02 g dye powder in 10 mL deionized water. Polyhydroxy fullerene (PHF) was synthesized in our laboratory according to the protocol of Gao et al.[75] Phosphate-buffered saline (PBS) solution was prepared by dissolving 12.36 g Na_2HPO_4, 1.80 g NaH_2PO_4 and 85.00 g NaCl in 1000 mL of deionized water and then diluting 10× immediately before use. PBS/SDS solution was prepared by adding 0.576 g sodium dodecyl sulfate (SDS) to 1000 mL of PBS and then autoclaving at 120°C and 16 bar for 15 minutes.

3.1.2 Microbe Culture and Enumeration

The culture media for *Staphylococcus aureus* (ATCC 25923) was tryptic soy agar and tryptic soy broth (Becton, Dickinson and Company, Sparks, MD), which were used for culturing and enumerating the bacteria. Agar plates were prepared by adding a mass of 40 g Tryptic soy agar powder to 1 L of deionized water and mixing thoroughly with heating to the boiling point. The solution was then autoclaved at 120 ºC and 16 bar for 15 minutes. Plates were made by pouring the autoclaved agar into 100×15 mm sterile plastic Petri dishes (Fisher Scientific) and air dried in a laminar flow hood (LABCONCO

[4] The phase of TiO_2 followed by its crystallite size was used to identify each TiO_2 powder in this study

purifier class 2 safe cabinet) for 24 hours. The dried agar plates were used immediately or stored in inverted position in a refrigerator at 4°C. Broth was prepared by adding a mass of 32 g tryptic soy broth powder to 1 L of deionized water and mixing thoroughly with heating to the boiling point. The solution was then autoclaved at 120 ºC and 16 bar for 15 minutes. Autoclaved tryptic soy broth was used immediately or stored in a refrigerator at 4°C.

The *S. aureus* was maintained by streaking the bacteria on tryptic soy agar in a Petri dish. The inoculated plate was inverted and incubated at 37ºC for 24 hours. An inoculation loop was used to transfer a loop full of *S. aureus* from the plate to a 250 mL Erlenmeyer flask containing 100 mL of tryptic soy broth. The flask with *S. aureus* was incubated at 37ºC for 24 hours. A volume of 1 mL of 24-hour *S. aureus* suspension was added to ten centrifuge tubes, respectively. Each tube contained 1 mL of 50% glycerol as cryoprotectant. The mixture of *S. aureus* and glycerol was stored at -84ºC.

S. aureus was cultured by adding a 2 ml aliquot of *S. aureus* that was previously frozen at -84ºC in 25% glycerol to a 250 mL Erlenmeyer flask containing 100 mL of sterile tryptic soy broth. The culture was incubated in a shaker-incubator at 150 rpm and 37ºC for 24 hours. The suspension was washed three times with sterile deionized water and the final pellet was resuspended in 15 mL of deionized water.

The number of colony forming units in a suspension of *S. aureus* was determined by serial dilution and viable plate counts. A series of 10-fold dilutions (10^{-1} to 10^{-7}) was prepared from the *S. aureus* suspension by adding 0.333 mL of sample to 3.0 mL sterile deionized water in a dilution tube, followed by vortexing for 10 seconds. A volume of 0.1 mL of diluted sample was spread over the surface of tryptic soy agar using a Teflon rod

in each of three 100×15mm Petri dishes. The inoculated plates were inverted and then incubated at 37ºC for 24 hours. Where possible, results were taken from plates that contained between 30 and 300 colonies.

3.1.3 Coating Preparation and Testing

The steps of coating preparations are described below

Step 1–Ten mg of TiO_2 or SiO_2 was added to 10 mL of deionized water in a 20 mL scintillation vial. The suspension was sonicated (Misonix Sonicator 3000, Farmingdale, NY) at the highest power level (providing 180–200 W) for 30 minutes total (10 min on/2 min off × 3). PHF/TiO_2 nanocomposite was prepared by adding ten mg of anatase7 to 9 mL of deionized water in a 20 mL scintillation vial. The anatase7 suspension was sonicated (Misonix Sonicator 3000, Farmingdale, NY) at the highest power level (providing 180–200 W) for 30 minutes total (10 min on/2 min off × 3). A volume of 1 mL of PHF solution, containing 1000, 500, 100, 50 or 0 mg/L PHF, was then added to the anatase7 suspension, mixed with magnetic stirrer for 10 minutes in dark. The Bioshield NuTiOTM TiO_2 and Bioshield Primer formulations were applied directly from the manufacturer's containers.

Step 2– Ceramic tiles were used to test photocatalytic degradation of organic dye and inactivation of microbes. Tiles (2.5 cm × 2.5 cm) were obtained from American Olean Inc. (Dallas,TX). The tile surfaces were almond-colored with a matte finish. A volume of 0.4 mL of TiO_2 or SiO2 (as inert control) suspension or Bioshield Primer was pipetted on the tile surface as a bottom coat. The coated surfaces were dried overnight at room temperature. A second coat of TiO_2, PHF/TiO_2 nanocomposite, SiO_2 or Bioshield NuTiO was applied following the same procedure as described above. This gave final surface TiO_2 loadings of 128 µg/cm^2 (TiO_2 on TiO_2), 64 µg/cm^2 (SiO_2 on TiO_2)

or 0 μg/cm^2 (SiO_2 on SiO_2). The TiO_2 surface loadings of coatings with either Bioshield Primer or Bioshield NuTiO were not determined.

Step 3–Organic dye or *S. aureus* suspension was applied to the test surfaces.

(a) Testing with organic dye. A volume of 0.01 mL of Procion red MX-5B solution (2000 mg/L) was pipetted onto coated tile and allowed to spread. The dye was dried at 50ºC for 20 minutes before testing.

(b) Testing with *S. aureus*. A volume of 0.1 mL of *S. aureus* suspension (2–3×10^5 CFU/mL) was pipetted onto each coated tile surface and allowed to spread, giving a surface loading of 6400–9600 CFU/cm^2. The tiles with *S. aureus* were dried in the dark in a biosafety cabinet for 3 hours.

Step 4–The photocatalytic experiments were carried out under fluorescent lamps (General Electric model T8 Ultramax F28T8-SPX41) at an irradiance of 1.8~2.0 W/m^2. UVA irradiance was measured by a PMA2110 meter with a PMA 2110 UVA Detector or PMA 2140 Global Detector (Solar Light Co., Glenside, PA).

Dye degradation was based on absorbance, as calculated from reflectance measured at 538 nm after 0, 3, 6, 12 and, sometimes, 24 hours of exposure to fluorescent light. Reflectance of coated or uncoated tile surfaces was measured with a Perkin-Elmer Lambda 800 with PELA-1000 Reflectance Spectroscopy Accessory. Absorbance was calculated as the negative $\log_{10}$ of reflectance expressed as fraction. Coated tiles without dye were used as the internal reference in the measurement. Dye degradation was calculated according to:

$$\% \text{ dye degradation} = \frac{A_0 - A_t}{A_0} \times 100 \qquad (3\text{-}1)$$

where A_0 is the calculated absorbance of dye coated on photocatalytic or bare grout surface before exposure to fluorescent light and A_t is the absorbance of dye coated on photocatalytic or grout surface after exposure to fluorescent light at a given time. Because the color of bare grout varied somewhat, it was necessary to subtract this background color. Therefore, A_0 and A_t were calculated from

$$A_0=A_{0'}-A_b \quad (3\text{-}2)$$

$$At=A_{t'}-A_b \quad (3\text{-}3)$$

where $A_{0'}$ and $A_{t'}$ are the measured absorbance of dye on grout at time zero and time t, respectively, and A_b is the measured absorbance of the bare or photocatalytically coated grout surface without dye at a given time.

Photocatalytic inactivation of microbes was based on viable counts after exposure of spores on test surfaces to fluorescent light. Bacteria were recovered by immersing a tile in 20 mL PBS/SDS within a polypropylene centrifuge tube and vortexing for 15 seconds. The tube was then sonicated at highest power for 1 minute. During sonication, the tube was immersed in a flowing water bath at 28 ºC. After sonication, the tube was vortexed for 15 seconds. The viable bacteria in a volume of 0.1 mL suspension from the centrifuge tube were enumerated as described previously. Inactivation was calculated from

$$\%Inactivation = \frac{CFU_0 - CFU_t}{CFU_0} \times 100\% \quad (3\text{-}4)$$

where CFU_t is the number of colonies after time t and CFU_0 is the number of colonies at time zero.

3.1.4 Characterization of TiO_2 Particles and Coatings

X-ray photoelectron spectroscopy. X-ray photoelectron spectroscopy (XPS) was used to measure the purity of the TiO_2 powders used in this study. XPS analysis was performed with an XPS/ESCA Perkin-Elmer PHI 5100ESCA system using a wafer as a substrate, followed by spectrum analysis with AugerScan software (Thermo Fisher Scientific, Waltham, MA). When a material is irradiated with a beam of aluminum or magnesium X-rays, XPS simultaneously measures the kinetic energy (KE) and electrons escaping from the top 1 to 10 nm of the material. The electron binding energy (BE) can be determined based on the equation:

$$E_{binding} = E_{photon} - E_{kinetic} - \Phi \quad (3\text{-}5)$$

where $E_{binding}$ is the energy of the electron emitted from one electron configuration within the atom; E_{photon} is the energy of the X-ray photons being used; $E_{kinetic}$ is the kinetic energy of the emitted electron as measured by the instrument and Φ is the work function of the spectrometer.

BET surface area. Specific surface area of TiO_2 was measured under nitrogen using a NOVA 1200 with multipoint BET (Quantachrome Instruments, Boynton Beach, FL). TiO_2 powder was degassed and dried under vacuum at 110ºC prior to measurement.

X-ray diffraction. Powder X-ray diffraction was measured on a APD 3720 diffractometer (Philips, Andover, MA) with Cu-K_α radiation (40 kV, 25 mA) and diffracted beam monochromator, using a step scan mode with the step of 0.075° (2θ) and 4 s per step. Crystal structure was identified according to the database of International Centre for Diffraction Data.

The crystallite size of TiO_2 was determined from the Scherrer equation:[89]

$$L = \frac{K\lambda}{(B-b)\cos\theta} \quad (3\text{-}6)$$

where L is the average crystallite size, K is the shape factor (0.9), λ is the x-ray wavelength of Cu-K_α radiation (1.54 Å), B is the overall line broadening in radians at the full width at half maximum (FWHM) intensity, b is the line broadening in radians at the FWHM intensity caused by the instrument itself (0.07) and θ is the Bragg angle, i.e., the angle at which highest intensity was observed. The crystallite size measured from XRD was used to compute an estimate of the specific surface area of TiO_2 for comparison with the measurement from BET surface area, according to the following equation:

$$SA = \frac{6}{\rho d} \quad (3\text{-}7)$$

where ρ is the density of TiO_2 form and d is the crystallite size of TiO_2, as determined by XRD.

Scanning electron microscopy. Scanning electron microscopy (JOEL 6335F FEG-SEM) was used to observe the ultrastructure of TiO_2 coating at the conditions of 10 kV accelerating voltage and 10 mm working distance.

UV/VIS reflectance spectroscopy. A Perkin-Elmer Lambda 800 UV/VIS spectrophotometer with PELA-1000 reflectance accessory was used to measure light adsorption by TiO_2 over a range of 300 to 700 nm. The band gap energy was determined from:

$$E = hc/\lambda \quad (3\text{-}8)$$

where λ is the wavelength at which a strong cut off in adsorption was observed, h is the Plank constant (4.14×10^{-15} eV·s) and c is the speed of light in vacuum (3.00×10^{8} m/s). A

volume of 0.4 mL of 1 wt%[5] TiO_2 suspension was pipetted onto a tile surface, followed by drying overnight in a biosafety cabinet. A white Teflon plate was used as the internal reference.

3.1.5 Adsorption

PHF was combined with anatase7 as described previously in the section on coating preparation and testing. A 2 mL volume of the mixture was transferred to a centrifuge tube, followed by 30-minute centrifugation at 20,800×g. The supernatant was carefully removed by pipette and the procedure was repeated two more times. The concentration of free PHF in the final supernatant was measured by UV/Vis spectroscopy at 330 nm.[77, 78] The extent of adsorption was found to follow the Langmuir relationship:

$$\Gamma = \Gamma_{max} \frac{Kc}{1+Kc} \tag{3-9}$$

where Γ is the mass PHF adsorbed per mass TiO_2 , c is the concentration of free PHF in equilibrium with TiO_2, Γ_{max} is the maximum mass PHF adsorbed per mass TiO_2 and K is the Langmuir equilibrium constant. The Langmuir parameters Γ_{max} and K were estimated by least squares non-linear regression.

The fraction of surface coverage of TiO_2 by PHF was calculated from

$$\text{Surface coverage} = \frac{\Gamma N_A A_P}{m_P A_S} \tag{3-10}$$

where N_A is Avogadro's constant, A_P is the projected area of a PHF molecule (1.33 nm^2 [58], m_P is the molecular weight of PHF (1094 g/mol from the empirical formula $C_{60}(OH)_{22}$)

[5] The concentration of TiO_2 suspension was ten times higher in order to increase signal to noise ratio of TiO_2 and eliminate signals coming from the bare tile surface.

and A_S is the specific surface area of anatase with a crystallite size of 7 nm (231 m^2/g as measured in the present study).

3.1.6 Data Analysis

First-order fits between the extent of dye degradation or microbe inactivation and UVA exposure time were based on the equation

$$\ln \frac{c_t}{c_0} = kt + b \tag{3-11}$$

and second-order fits were based on the equation

$$\frac{1}{c_t/c_0} = k't + b' \tag{3-12}$$

where c_t and c_0 represent absorbance or colony forming units at times t and t_0, respectively, k and k' are the reaction rate coefficients for the first and second order fits, respectively, and b and b' are arbitrary constants.

The parameter values (k, b, k', b') for the fits were determined by least squares linear regression.

One-way ANOVA and post-hoc testing were carried out using the Dunnett's two-sided tests through NCSS statistical analysis and graphics software (NCSS, Kaysville, UT). The significance of differences between R^2 values of least square fits to experimental data was determined using the Fisher r-to-z transformation.[79]

3.2 Results

3.2.1 Characterization

XPS gives a measure of the elemental composition of a powder to a depth of 1 to 10 nm. The XPS spectrum of the TiO_2 particles used in this study is displayed in Figure 3-1. Each of the powders contained titanium, oxygen and carbon (Table 3-2). The carbon is present as surface impurity due to exposure of the powder to the laboratory

atmosphere. P25 contained a small amount of silicon and rutile22 contained a small amount of aluminum in addition to Ti, O and C. Binding energies are given in Table 3-3. The binding energies exhibited a shift of 3.7–7 eV above the binding energies published in the NIST X-ray Photoelectron Spectroscopy Database.[90] Because the shifts between the measured and database binding energies for electrons are consistent both in magnitude and direction, the measurements were considered to be consistent with the database.

The BET specific areas of rutile22, rutile99, anatase7, anatase15 and P25 were 35, 1, 231, 110 and 44 m^2/g, respectively (Table 3-4). These values deviated slightly from the specific surface area calculated on the basis of the crystallite sizes calculated from XRD and spherical particles.

X-ray diffraction gives information about the crystallographic structure of powders. X-ray diffraction patterns of the TiO_2 powders used in this study are shown in Figure 3-2. Diffraction patterns of characteristic of both anatase and rutile were found by XRD analysis of P25. This indicates that P25 has a mixed phase structure.[91] The diffraction patterns of rutile22 and rutile99 were in good agreement with the pattern for rutile from the database of International Centre for Diffraction Data (ICDD).[92] The diffraction pattern of anatase7 was in good agreement with the diffraction pattern for anatase from the ICDD database, whereas anatase15 contained a small peak at Miller index 110, which is indicative of a slight rutile impurity. The mean crystallite size calculated on the basis of XRD was 22 nm for rutile22, 99 nm for rutile99, 7 nm for anatase7, 15 nm for anatase15 and 25 nm for P25 (Table 3-5). The x-ray diffraction parameters used for these calculations are also given in Table 3-5.

Scanning electron micrographs of TiO_2 powders employed in this research are given in Figure 3-3. The aspect ratio of anatase crystallites was noticeably higher than that of rutile or P25. The anatase coating also appears less dense than the rutile or P25 coatings. The smaller dimension of the crystallites was 23–28 nm for rutile22 (Fig. 3-3A), 97–280 nm for rutile99 (Fig. 3-3B), 16–25 nm for anatase7 (Fig. 3-3C), 21–59 nm for anatase15 (Fig. 3-3D) and 30–47 nm for P25 (Fig. 3-3E). Table 3-6 gives a comparison of crystallite size based on XRD and SEM.

The light absorption spectra of TiO_2 coatings used in this study are shown in Figure 3-4. The band gaps were determined to be 3.0 eV for rutile22, 3.0 eV for rutile99, 3.2 eV for anatase7, 3.2 eV for anatase15 and 3.1 eV for P25 (Table 3-7). These values are consistent with band gaps for these materials that are reported in the literature.[93, 94]

3.2.2 Photocatalytic Performance of TiO_2 with Different Crystallite Sizes

Top coats of a commercial photocatalyst (NuTiO TiO_2), P25 and anatase15 on bottom coats of NuTiO Primer, rutile99 and SiO_2 was screened for their ability to degrade organic dye under visible light, as shown in Figure 3-5. Dye degradation on bare tile over the 4-days of exposure to visible light was minimal. NuTiO TiO_2 appeared to have almost no photocatalytic activity. P25 and anatase15 exhibited modest photocatalytic activity with bottom coat of NuTiO Primer, and almost complete photocatalytic dye degradation on bottom coats of rutile99 and SiO_2.

The visible light photocatalytic performance of coatings made from rutile22 or anatase7, as well as coatings made from rutile99, anatase15 and P25, is shown in Figure 3-6. The largest particles, rutile99, were inactive. TiO_2 coatings made from powders with crystallite size smaller than P25 outperformed P25. Rutile22 exhibited the highest photocatalytic activity.

Table 3-8 summarizes model fits to the time-dependent dye degradation data with first order and second order reaction kinetics. There is no significant difference between the correlation coefficients of the first order and the second order fits. In the case of UVA experiments, as reported in Chapter 2, second order fits were significantly better for dye degradation. In order to maintain consistency with the Chapter 2 results, the second order reaction rate coefficients are used to compare dye degradation performance of alternative coatings.

The second order dye degradation rate coefficients are compared in Figure 3-7 in relation to crystallite size. The reaction rate coefficient for rutile99 is near zero, significantly lower than the coefficients of other coatings. All coatings except rutile99 have significantly higher reaction rate coefficients than P25. The dye degradation rate coefficient for rutile22 was significantly greater than that for the other coatings. Anatase7 and anatase15 were equivalent in performance. The coatings of anatase7 and rutile22 were more uniform and transparent than coatings of other powders. Due to their ability to produce coatings with excellent visible light activity and transparency, rutile22 and anatase7 were selected for further development.

3.2.3 Light Utilization by Rutile22 and Anatase7

The light source used in this study was fluorescent lamp, which contained a wide spectrum of electromagnetic radiation ranging from far end of UVA to near infrared. The emission spectrum of the fluorescent light used in this study (Fig. 3-8) indicated that only a small peak in intensity was present below 400 nm, comprising less than 3% of the total intensity. Two peaks are present between 400 and 500 nm, together accounting for 17% of total intensity. Light from 500 to 700 nm constitutes 80% of total intensity.

Optical filters were used to identify the effect of different portions of the spectrum of fluorescent light on photocatalytic activity of rutile22 and anatase7. The 400 nm cut-off filter has zero transmission below 380 nm, with a transition to 90% transmission between 380 and 400 nm. The 495 nm cut-off filter has zero transmission below 470 nm, with a transition to 90% transmission between 470 and 495 nm (Table 3-9 and 3-10). The effects of the optical filters on dye degradation are shown in Figure 3-9. Application of the 400 nm cut-off filter reduced dye degradation by rutile22 by 22% relative to the dye degradation obtained under neutrally filtered light (Table 3-11), indicating that about one fourth of the activity of this photocatalyst is due to UVA. Application of the 495 nm cut-off filter further decreased dye degradation by 62% relative to the neutral filter, indicating that about one-half of the activity of rutile22 is due to light between 400 and 495 nm. Thus, most of the activity of rutile22 appears to derive from sub-495 nm light. In the case of anatase7, application of the 400 nm cut-off filter reduced dye degradation by 22% relative to the neutral filter, indicating that about one fourth of the activity of this photocatalyst, as with rutile22, is due to UVA. Application of the 495 nm cut-off filter further decreased dye degradation by only 4% relative to the neutral filter, indicating that almost none of the activity of anatase7 is due to light between 400 and 495 nm. Thus, most of the activity of anatase7 appears to derive from sub-400 nm and supra-495 nm light.

3.2.4 Photocatalytic Performance of PHF/anatase7

Since anatase7 and rutile22 utilize different spectrum of fluorescent light, the combination of these TiO_2 particles as part of a coating system can be expected to exhibit superior photocatalytic activity. Scanning electron micrographs of anatase7 and rutile22 (Fig. 3-10) shows that a two-layer rutile22 coating is more uniform and denser

than a two layer anatase7 coating. In Figure 3-10B, some bare area seemed to appear in addition to aggregates on the antase7 coating. However, this area was covered with ultrafine, sparsely distributed anatase7 particles (16–25 nm) as shown previously in Figure 3-3. As a result, the coating design with rutile22 as a dense and uniform bottom coat and with the ultrafine anatase7 or PHF/anatase7 nanocomposite as top coat was expected to maximize the photocatalytic performance of the coating.

The isotherm for adsorption of PHF on anatase7 is given in Figure 3-11. The theoretical maximum adsorption of PHF on anatase was 39.7 mg/g, whereas the highest level reached experimentally was 31 mg/g at the PHF/anatase7 ratio of 0.1.

The effectiveness of PHF/anatase7 nanocomposite with ratios of 0, 0.005, 0.01, 0.05 and 0.1 as top coat with rutile22 as bottom coat was tested. Figure 3-12 describes the time-dependent degradation of procion red MX-5B dye on this coating system under fluorescent light. A dark control with anatase7 as top coat and rutile22 as bottom coat suggested that no dye degradation took place in dark. Previously (Fig. 3-5), it was shown that dye photolysis under visible light is negligible. TiO_2 photocatalysis was definitely enhanced even with small amount of PHF. After 3-hour exposure to fluorescent light, up to 2.3 times enhancement was observed for PHF/anatase7 at the ratio of 0.1, and the extent of dye degradation for other ratios of PHF/anatase7 (0.005, 0.01 and 0.05) were also significantly different from that of anatase7 coating. After 6 hours, the speed up was1.4 times for PHF/anatase7 ratios of both 0.05 and 0.1. The second-order dye degradation rate coefficient was found to be significantly correlated ($P = 0.001$) with the PHF/anatase7 ratio, as shown in Figure 3-13.

3.2.5 Photocatalytic Inactivation of *Staphylococcus aureus*

The time dependent inactivation of *S. aureus* on photocatalytic and non-photocatalytic surfaces under fluorescent light is shown in Figure 3-14. There was 42% inactivation over 24 hours without light, which can be attributed to desiccation of *S. aureus* on a surface. Under visible light, on the SiO_2/rutile22 coating, there was 80% inactivation of *S. aureus*. Under visible light, on the photocatalytic coatings, there was 91% to 97% inactivation. The effect of PHF was most pronounced in the first 6 hours of the experiment. At this time, the concentrations of viable *S. aureus* remaining on the coatings of PHF/anatase7 nanocomposite were significantly lower than the remaining concentration on anatase7 (α=0.05). The nanocomposite at PHF/anatase7 ratios of 0.01 and 0.1 gave inactivation rates of 1.5× and 2.0× times the rate obtained with anatase7, respectively.

3.3 Discussion

3.3.1 Visible Light Photocatalysis

The anatase and rutile phases of TiO_2 are generally regarded as inactive under visible light. However, anatase and rutile with smaller crystallite size were found to be active in this study. Possible reasons for the observed visible light photocatalytic activity of rutile and anatase are the presence of dopants in the crystal lattice, sufficiently small crystallite size or stray UVA.

The XPS data suggested that rutile99, anatase7 and anatase15 powders exhibited high purity, whereas rutile22 contained 4.9 atomic% of aluminum and P25 contained 3.5 atomic% of silicon. The presence of impurity can exist as dopants or surface contaminants. Kim *et al.*[95] suggested that in aluminum (6–12 atomic%) doped TiO_2 film, peak at binding energy (Al bonding with Ti) at 530 eV was present. It was reported that

TiO_2 doped with aluminum usually exhibits an increase in band gap energy.[96] Neither of these phenomena was observed in our measurements based on XPS and UV/Vis measurement. This suggests that aluminum is present as surface contamination only and does not act as a dopant. The small amount of silicon present in P25 is also due to surface contamination. Yan *et al.*[97] indicated that TiO_2 doped with Si exhibited an increase of band gap energy. This was not observed in our study. The characterization studies (XPS, XRD and UV/Vis) indicated that rutile22, rutile99, anatase7 and anatase15 are dopant free, highly crystalline single phase photocatalyst, whereas P25 is dopant free, highly crystalline mixed phase photocatalyst. The observed visible light photocatalytic activity is not due to dopants in the crystal lattice of TiO_2.

The photocatalytic activity of rutile22, rutile99, anatase7, anatase15 and P25 differed widely. Rutile with crystallite size of 22 nm is the most active photocatalyst in this study, whereas rutile with crystallite size of 99 nm is the least active one. Rutile can adsorb a small portion of visible light, but was generally reported to be less active than anatase due to a relatively smaller band gap (3.0 eV), which cause rapid recombination of electron-hole pairs. Harada *et al.*[98] argued that as the size of rutile is less than 40 nm, the photocatalytic activity increases dramatically. This is due to combined effect of larger reactive surface area and shorter diffuse distance between the point of ejection of electrons to conduction band and the particle surface. Thus, the observed photocatalytic activity of rutile22 may be due to small crystallite size.

In order to test this hypothesis, the photocatalytic performance of rutile at different size was normalized at the same surface area basis by adjusting the concentration of rutile suspension. BET surface area measurement indicated that the ratio of specific

surface area of rutile22 to rutile99 rutile is about 50. Therefore the suspension concentration of rutile99 used in preparing the coating was increased to 5 wt%, as compared to concentration of rutile22 at 0.1%. The corresponding calculated coating thicknesses[6] were 0.48 μm for rutile22 and 23 μm for rutile99.

The micrograph in Figure 3-15 suggests that the crystallite is crucial in controlling surface coverage of photocatalyst. Under the same weight basis, as the crystallite size of TiO_2 increases, surface will be less covered by photocatalyst. Figure 3-15A indicates that the coating of rutile22 is uniform with high surface coverage of photocatalyst. Figures 3-15B and 3-15C show the appearance of a rutile99 coating is not completely covered with photocatalyst (less than 40%). Figures 3-15D and 3-15E indicate that the coating of rutile99 at higher dose gave complete surface coverage and much bigger rutile99 aggregates. As shown in Figure 3-16, dye degradation on less covered rutile99 surface (Rutile99 in the figure legend) resulted in the poorest performance. As the surface loading and, concomitantly, surface coverage increase, dye degradation performance also increase. Interestingly, rutile22 coating with smaller crystallite size and high surface coverage performed equally as well as rutile99 with larger crystallite size at 50-time higher dose. Figure 3-17 relates the dye degradation rate coefficient to the surface loading. This correlation is significant ($P<0.0001$). The dye degradation rate coefficient of rutile99 with 50 times higher surface loading is comparable to the rate coefficients of rutile22 and anatase7. Apparently, coatings with high surface coverage, even with a very thin layer, can contribute to highly active photocatalytic surfaces. Thus, the observed visible light photocatalytic activity in this study is not due to smaller

[6] The method to calculate thickness was described in Equation 2-1 in Chapter 2. v

crystallite size. Photocatalyst with smaller crystallite size is beneficial to construct thin coatings with high photocatalytic activity.

Some literature suggested that TiO_2 photocatalysis can take place even under ultralow UVA intensity (360 μW/m^2–100 mW/m^2).[99–101] The dye degradation experiment with optical filters suggested that rutile22 and anatase7 did utilize stray UVA, which contributed a quarter of the total photocatalytic activity. The rest of the total activity came from visible light.

Anatase, without any dopant, is generally reported in the literature to be inactive under visible light. In contrast, results of the present study indicated that anatase with crystallite sizes of 7 nm is able to utilize significant amount of visible light beyond 495 nm, whereas hardly uses visible light between 400 and 495 nm. Rutile with crystallite size of 22 nm is able to utilize visible light between 400 and 495 nm, whereas only use slight amount of visible light beyond 495 nm. This result contradicted many existed literature, which suggests that photon energy is a prerequisite for photocatalysis. Only when photon energy is high enough (≥3.2 eV), the electron hole pair can be generated and migrate to surface, reacting with other species. Nevertheless, the dye degradation experiment indicated that pure anatase and rutile phase of TiO_2 can utilize visible light for photocatalytic degradation of organic dye. One study conducted by Ariga *et al.*[30] synthesized a rutile (001) surface, of which the band gap is 2.3 eV (530 nm cut-off wavelength) in spite of its bulk band gap is 3.0 eV. The study by Ariga et al. was the first to investigate the photocatalytic reaction on a single crystal surface of TiO_2, instead of the bulk reaction, using scanning tunneling microscopy. The rutile22 used in the present study also exhibited photocatalytic activity under visible light (400–495 nm) even though

its bulk band gap is 3.02 eV (410 nm cut-off wavelength). Thus, it is possible that the surface band gap of rutile22 is much lower than its bulk band gap, allowing utilization of low photon energy in the visible range. Anatase7 is expected to have a much lower surface band gap, which allow it to use even lower photon energy (wavelength > 495 nm). Further study is required to identify the visible light photocatalytic activity of rutile22 and antase7.

3.3.2 Unified Model for the Effect of PHF on TiO_2 Photocatalysis

The enhancement effect of PHF on TiO_2 photocatalysis, under both UVA and visible light, is given in Table 3-12. The adsorption of PHF was estimated from isotherms for PHF adsorption on anatase with a crystallite size of 15 nm, as used in the experiment with UVA (Fig. 2-2), and anatase with a crystallite size of 7 nm, as used with visible light (Fig. 3-11). Interestingly, anatase7 (39.7 mg/g) exhibited much higher adsorption of PHF than anatase15 (7.2 mg/g) under the same pH. This can be attributed to much larger specific surface area of anatase7. Another possible reason is that the electrostatic attraction between anatase7 and PHF is much stronger than that between anatase15 and PHF. Further experiments to identify the IEP of anatase7 and anatase15 may help explain this differential adsorption effect.

As shown in Figure 3-18, the enhancement of TiO_2 photocatalysis by addition of PHF is highly correlated with the surface coverage of PHF on anatase. Notably, data obtained with two different sizes of anatase follow the same relationship.

3.4 Summary

- Photocatalytic performance of anatase and rutile coatings is influenced by the surface coverage.
- Most of the photocatalytic activity of rutile with a crystallite size of 22 nm is obtained with light below 500 nm.

- Anatase with a crystallite size of 7 nm can use light below 400 nm and above 500 nm, but cannot use light between 400 and 500 nm.
- Anatase visible light photocatalysis is effective for inactivating *Staphylococcus aureus*.
- The enhancement of anatase photocatalysis by addition of PHF is controlled by the surface coverage of PHF.

Table 3-1. Properties of photocatalysts employed in present research, as provided by manufacturers

Photocatalyst	Component	Manufacturer	Product Name	Primary Particle Size (nm)	Mass Density (g/cm^3)
Rutile22	Rutile	MKnano (Missisauga, Ontario, Canada)	MKN-TiO2-R050P	50	4.23
Rutile99	Rutile	Sigma Aldrich (St. Louis, MO)		N/A*	4.17
Anatase7	Anatase	MKnano	MKN-TiO2-C7	7	3.9
Anatase15	Anatase	Alfa Aesar (Ward Hill, MA)		5	3.9
P25	Mixed phase particles	Evonik Industries AG (Essen, Germany)	P25	N/A	4.26

*Not available in manufacturer's description

Table 3-2. Elemental composition of TiO_2

	Rutile22	Rutile99	Anatase7	Anatase15	P25
Ti %	12.6	16.5	17.1	16.2	17.9
O %	57.3	55.4	55.0	50.5	35.8
C %	25.2	28.1	27.9	33.3	42.8
Al %	4.9	0.0	0.0	0.0	0.0
Si %	0.0	0.0	0.0	0.0	3.5

Table 3-3. Binding energy (eV) of TiO_2

Element/ orbital	Rutile22	Rutile99	Anatase7	Anatase15	P25	NIST Database
Ti 2s	569	568	568	569	568	561
Ti 2p1/2	469	468	468	468	468	464.3–464.6
Ti 2p3/2	463	462	462	462	462	458.3–459.2
O 1s	534	533	533	533	533	529.7–530.2
C 1s	290	289	288	289	289	284.5–285.0
Al 2s	124	N/D*	N/D	N/D	N/D	116.2–121.0
Al 2p	79	N/D	N/D	N/D	N/D	72.0–76.7
Si 2s	N/D	N/D	N/D	N/D	158	149.3–154.6
Si 2p	N/D	N/D	N/D	N/D	107	98.0–104.0

* not detected by XPS

Table 3-4. BET specific surface area and calculated specific surface area based on mean crystallite size

	Rutile22	Rutile99	Anatase7	Anatase15	P25
BET specific surface are (m^2/g)	35	0.7	231	110	44
Calculated specific surface area (m^2/g)	66	15	200	95	56

Table 3-5. X-ray diffraction parameters used for calculation of mean crystallite size of P25, anatase and rutile

	Rutile22	Rutile99	Anatase7	Anatase15	P25
K: shape factor	0.9	0.9	0.9	0.9	0.9
λ: x-ray wavelength (Å)	1.54	1.54	1.54	1.54	1.54
B: line broadening in FWHM intensity (°)	0.45	0.153	1.210	0.618	0.391
b: line broadening in FWHM intensity caused by instrument (°)	0.07	0.07	0.07	0.07	0.07
2θ: 2×Bragg angle (°)	27.598	27.662	25.401	25.409	25.402
L: mean crystallite size (nm)	22	99	7	15	25

Table 3-6. Comparison of crystallite size in nanometers based on XRD and SEM

Technique	Rutile22	Rutile99	Anatase7	Anatase15	P25
XRD	22	99	7	15	25
SEM	23–28	97–280	16–25	21–59	30–47

Table 3-7. Band gap of TiO_2

	Rutile22	Rutile99	Anatase7	Anatase15	P25
Cut off wavelength (nm)	410	418	385	386	407
Band gap energy (eV)	3.02	2.97	3.22	3.21	3.05

Table 3-8. Comparison of first-order fits and second-order fits to photocatalytic dye degradation data*

Treatment	First-Order Reaction Kinetics		Second-Order Reaction Kinetics		1st-order ≠ 2nd-order
	Equation	R^2	Equation	R^2	P
Rutile22	y=-0.1311x-0.0968	0.98	y=0.352x+0.8244	0.99	0.46
Rutile99	y=-0.0015x-0.0249	0.21	y=-0.0026x+1.0354	0.50	0.41
Anatase7	y=-0.0813x-0.0184	0.99	y=0.1485x+0.919	0.95	0.08
Anatase15	y=-0.0765x-0.0893	0.95	y=0.1342x+1.0328	0.98	0.32
P25	y=-0.0457+0.0265	0.99	y=0.0611x+0.949	0.98	0.46

* 1st-order: y is ln c/c_0; 2nd-order: y is c_0/c

Table 3-9. Optical properties of filter FGL400*

	Range of Wavelength (nm)		
	200–380	380–400	400–1800
%Transmission	0	<10	90

* Thorlabs (Newton, NJ)

Table 3-10. Optical properties of filter FGL495*

	Range of Wavelength (nm)		
	200–470	470–495	495–1800
%Transmission	0	<50	90

* Thorlabs (Newton, NJ)

Table 3-11. Relative activity of photocatalysts under filtered light

	Rutile22		Anatase7	
	%Dye degradation*	Relative activity**	%Dye degradation*	Relative activity**
Neutral filter	51	100	46	100
400 nm cut-off filter	40	78	36	78
495 nm cut-off filter	8	16	34	74

* after 12 hours

** as percent of the activity with neutral filter

Table 3-12. Comparison of enhancement ratio* of PHF/anatase to anatase alone under UVA and visible light

	UVA			Visible light			
PHF/anatase ratio**	0.005	0.01	0.02	0.005	0.01	0.05	0.1
Estimated Γ (mg PHF/g anatase)***	4.7	7.0	7.1	5.0	9.6	22	31
Surface coverage of PHF to anatase (%)	3.1	4.7	4.7	1.6	3.0	6.8	9.8
Enhancement ratio	1.1	1.8	1.9	1.7	1.9	2.5	3.1

* The enhancement ratio (E) was calculated from:

$$\mathrm{E} = \frac{k_n' - k_c'}{k_a' - k_c'} \qquad (3\text{-}13)$$

where k_n' is the second order rate coefficient with the PHF/anatase nanocomposite, k_a' is the second order rate coefficient with anatase and k_c' is the second order rate coefficient with non-photocatalytic surface.

** Anatase with a crystallite size of 15 nm was used in the experiments under UVA, whereas anatase with a crystallite size of 7 nm was used in the experiments under visible light

*** Γ is estimated from the isotherms in Figures 2-2 and 3-11 for a suspension pH of 6.

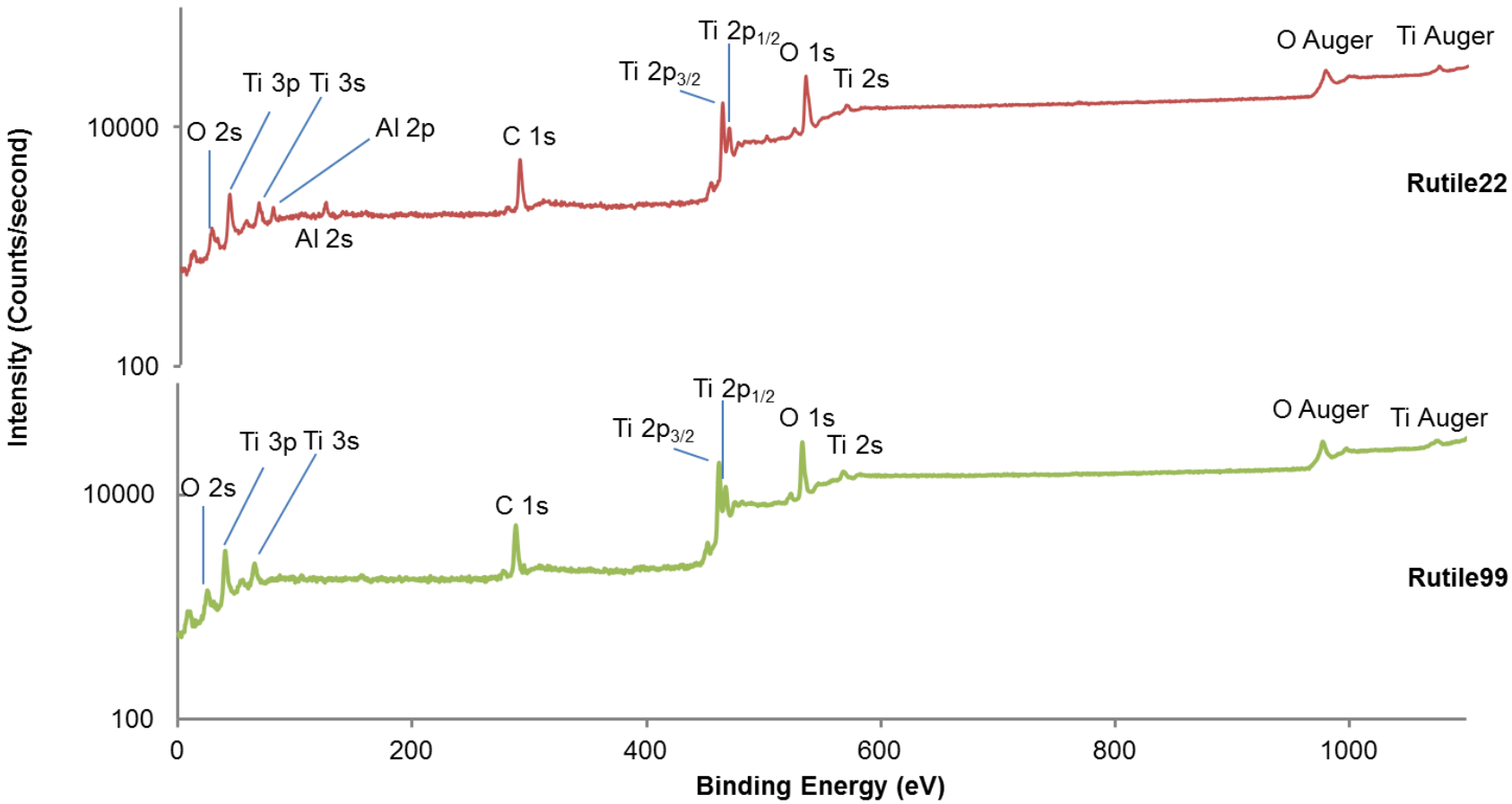

Figure 3-1. XPS spectrum of TiO_2 powders

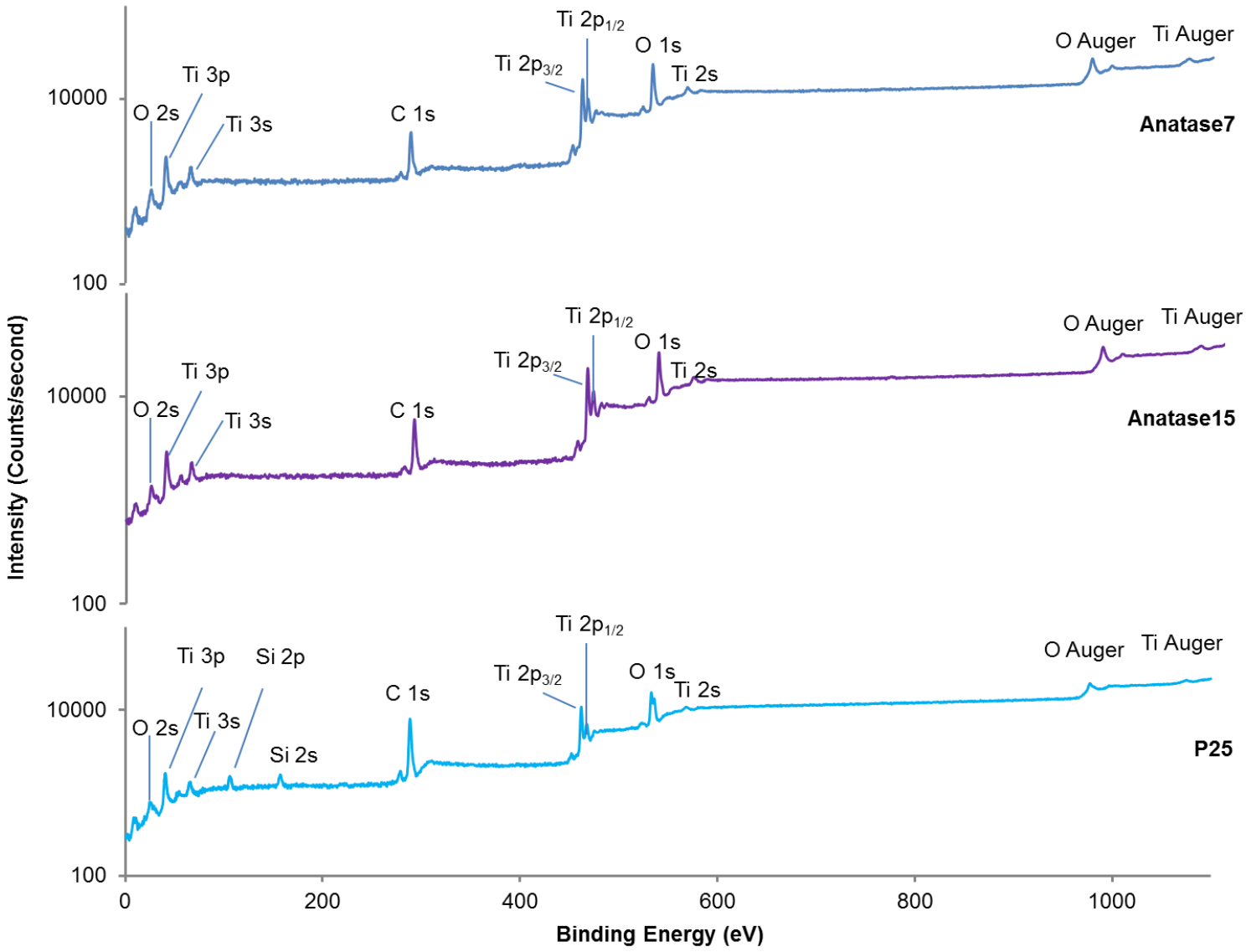

Figure 3-1. continued

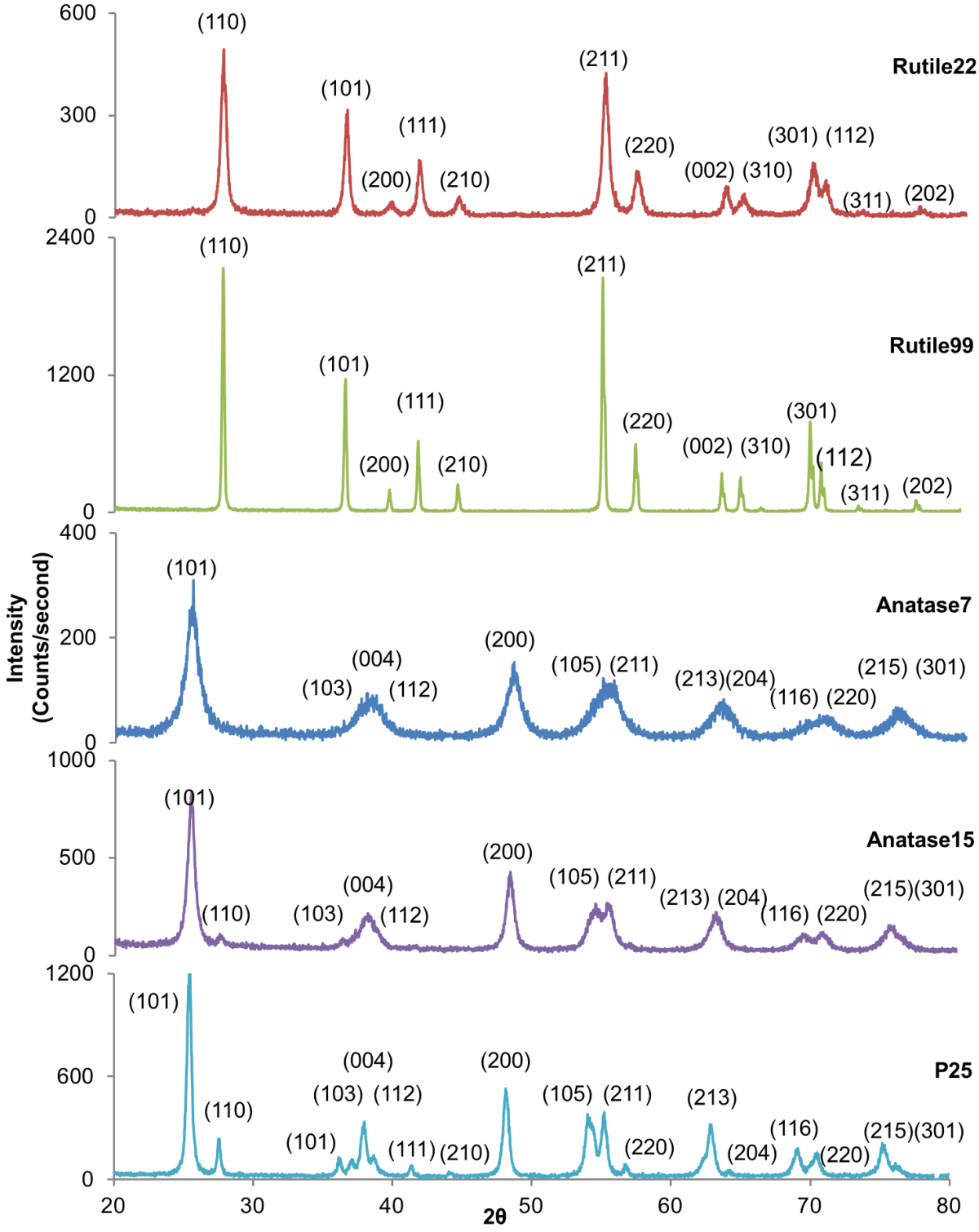

Figure 3-2. X-ray diffraction pattern of TiO_2

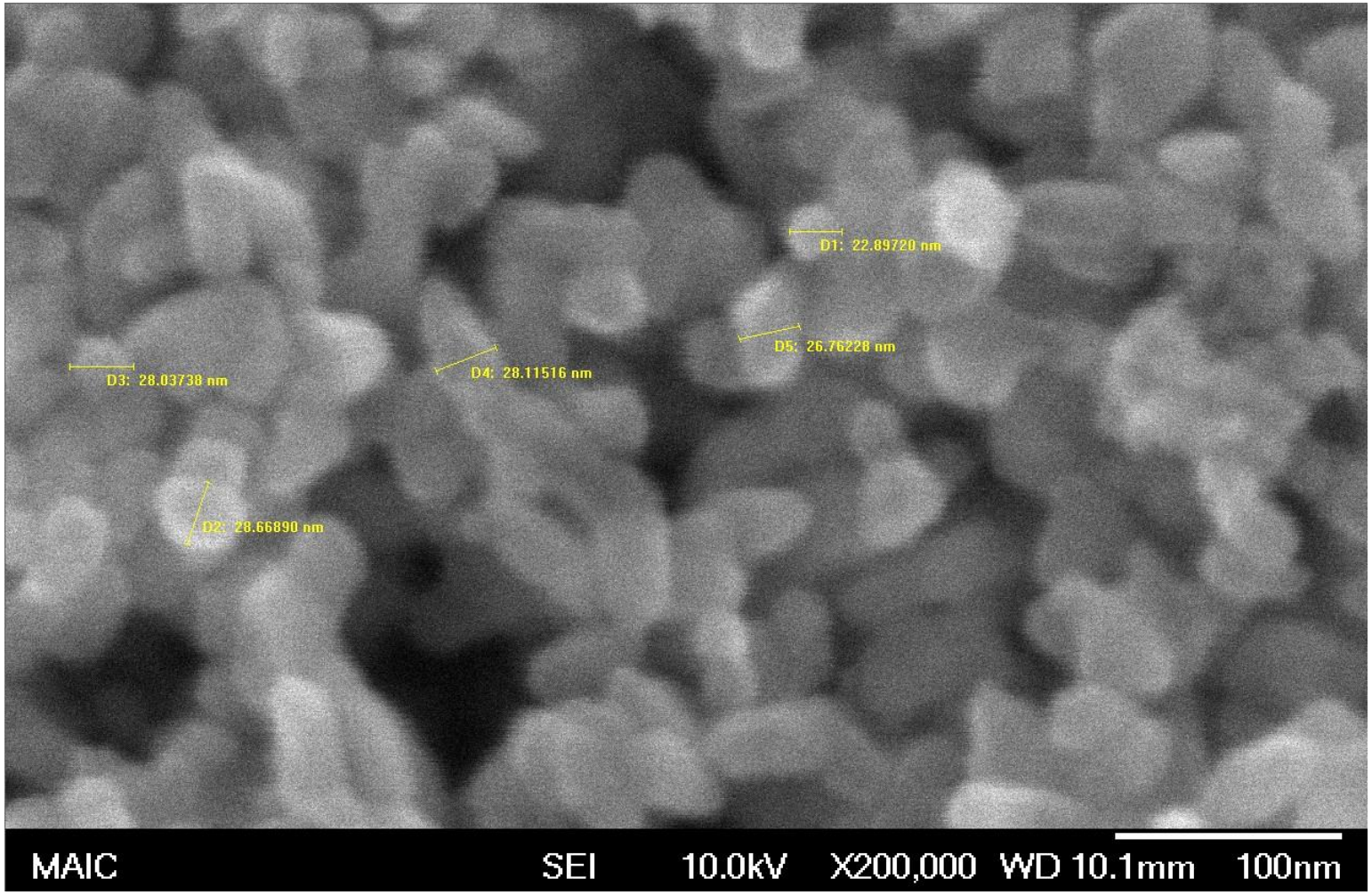

A

Figure 3-3. Scanning electron micrographs of TiO_2 powders. A) Rutile22. B) Rutile99. C) Anatase7. D) Anatase22. E) P25

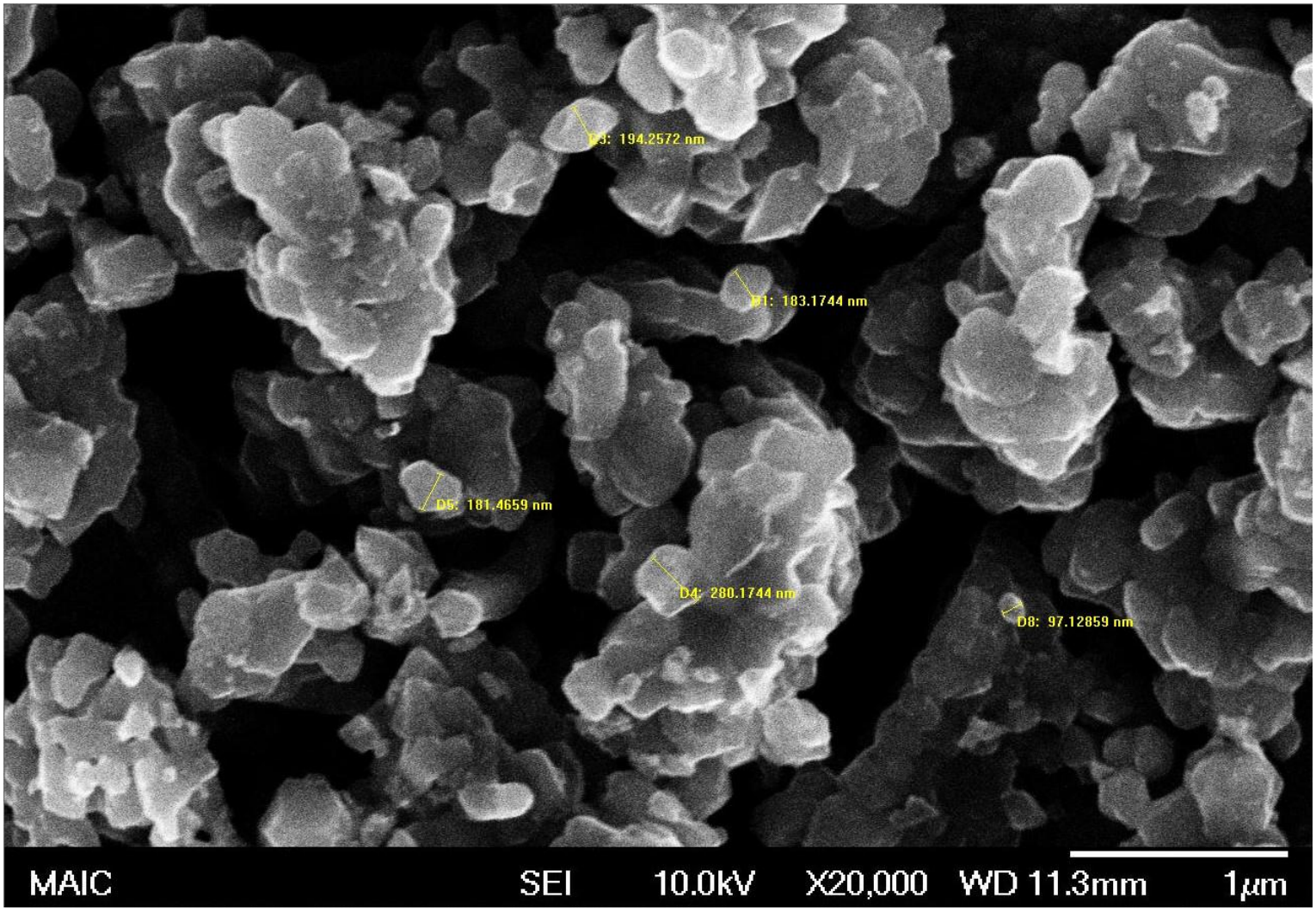

B

Figure 3-3. Continued

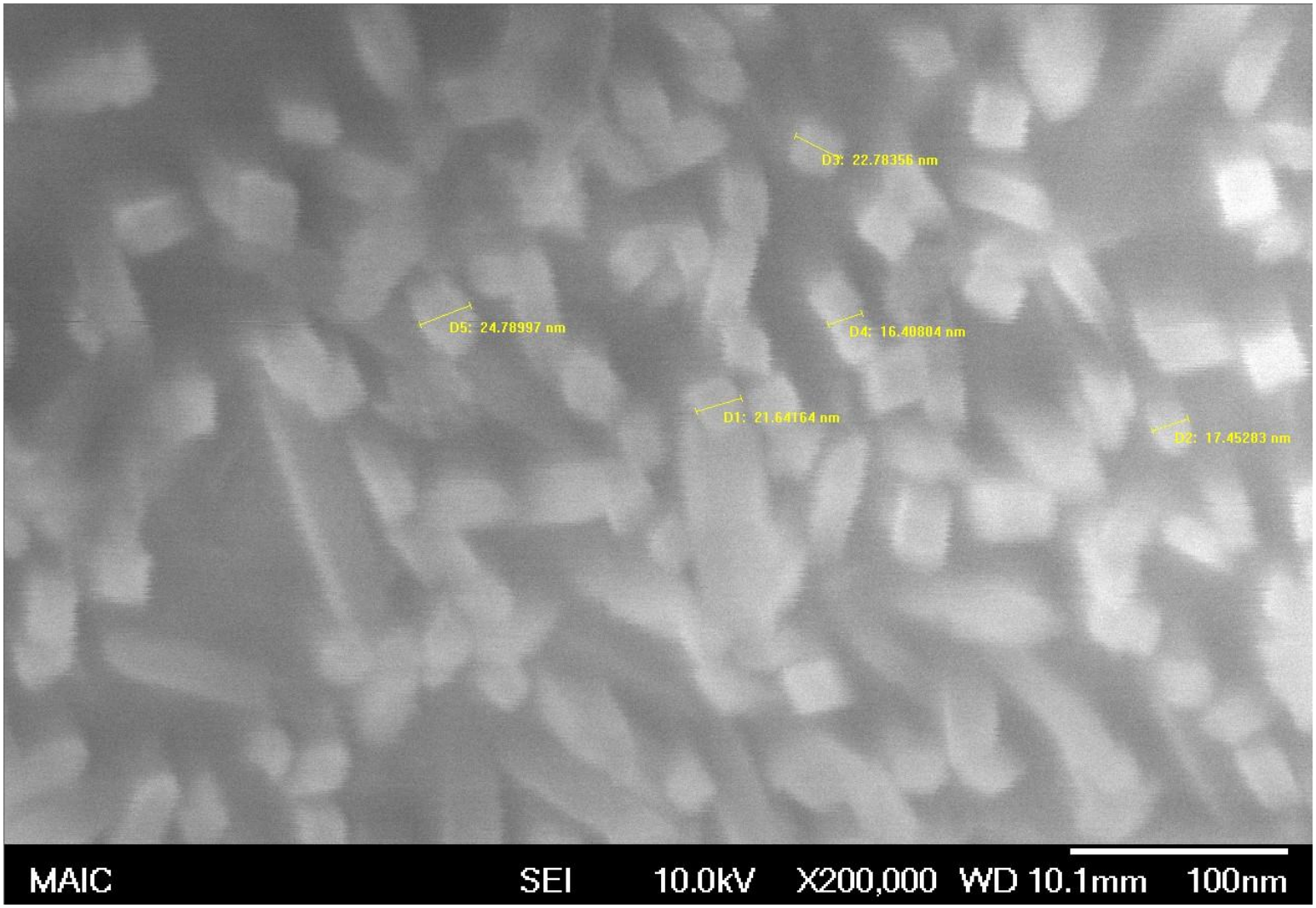

C

Figure 3-3. Continued

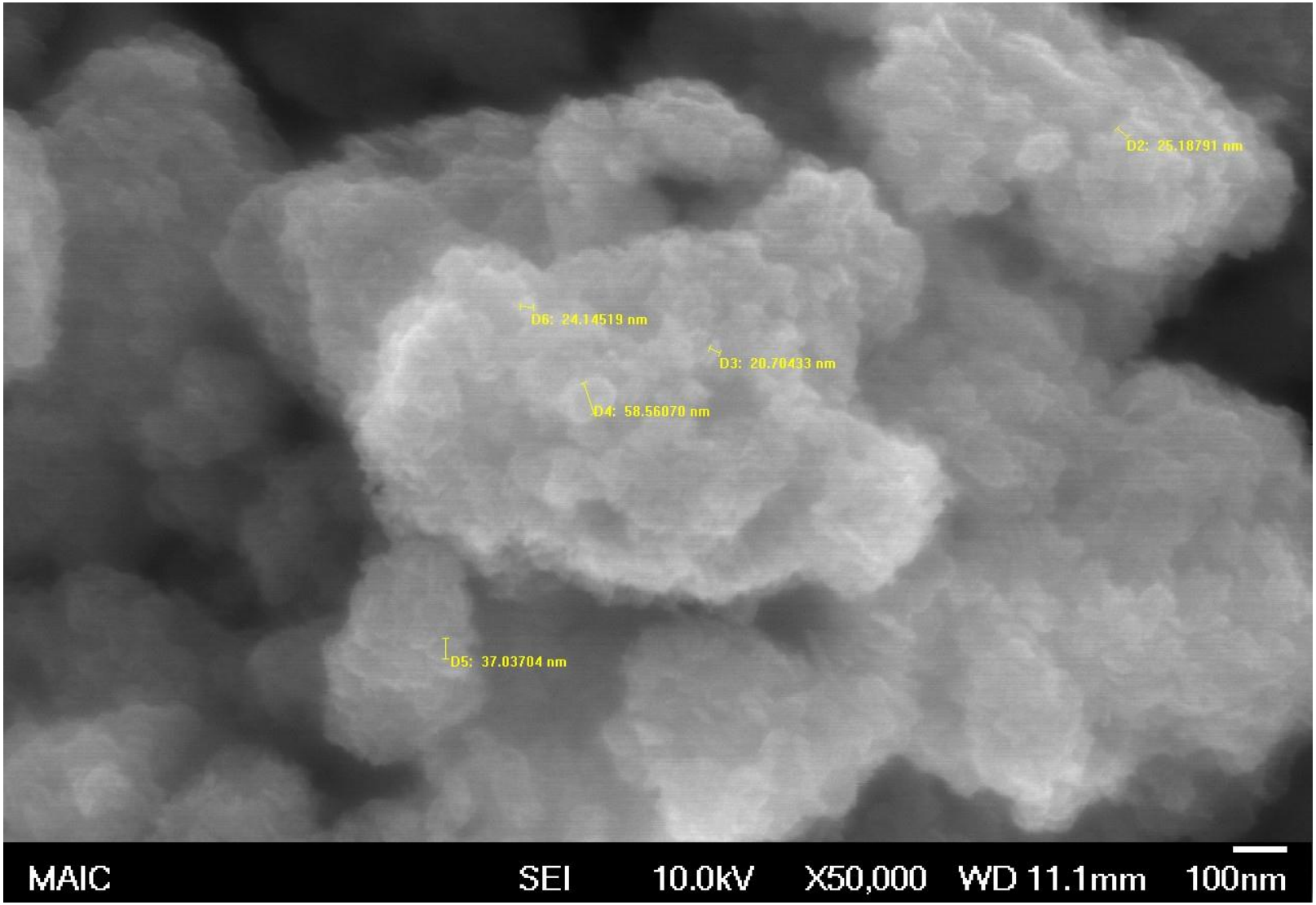

D

Figure 3-3. Continued

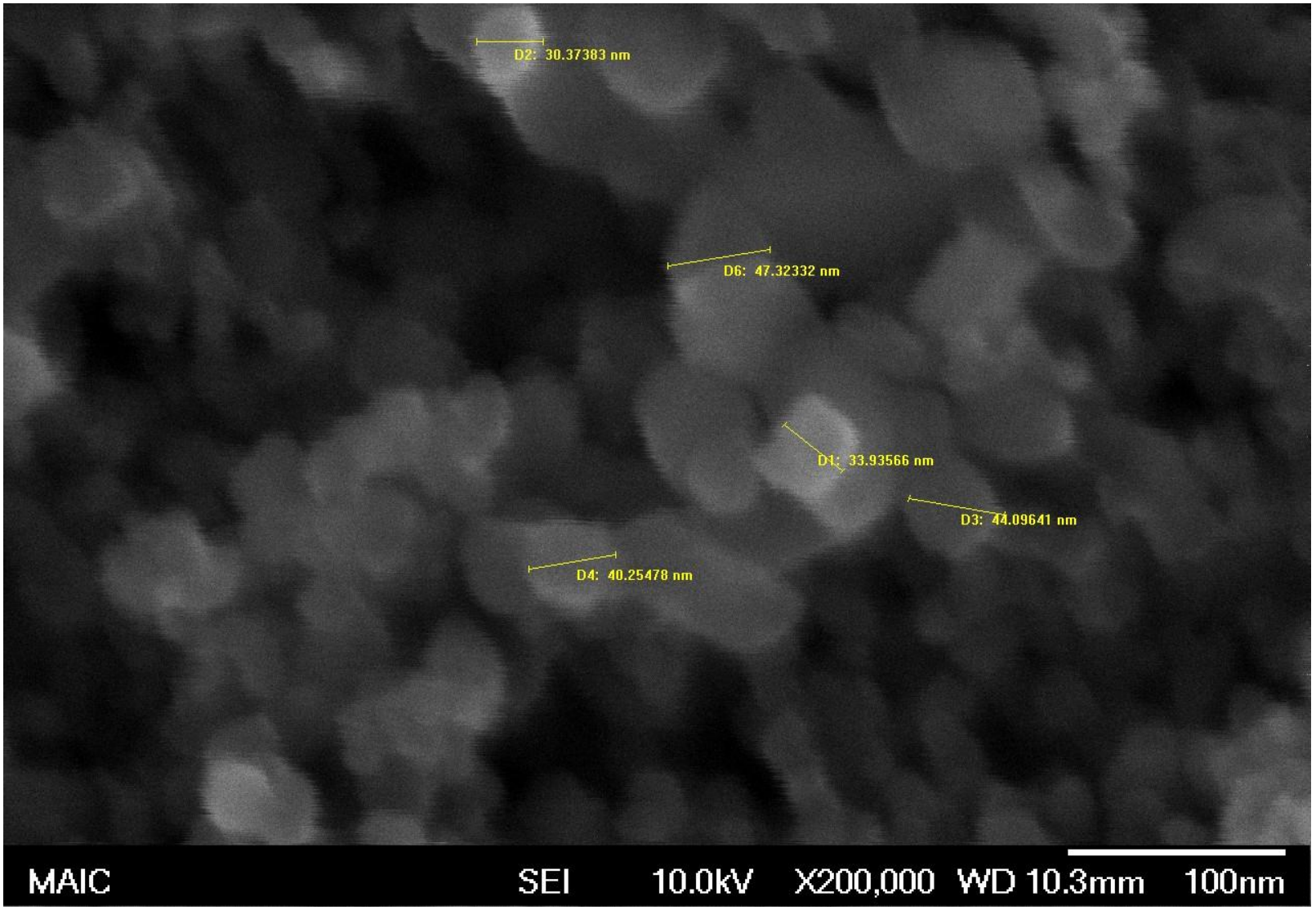

E

Figure 3-3. Continued

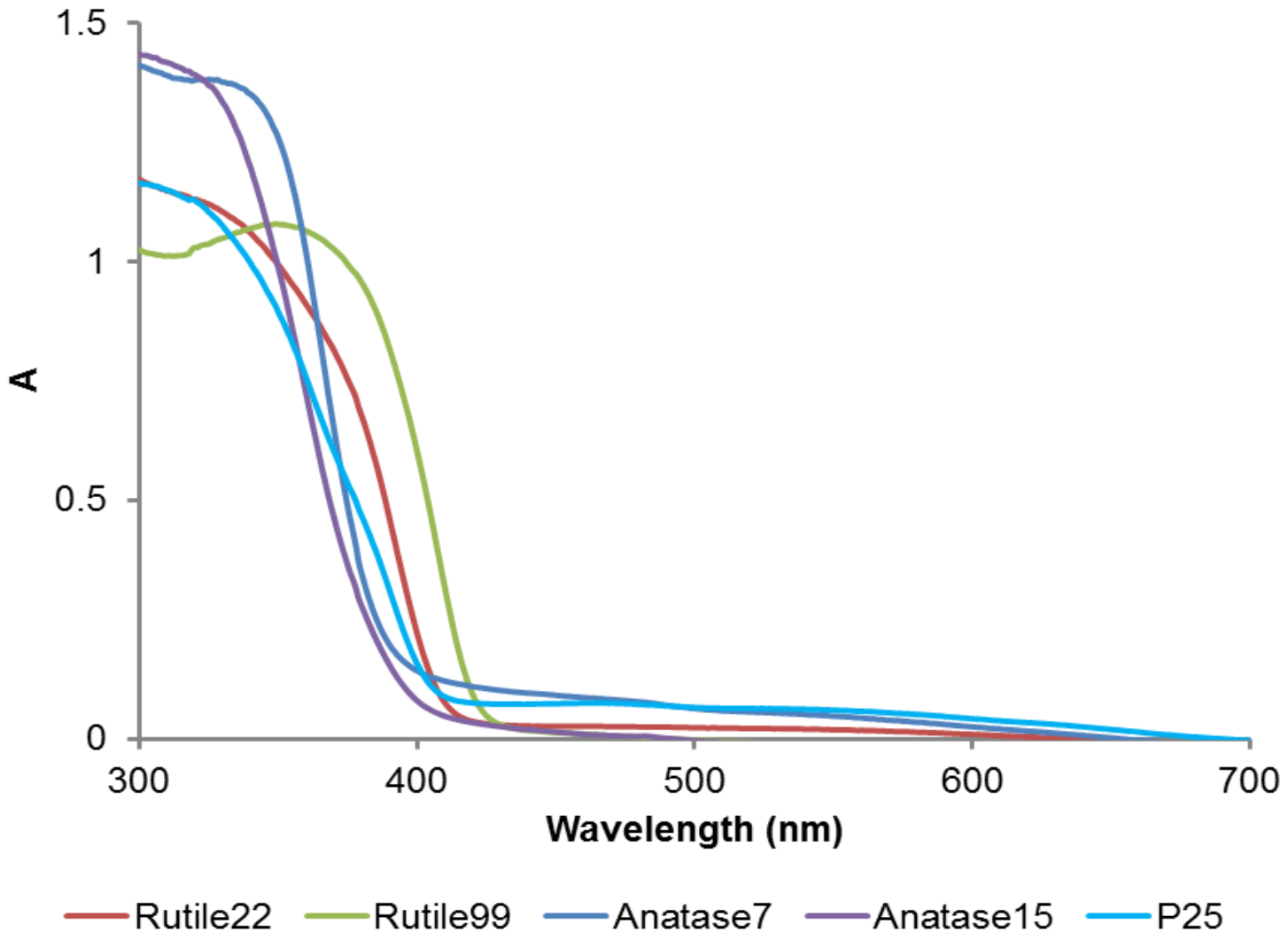

Figure 3-4. Absorbance spectrum of TiO_2 coating made from 1 wt% suspension. A white Teflon plate was used as reference

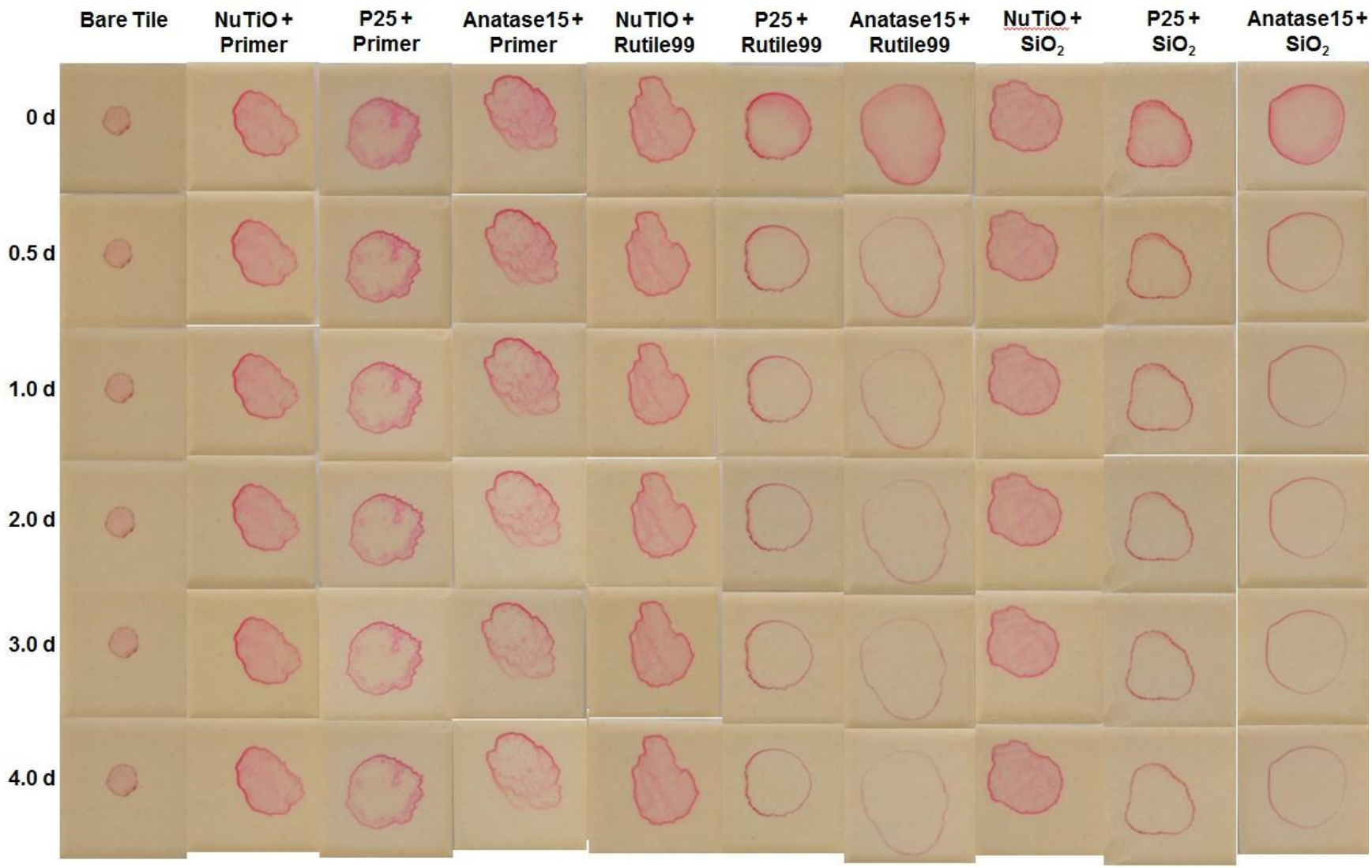

Figure 3-5. Screening of alternative photocatalysts for visible light photocatalysis (Visible light irradiance = 2 W/m^2, UVA irradiance = 0.01 W/m^2). Photos were taken with a Nikon D90 with AF-S DX NIKKOR 35mm f/1.8G lens using a SB-400 flash at 90° to horizontal

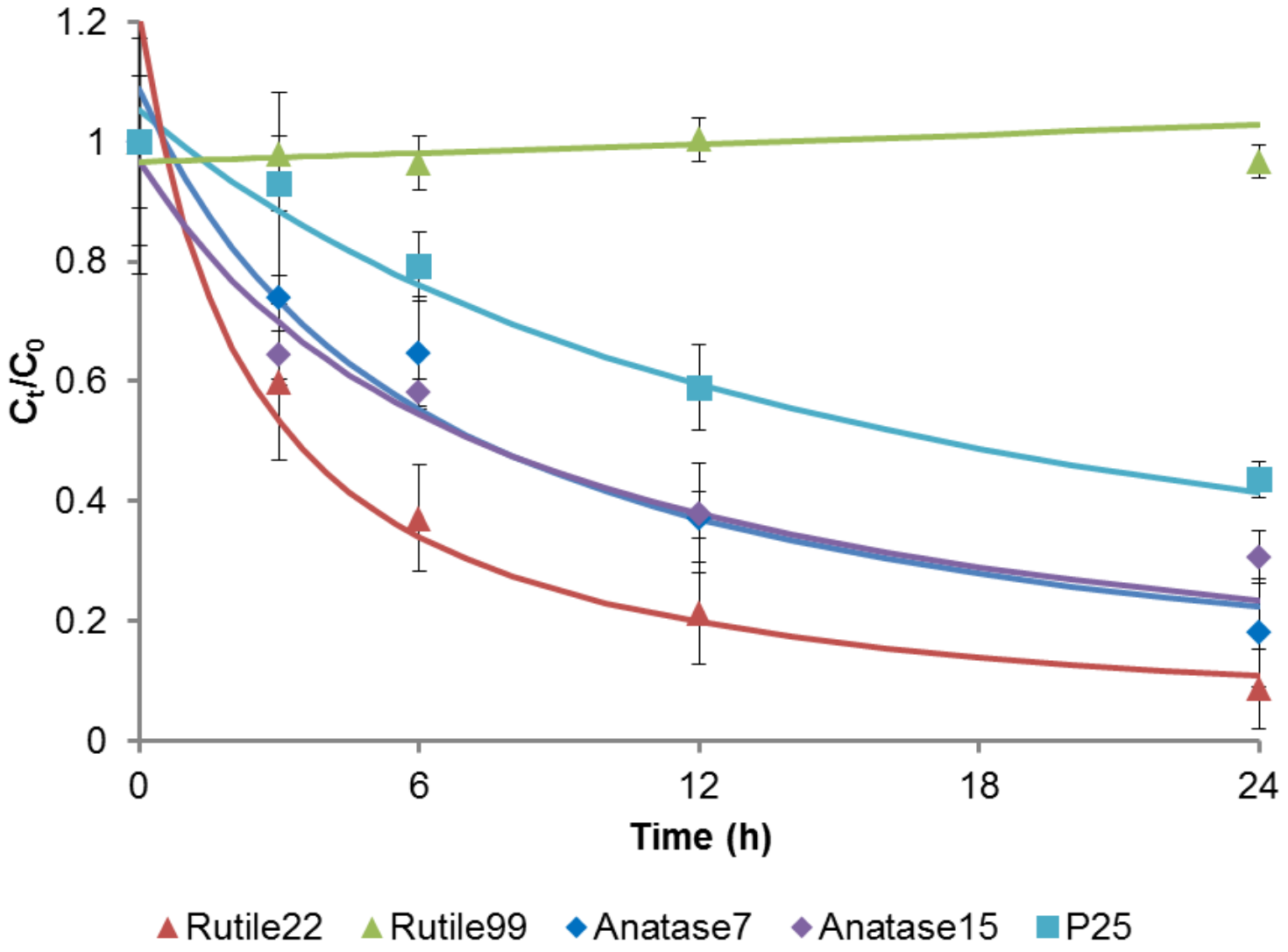

Figure 3-6. Dye degradation on coating made from TiO_2 with different phase and crystallite size under visible light (2 W/m^2). Model fits based on second order reaction kinetics

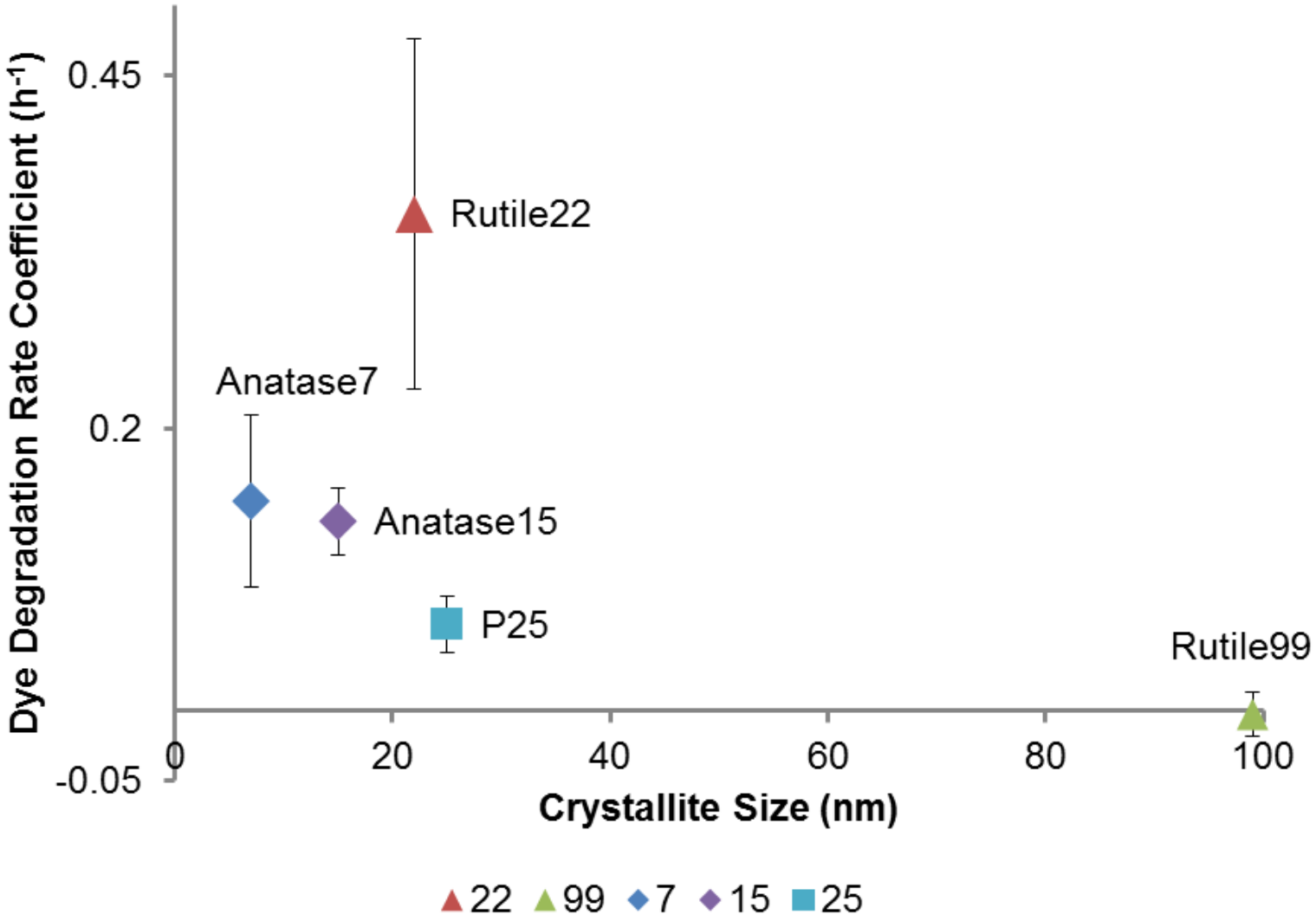

Figure 3-7. Comparison of the second order dye degradation rate coefficient on TiO_2 coatings under visible light (2 W/m^2) (α=0.05). Error bars represent a 95% confidence interval

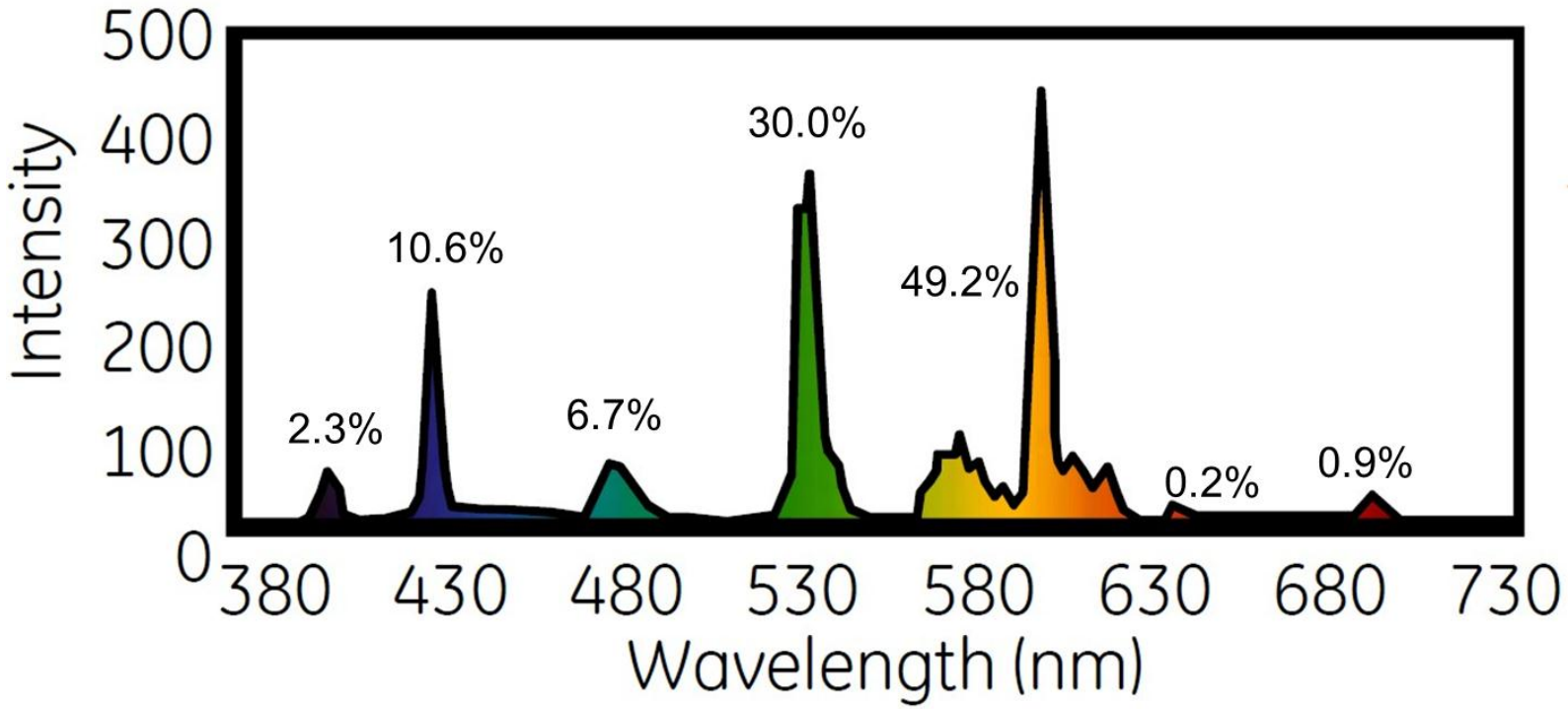

Figure 3-8. Fluorescent lamp spectra for General Electric model T8 Ultramax F28T8-SPX41

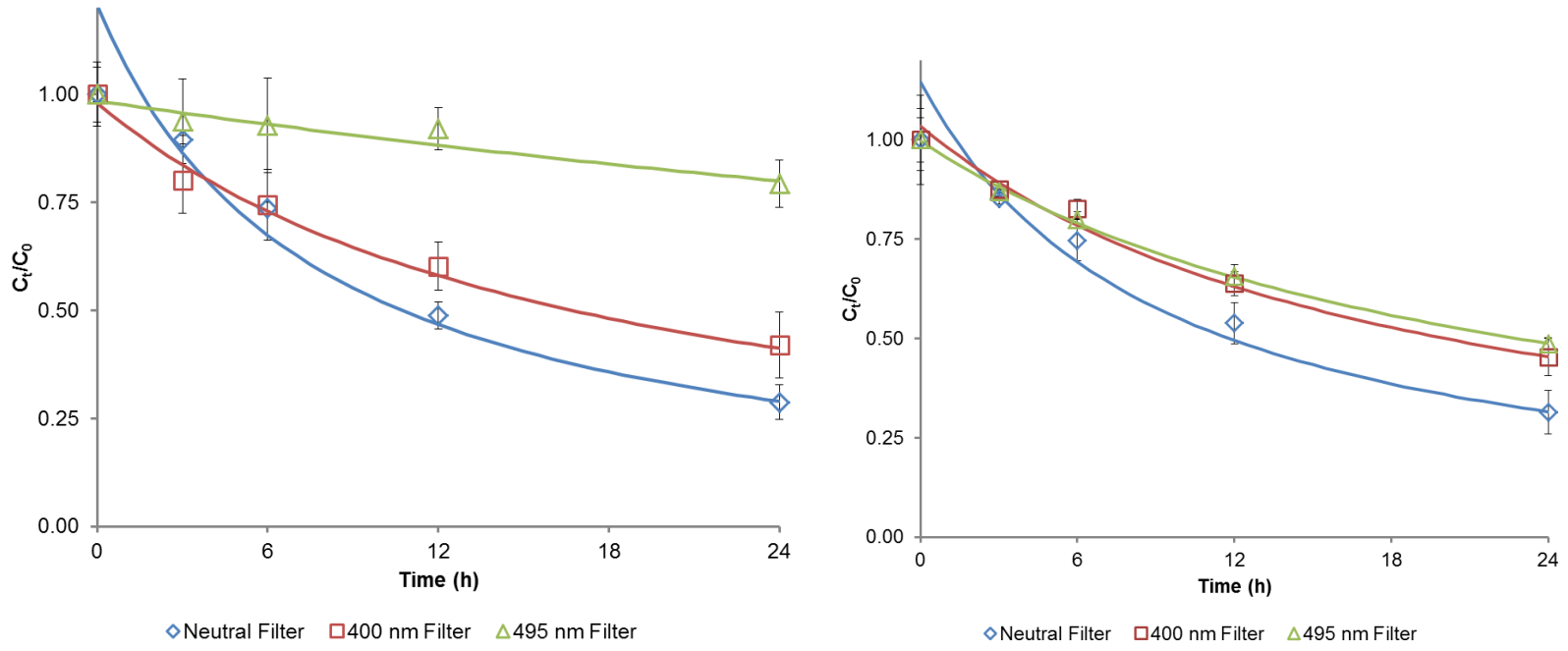

Figure 3-9. Dye degradation on two-layer coatings under visible light (1.5 W/m^2) with neutral or cut-off optical filters. A thin polystyrene Petri dish cover with 90% transmission above 300 nm was used as a neutral filter. A) Rutile22 coating. B) Anatase7 coating

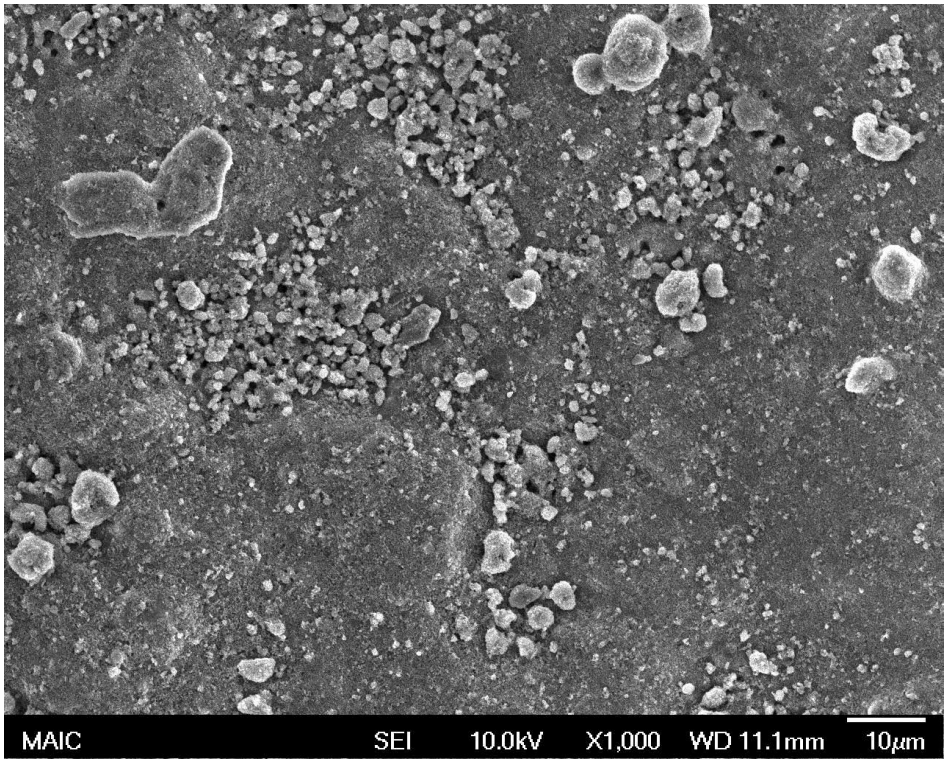

A

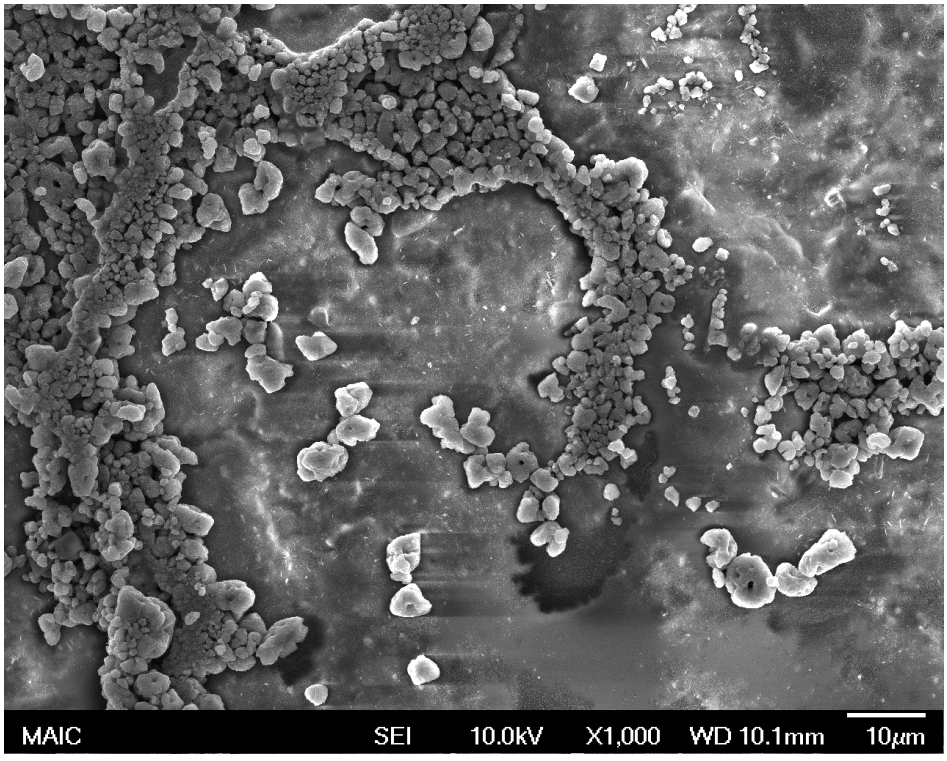

B

Figure 3-10. Appearances of two-layer coating. A) Rutile22 coating. B) Anatase7 coating

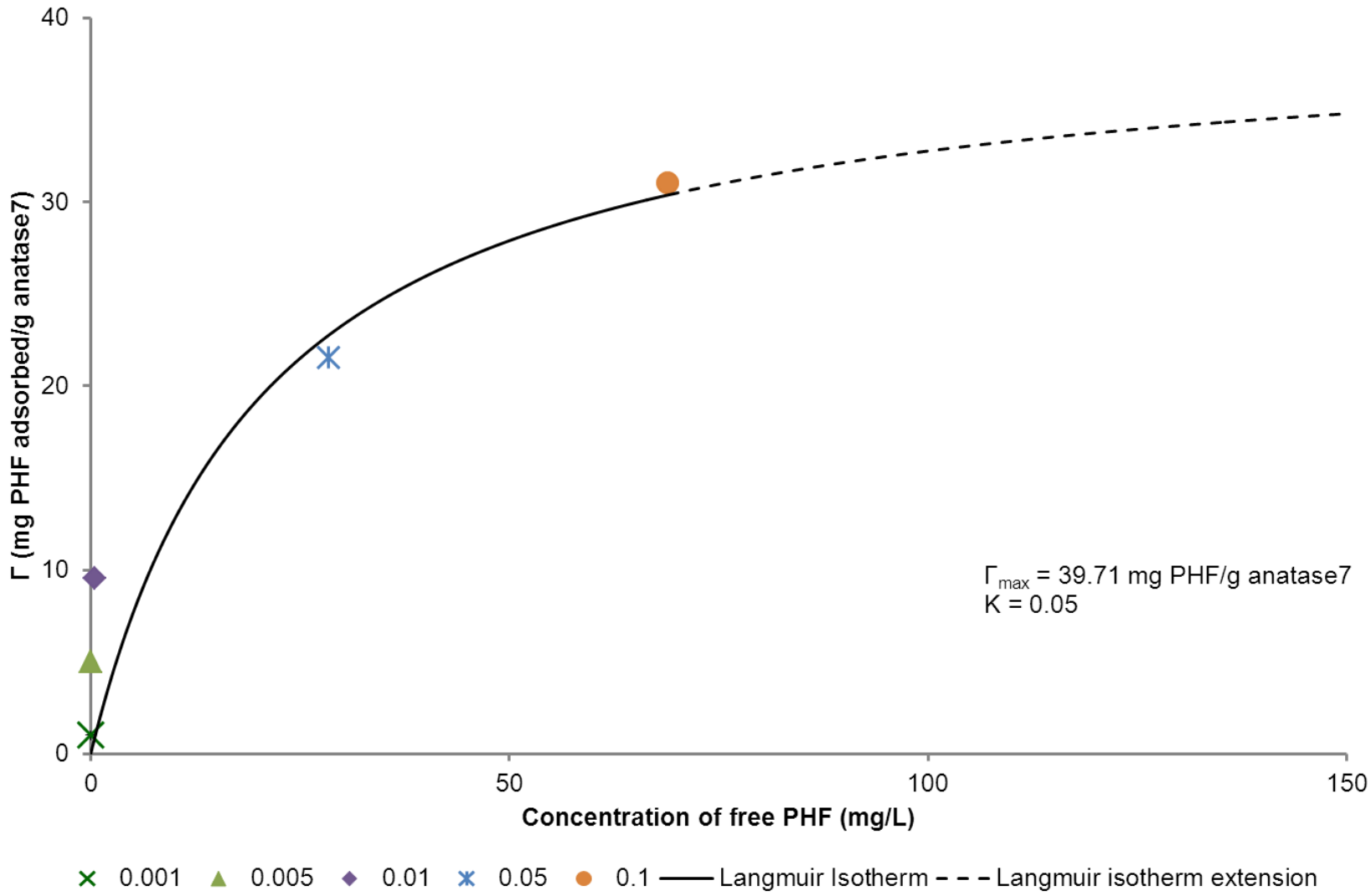

Figure 3-11. Langmuir isotherm for adsorption of PHF onto anatase7 at pH 6 and 25°C. The PHF to anatase ratios were 0.001, 0.005, 0.01, 0.05 and 0.1.

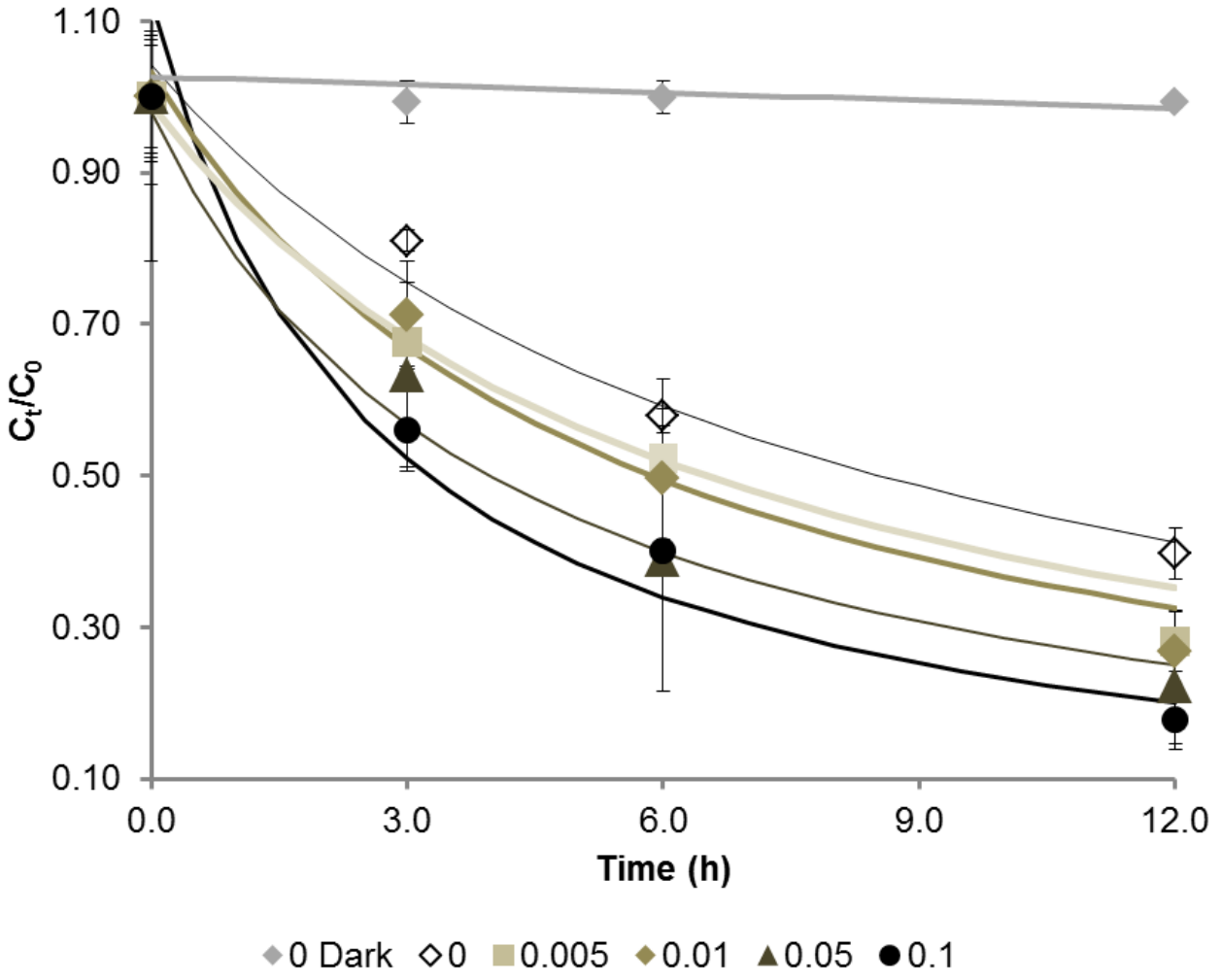

Figure 3-12. Time dependent dye degradation on two-layer coating with rutile22 as bottom coat and PHF/anatase7 as top coat. PHF/anatase7 ratios were 0, 0.005, 0.01, 0.05 and 0.1. Error bars represent ± 1.0 SD. Second-order model fits are shown.

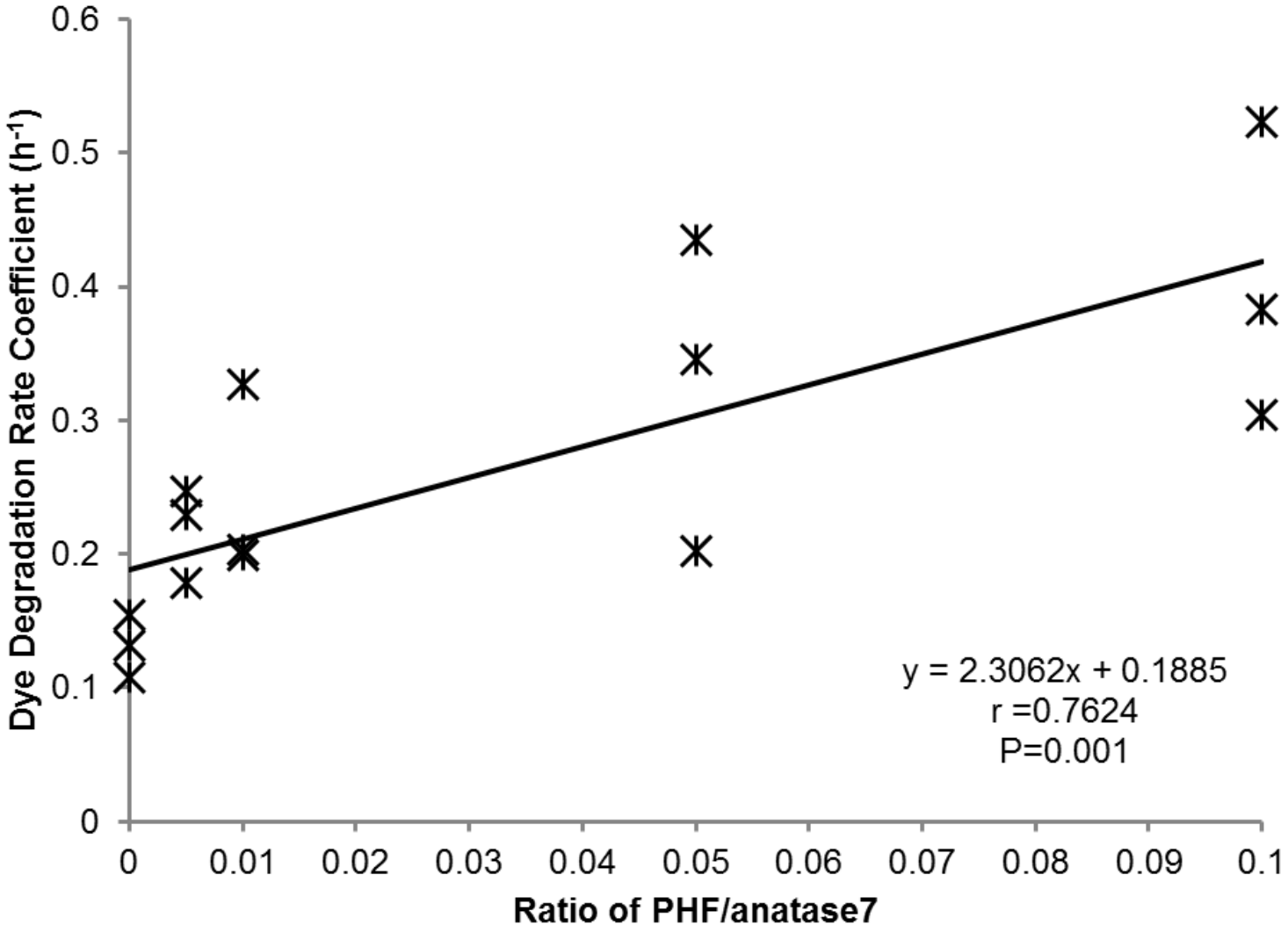

Figure 3-13. Comparison of second order dye degradation rate coefficients on two-layer coatings with rutile22 as bottom coat and PHF/TiO_2 (anatase7) nanocomposite at different weight ratios as top coat

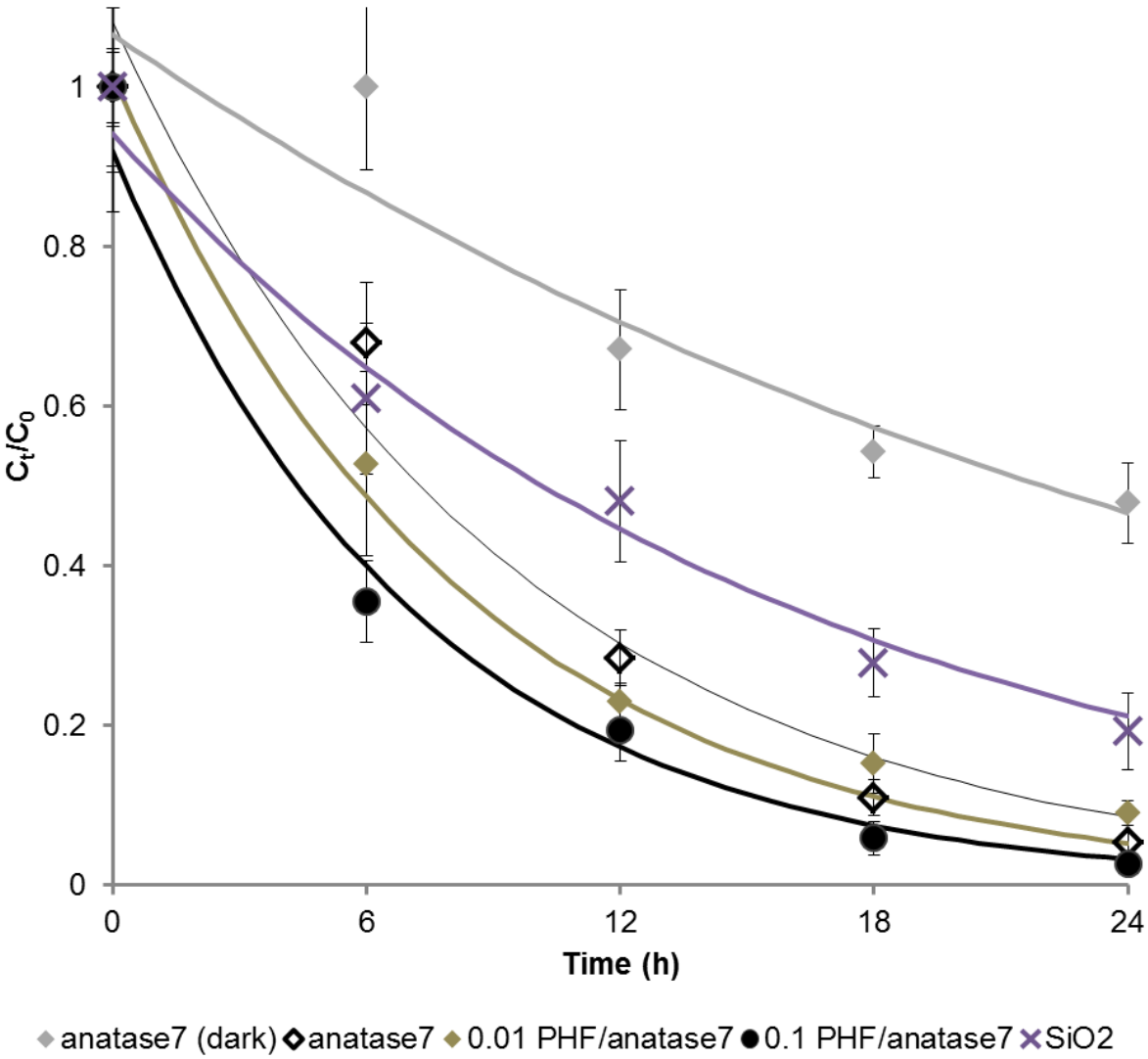

Figure 3-14. Time dependent *S. aureus* inactivation on two-layer coating system with rutile22 as bottom coat. Top coats were anatase7 (dark), anatase7, PHF/anatase7 weight ratios of 0.01 or 0.1 and SiO_2

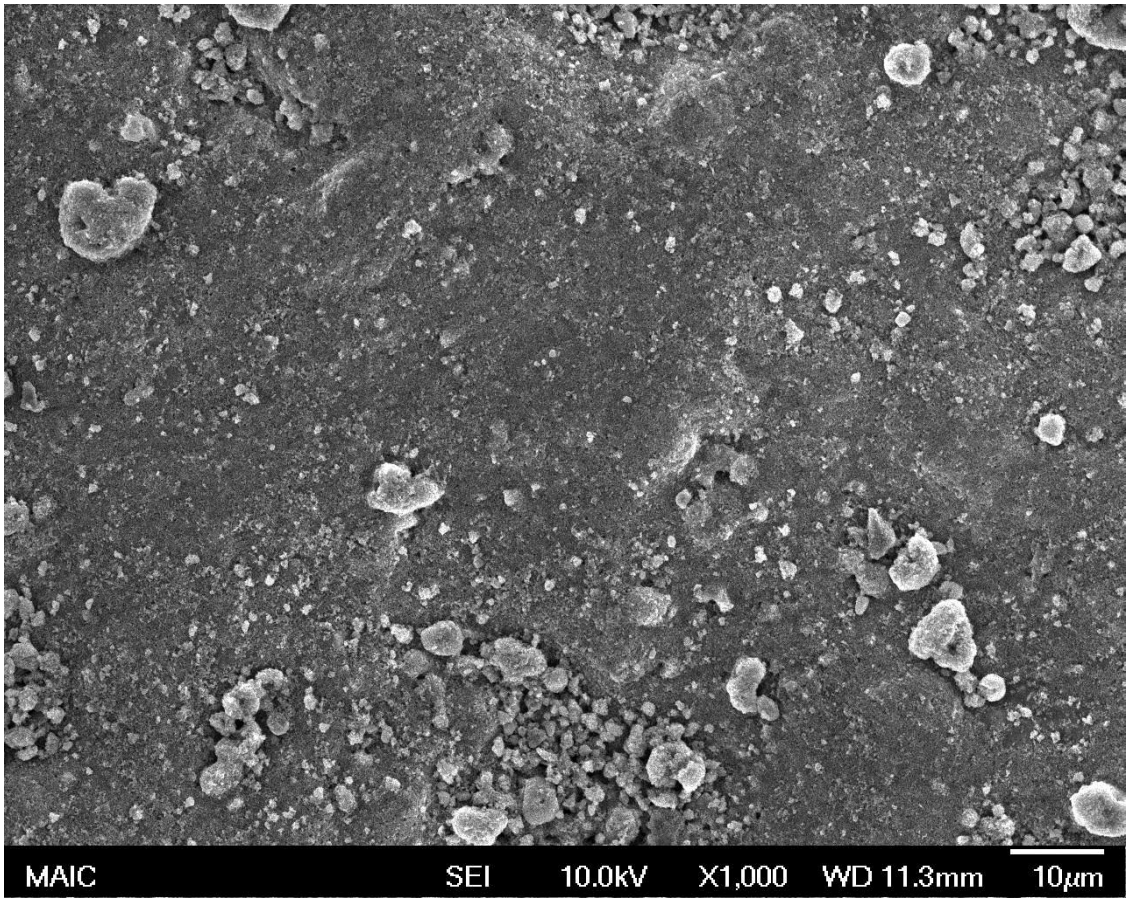

A

Figure 3-15. Coating appearance rutile22 and rutile99 at different surface loadings. A) 128 μg/cm^2 of rutile22. B) 128 μg/cm^2 of rutile99. C) 128 μg/cm^2 of rutile99 at higher magnification. D) 1280 μg/cm^2 of rutile99. E) 6400 μg/cm^2 of rutile99

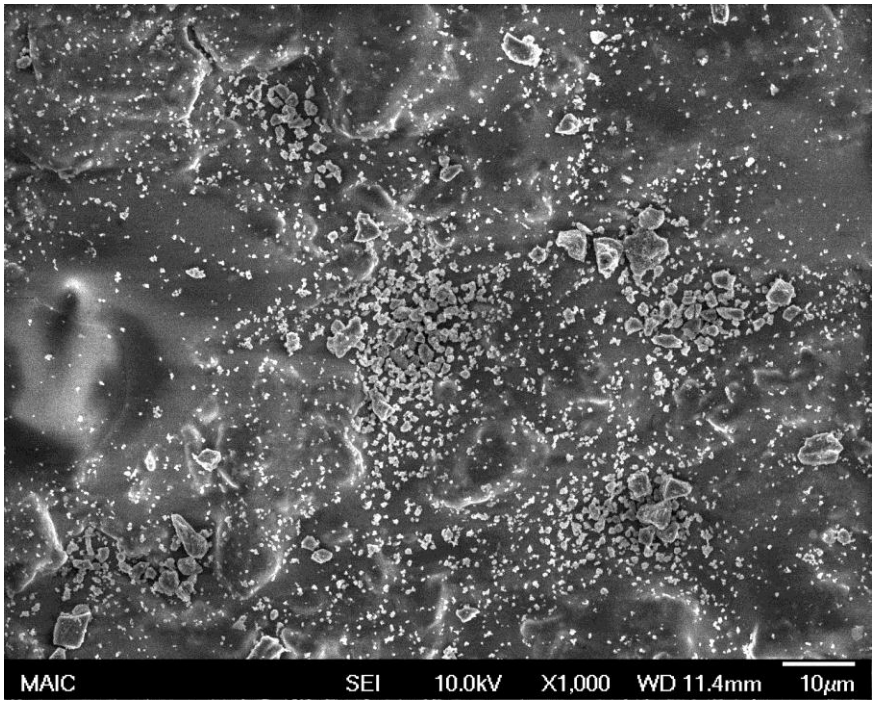

B

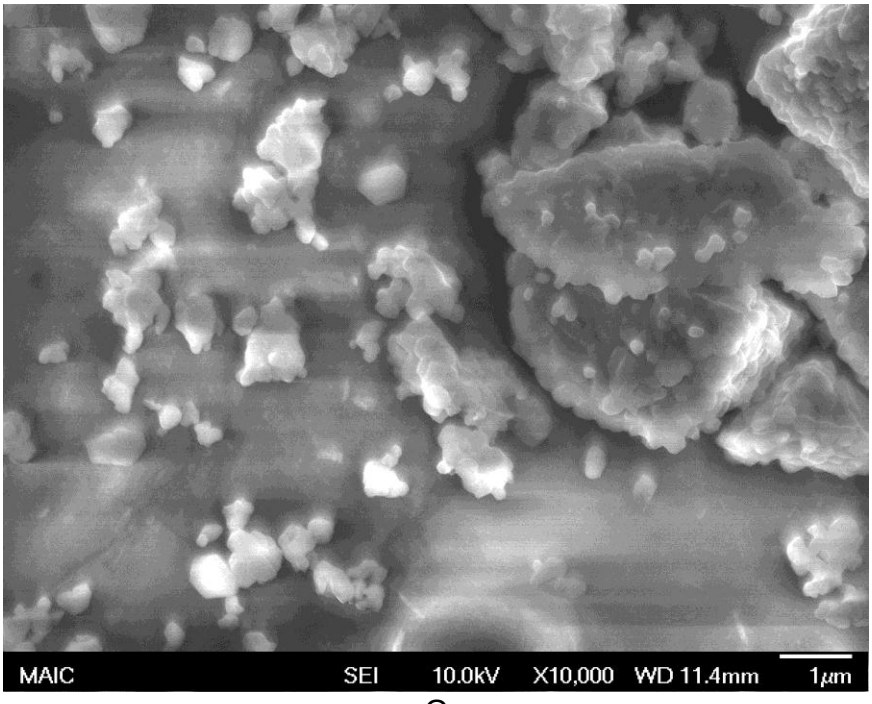

C

Figure 3-15. continued.

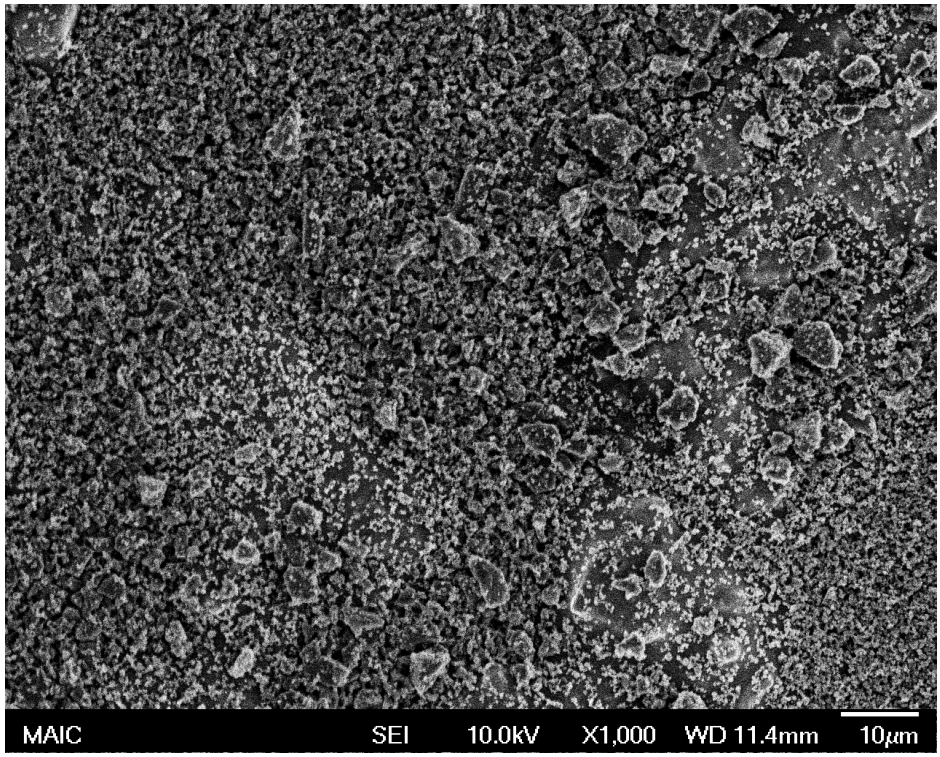

D

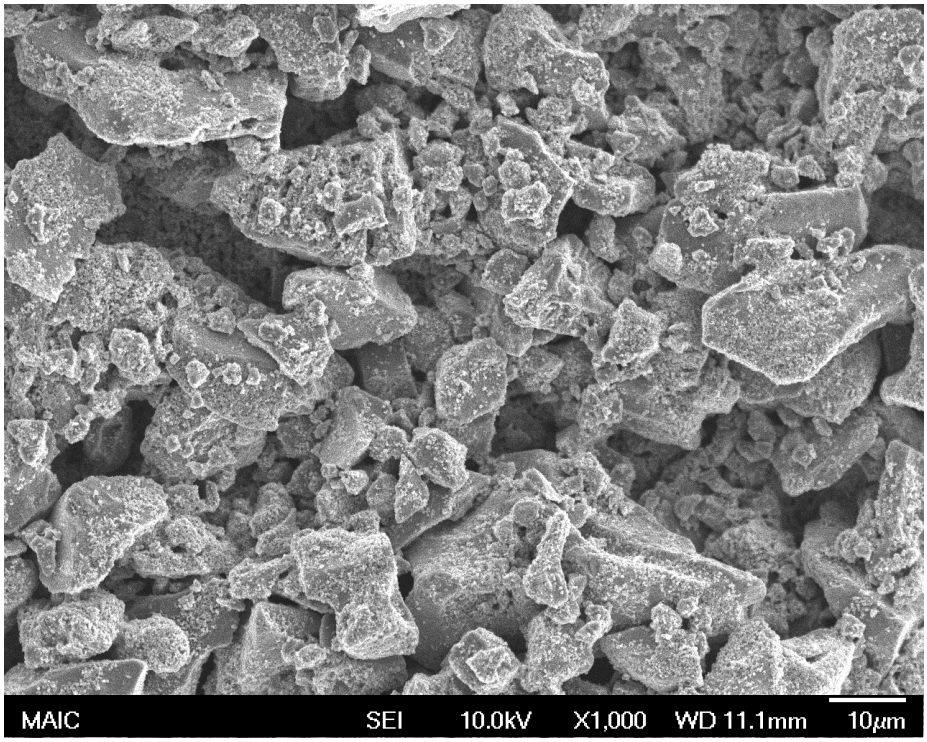

E

Figure 3-15. continued.

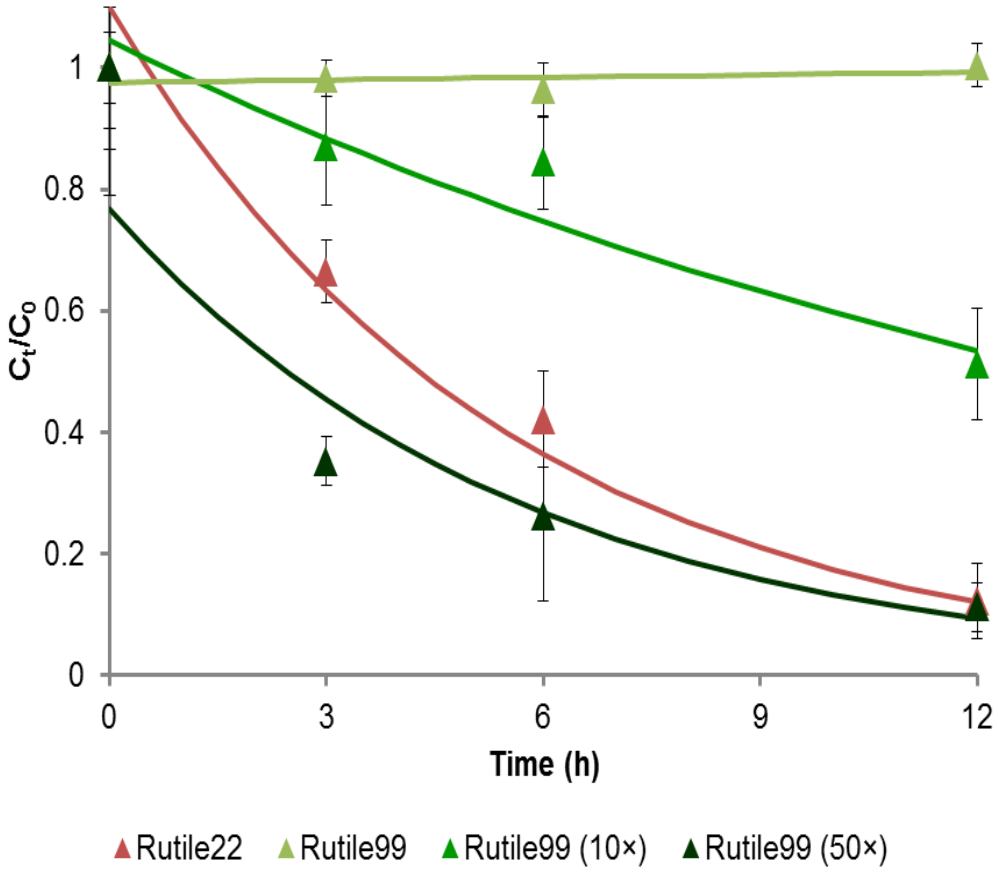

Figure 3-16. Time dependent dye degradation on rutile22 at the reference surface loading of 128 µg/cm^2, rutile99 at the reference loading, rutile99 at 10× reference loading and rutile99 at 50× reference loading

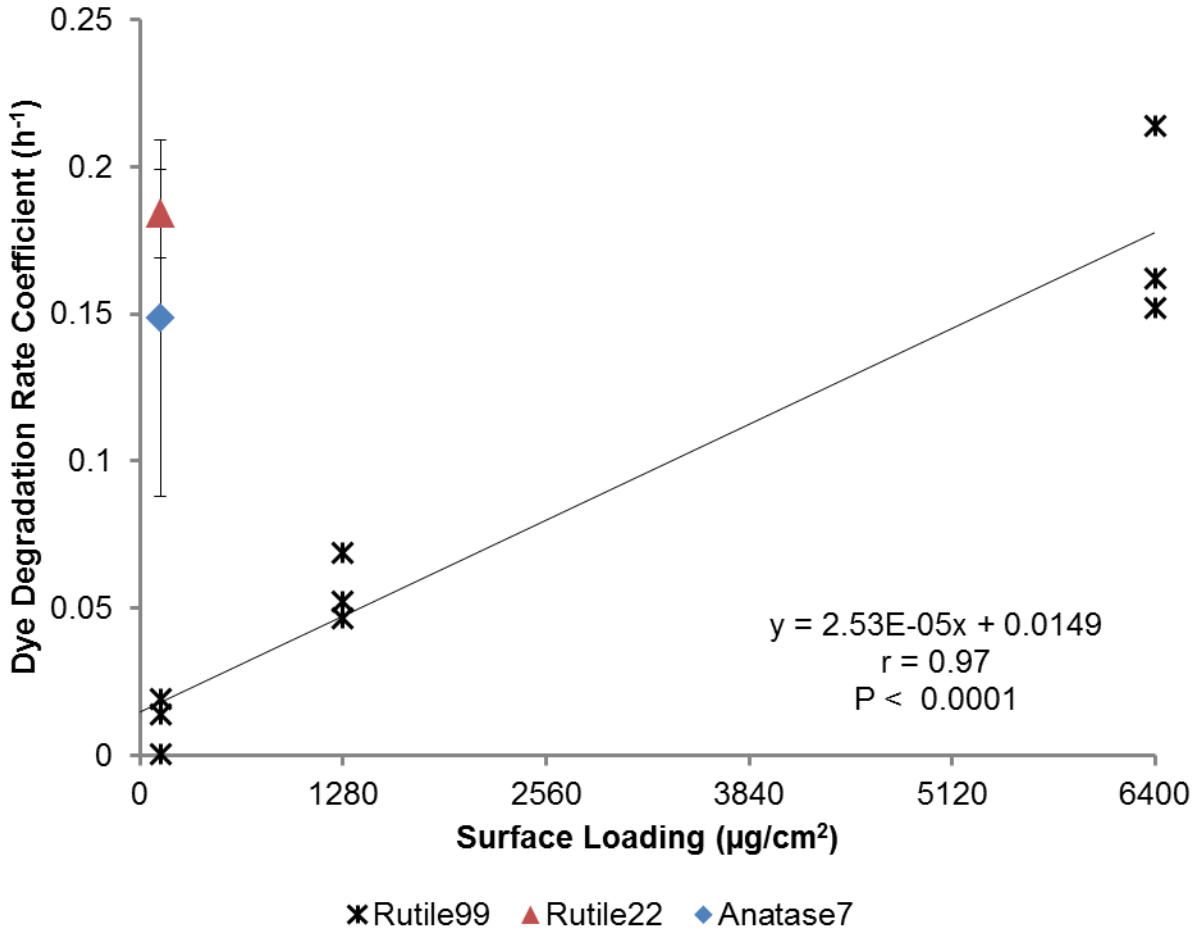

Figure 3-17. Effect of photocatalyst surface loading on second order reaction rate coefficient. The correlation shown is for rutile99

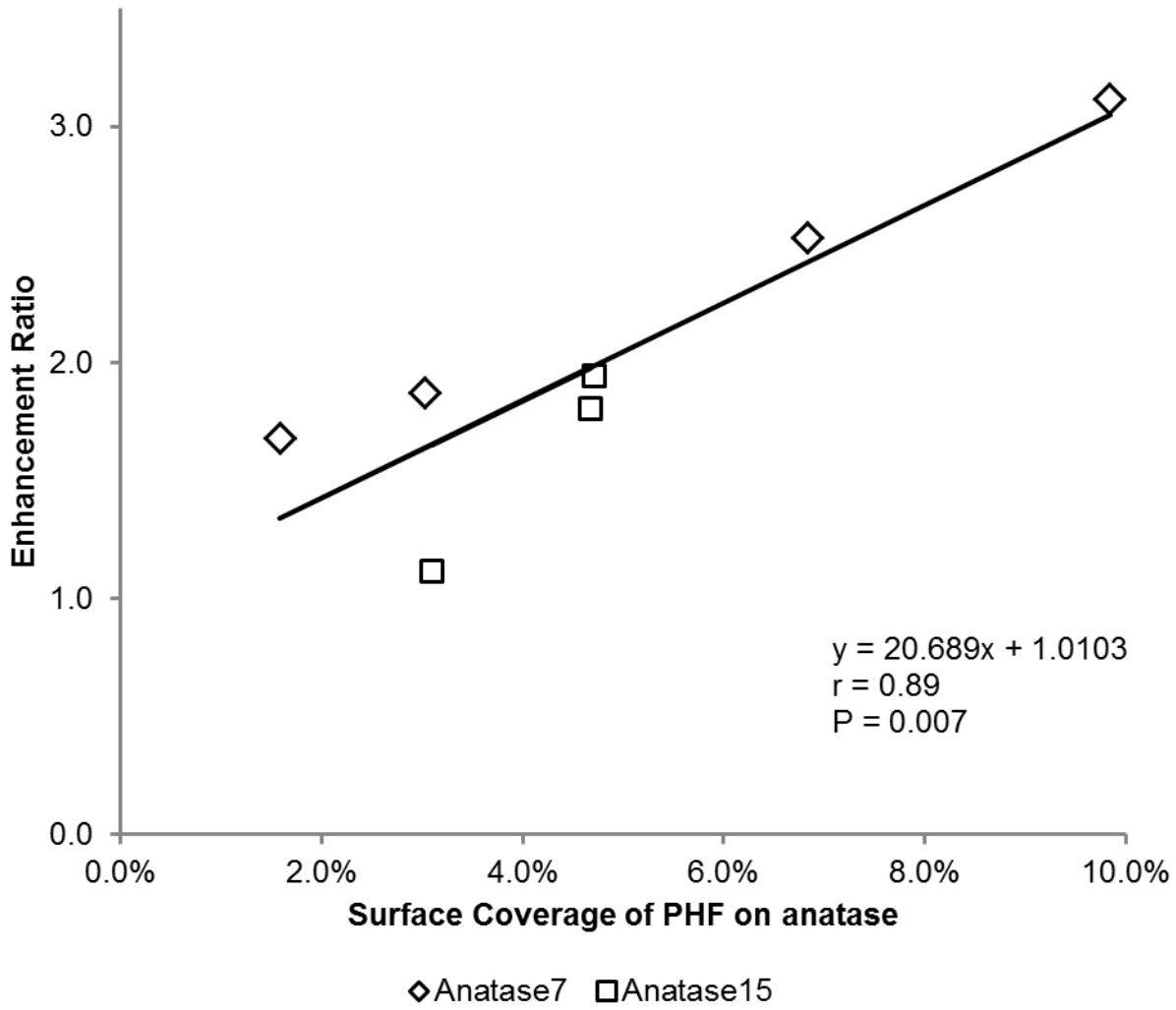

Figure. 3-18. The relationship of enhancement ratio and surface coverage of PHF on anatase under both UVA and visible light

CHAPTER 4
THE EFFECT OF DISPERSANT ON THE PERFORMANCE OF TITANIUM DIOXIDE COATING

A convenient method of applying TiO_2 coatings on walls, benches, tables and other indoor surfaces of buildings is to spray an aqueous suspension of TiO_2 onto the surfaces using a high volume, low pressure (HVLP) electric sprayer. The concentration of the TiO_2 suspension in the sprayer's feed reservoir should remain constant throughout the application period to obtain a consistent coating coverage. Also, the formation of large aggregates of TiO_2 that could clog the spray equipment should be prevented.

TiO_2 nanoparticles, suspended in aqueous system, are subject to random drifting caused by Brownian motion of water molecules. Random drifting of TiO_2 nanoparticles increases the probability of particle aggregation in aqueous system, which is caused by Van der Vaal attractive force. Once TiO_2 nanoparticles are aggregated, they tend to not fragment easily, eventually resulting in sedimentation. According to the DLVO theory,[102–104] the surface electrical charge of TiO_2 nanoparticles is an important factor controlling its aqueous stability. Manipulation of electrostatic repulsion in TiO_2 suspension by pH can change the surface potential of TiO_2 nanoparticles, giving stable suspension. The isoelectric point (IEP) of TiO_2 ranges from 3.9 to 8.2, depending on the crystal structure, crystallographic orientation or synthesis procedure.[91, 105, 106] The electrical charge of TiO_2 surface varies as a function of pH:

$$TiOH_2^+ \overset{H^+}{\longleftrightarrow} TiOH \overset{OH^-}{\longleftrightarrow} TiO^- \qquad (4\text{-}1)$$

As the pH of TiO_2 suspension decreases below IEP, the surface of TiO_2 is protonated, giving a net positive charge. Conversely, a net negative charge is developed on TiO_2 surface with elevated pH beyond IEP. Further increase or decrease pH away from IEP significantly increases the electrical charge of TiO_2 surface, leading to a stable suspension.

Addition of surfactants can stabilize TiO_2 suspensions through electrostatic forces or steric hindrance. Surfactants form a monolayer on particle surfaces when the free surfactant concentration is low. At higher free surfactant concentration, surfactant structures, such as micelles, are formed and these structures can adsorb to the particle surfaces. The minimum concentration of free surfactant at which micelles form is called the critical micelle concentration (CMC).

The purpose of the research described in the present chapter was to design a chemical dispersant system to prevent or limit aggregation of TiO_2 and thus make it compatible with spray application equipment. Chemical dispersion of the TiO_2 would also make it easier to keep the suspension well mixed during the application period. The approaches tested were to increase electrostatic repulsion or steric hindrance between TiO_2 particles. Adjustment of pH by adding sodium hydroxide and adsorption of anionic surfactant (sodium dodecyl sulfate) were tested for increasing electrostatic repulsion, whereas addition of nonionic surfactant (Tween 20) was tested for creating steric hindrance. P25 was used as the model photocatalyst in the experiments for dispersant selection. Once a dispersant was chosen, further experiments designed to refine the dispersant

system were carried out on a simple mixture of anatase with a crystallite size of 7nm and rutile with a crystallite size of 22 nm. These two photocatalysts were discovered to be more active than P25 under visible light, as reported in chapter 3. The long-term stability of the nanocomposite suspension was tested with the criteria that the suspension remains stable for a minimum of a week and is compatible with HVLP sprayers. Performance evaluation was carried out to determine the effect of alternative dispersant systems on photocatalytic activity.

4.1 Experimental

4.1.1 Chemicals and Reagents

The two model photocatalysts used were the mixed-phase (anatase and rutile) P25, manufactured by Evonik Industries AG (Essen, Germany), and a simple 1:1 mixture of rutile and anatase powders obtained from MKnano (Missisauga, Ontario, Canada). Properties of these photocatalysts are given in Table 4-1. A solution of Procion red MX-5B dye (Sigma-Aldrich Inc., St. Louis, Missouri) was prepared at a concentration of 2000 mg/L by dissolving 0.02 g dye powder in 10 mL deionized water. Non-ionic surfactant Tween 20 (Sigma-Aldrich Inc.), anionic surfactant sodium dodecyl sulfate (Fisher Scientific, Waltham, Massachusetts) or sodium hydroxide (Acros Organics, New Jersey) was used to increase the stability of TiO_2 suspension.

4.1.2 Characterization of TiO_2 Particles

BET surface area. Specific surface area of TiO_2 was measured under nitrogen using a NOVA 1200 with multipoint BET (Quantachrome Instruments, Boynton Beach, FL). TiO_2 powder was degassed and dried under vacuum at 110ºC prior to measurement.

X-ray diffraction. Powder X-ray diffraction was measured on a APD 3720 diffractometer (Philips, Andover, MA) with Cu-K_α radiation (40 kV, 25 mA) and diffracted beam monochromator, using a step scan mode with the step of 0.075° (2θ) and 4 s per step. Crystal structure was identified according to the database of International Centre for Diffraction Data. The crystallite size of TiO_2 was determined from the Scherrer equation:[89]

$$L = \frac{K\lambda}{(B-b)\cos\theta} \quad (4\text{-}2)$$

where L is the average crystallite size, K is the shape factor (0.9), λ is the x-ray wavelength of Cu-K_α radiation (1.54 Å), B is the overall line broadening in radians at the full width at half maximum (FWHM) intensity, b is the line broadening in radians at the FWHM intensity caused by the instrument itself (0.07) and θ is the Bragg angle, i.e., the angle at which highest intensity was observed. The crystallite size measured from XRD was used to compute an estimate of the specific surface area of TiO_2 for comparison with the measurement from BET surface area, according to the following equation:

$$SA = \frac{6}{\rho d} \quad (4\text{-}3)$$

where ρ is the density of TiO_2 form and d is the crystallite size of TiO_2, as determined by XRD.

Scanning electron microscopy. Scanning electron microscopy (JOEL 6335F FEG-SEM) was used to observe the ultrastructure of TiO_2 coating at the conditions of 10 kV or 15 kV accelerating voltage and 10 mm working distance. In addition to the secondary electron imaging mode, the backscattering electron imaging mode was used to get elemental contrast if necessary.

4.1.3 Dispersion

A series of dispersant concentrations with a constant weight percentage (0.1 wt%) of P25 was prepared as follows.

P25 dispersed with NaOH was prepared by adding 1.0 mL of 25 M NaOH to 24.0 mL of deionized water, giving a concentration of 1 M, which was then serially diluted (10× each dilution) to 10^{-6} M in deionized water. A mass of 10 mg of P25 was added to 10 mL of each dilution, followed by sonication (Misonix Sonicator 3000, Farmingdale, NY) at the highest power level (providing 180–200 W) for 30 minutes total (10 min on/2 min off × 3). Each suspension of P25 with a specific NaOH concentration was used within 1 hour.

P25 dispersed with sodium dodecyl sulfate (SDS) was prepared by adding 0.29 g of SDS to 10 mL of deionized water, giving a concentration of 0.1 M, which was then serially diluted to 10^{-6} M. A mass of 10 mg of P25 was added to 10 mL of each dilution, followed by sonication (Misonix Sonicator 3000, Farmingdale, NY) at the highest power level (providing 180–200 W) for 30 minutes total (10 min on/2 min off × 3). There was moderate foaming as the TiO_2 was added to the SDS solutions, but no forming was observed during sonication. Each suspension of P25 with a specific Tween 20 concentration was used within 1 hour.

P25 dispersed with Tween 20 was prepared by adding 1.0 mL of Tween 20 to 9 mL of deionized water, giving a volume fraction of 0.1, which was then serially diluted to 10^{-6} v/v. A mass of 10 mg of P25 was added to 10 mL of each dilution, followed by sonication (Misonix Sonicator 3000, Farmingdale, NY) at the highest power level (providing 180–200 W) for 30 minutes total (10 min on/2 min

off × 3). There was moderate foaming as TiO_2 was added to the solution of Tween, but no foaming during sonication. Each suspension of P25 with a specific Tween 20 concentration was used within 1 hour.

The settling of P25 was monitored visually for 24 hours after sonication. The aqueous aggregate size, size distribution and zeta potential of P25 suspension was measured within one hour of sonication. Particle size and size distribution were measured by Nanotrac ULTRA (Microtrac Inc., York, PA). Zeta potential was measured by Brookhaven ZetaPlus (Brookhaven Instruments Corporation, Holtsville, NY).

Further studies into the effect of suspension pH on settling of TiO_2 particles and photocatalytic performance of coatings prepared with the suspension were carried out on a 1:1 mixture of anatase and rutile. Rutile/anatase dispersed with NaOH was prepared by adding 1.0 mL of 25 M NaOH to 24.0 mL of deionized water, giving a concentration of 1 M, which was then serially diluted (10× each dilution) to 10-6 M in deionized water. A mass of 5 mg of rutile and 5 mg of anatase were added to 10 mL of each dilution, followed by sonication (Misonix Sonicator 3000, Farmingdale, NY) at the highest power level (providing 180–200 W) for 30 minutes total (10 min on/2 min off × 3). Each suspension of rutile/anatase with a specific NaOH concentration was used to particle size analysis and coating preparation within 1 hour. The settling of the rutile/anatase suspension was observed over a period of one week.

4.1.4 Coating Preparation

Ceramic tiles were used as substrates for photocatalytic performance evaluation. Tiles (2.5 cm × 2.5 cm) were obtained from American Olean Inc.

(Dallas,TX). The tile surfaces were almond-colored with a matte finish. The coating was applied in two steps to be consistent with commercial TiO_2 coating practice. In the dispersant selection experiments, P25 coating was prepared by pipetting a volume of 400 µL of P25 suspension containing NaOH, Tween 20 or SDS onto the tile surface, followed by drying overnight in a biosafety cabinet. A second coat of P25 was then applied using the same procedure, giving a surface loading of 128 µg/cm^2. In the dispersant refinement experiments, rutile/anatase coating was prepared by pipetting a volume of 400 µL of rutile/anatase suspension containing NaOH onto the tile surface, followed by drying overnight in a biosafety cabinet. A second coat of rutile/anatase was then applied using the same procedure, giving a surface loading of 128 µg/cm^2.

4.1.5 Dye Degradation

The photocatalytic performance of TiO_2 coatings was determined based on organic dye degradation. A volume of 0.01 mL of Procion red MX-5B solution (2000 mg/L) was pipetted onto coated tile and allowed to dry in an oven (55ºC) for 20 minutes. Samples were exposed to fluorescent light (model, distance to the samples, detector) at an irradiance of 1.8~2.0 W/m^2. Dye degradation was based on absorbance, as calculated from reflectance measured at 538 nm after 0, 12 and 24 hours of exposure to fluorescent light. Reflectance of coated or uncoated tile surfaces was measured with a Perkin-Elmer Lambda 800 with PELA-1000 Reflectance Spectroscopy Accessory. Absorbance was calculated as the negative log10 of reflectance expressed as fraction. Coated tiles without dye were used as the internal reference in the measurement. Dye degradation was calculated according to:

$$\% \text{ dye degradation} = \frac{A_0 - A_t}{A_0} \times 100 \quad (4\text{-}4)$$

where A_0 is the calculated absorbance of dye coated on photocatalytic or bare grout surface before exposure to fluorescent light and A_t is the absorbance of dye coated on photocatalytic or grout surface after exposure to fluorescent light at a given time. Because the color of bare grout varied somewhat, it was necessary to subtract this background color. Therefore, A_0 and A_t were calculated from

$$A_0 = A_{0'} - A_b \quad (4\text{-}5)$$

$$At = A_{t'} - A_b \quad (4\text{-}6)$$

where $A_{0'}$ and $A_{t'}$ are the measured absorbance of dye on grout at time zero and time t, respectively, and Ab is the measured absorbance of the bare or photocatalytically coated grout surface without dye at a given time.

4.1.6 Statistical Analysis

First order fits between the extent of dye degradation and visible light exposure time were based on the equation

$$\ln \frac{c_t}{c_0} = kt + b \quad (4\text{-}7)$$

and second order fits were based on the equation

$$\frac{1}{c_t / c_0} = k't + b' \quad (4\text{-}8)$$

where c_t and c_0 represent absorbance at times t and t_0, respectively, k and k' are the reaction rate coefficients for the first and second order fits, respectively, and b and b' are arbitrary constants.

The parameter values (k, b, k', b') for the fits were determined by least squares linear regression.

One-way ANOVA and post-hoc testing were carried out using the Dunnett's two-sided tests through NCSS statistical analysis and graphics software (NCSS, Kaysville, UT).

4.2 Results

4.2.1 Characterization

X-ray diffraction patterns of the TiO_2 powders used in this study are shown in Figure 4-1. The diffraction pattern of P25 exhibited a combination of anatase and rutile patterns, which is due to its mixed phase structure.[91] The diffraction patterns of anatase and rutile from MKnano were in good agreement with the patterns shown in the database of International Centre for Diffraction Data (http://www.icdd.com). The mean crystallite size calculated on the basis of XRD was 25.4 nm for P25, 7.1 nm for anatase and 21.5 nm for rutile (Table 4-2). Scanning electron microscopy showed that the smaller dimension of primary particles of P25 was in the range of 28–59 nm (Fig. 4-2A). In the rutile/anatase coating (Fig. 4-2B), the smaller dimension of primary particles ranged from 15 to 38 nm.

The BET specific areas of P25, anatase and rutile were 44, 231 and 35 m^2/g, respectively (Table 4-3). These values deviated slightly from the specific surface area calculated on the basis of the crystallite sizes calculated from XRD, with assumed spherical particles.

4.2.2 Effects of Dispersant Systems on P25 Suspension Characteristics and Coating Performance

P25 suspended in deionized water containing no dispersant (pH = 6–7) completely settled within 24 hours (Fig. 4-3). P25 prepared in 10^{-2} or 10^{-3} M

NaOH (pH 10.4 or 9.2, respectively) remained in suspension for 24 hours, whereas P25 prepared in 10^{-4} or 10^{-5} M NaOH (pH 8.0 or 6.9, respectively) settled within 24 hours (Fig. 4-4).

In the concentration range of 10^{-2} to 10^{-6} v/v Tween 20, there was no settling of TiO_2 at the lowest dilution, and complete settling at dilutions of 10^{-3} to 10^{-6} v/v (Fig. 4-5A). A series of dilutions centered on 10^{-2} v/v confirmed this concentration was optimal for stabilizing P25 (Fig. 4-5B).

There was complete settling of P25 within 24 hours at SDS concentration of 10^{-3}, 10^{-4} and 10^{-5} M SDS. No settling occurred in 10^{-2} M SDS, whereas the 10^{-1} M concentration exhibited some settling (Figure 4-6).

The aqueous aggregate size and zeta potential of P25 suspensions with no dispersant and at the optimum NaOH, Tween 20 and SDS concentrations are shown in Figure 4-7. The aggregate size (mean diameter based on number distribution) was 179 nm with no dispersant. The size was not significantly decreased with Tween 20 (α=0.05). Aggregate size was significantly decreased to the range of 86 to 89 nm with NaOH or SDS. Zeta potential of P25 with no dispersant was 0 mV. Addition of Tween 20 significantly increased zeta potential to 8 mV, whereas addition of SDS or sodium hydroxide significantly decreased the zeta potential to the range of -38 to -42 mV.

Coatings of P25 with the three alternative dispersant systems were examined under SEM. Figures 4-8 and 4-9 indicate that the pH of the P25 suspension used to prepare the coatings did not change the appearance of the coatings with respect to surface coverage and granularity. The P25 coating

prepared with Tween 20 as dispersant is shown in Figure 4-10. At 200×, this coating was similar in appearance to that of coating prepared with the pH-stabilized suspension. At 5,000×, this coating appeared to be very uniform with no granularity. Figure 4-11a indicates that addition of SDS to the P25 suspension resulted in a coating exhibiting a ridge and valley pattern. At higher magnification, segregation of the coating components is apparent, with P25 (bright areas in backscattering mode) overlaying SDS (dark areas in backscattering mode) (Fig. 4-11C and 4-11D).

Dye degradation under visible light by P25 coatings made with optimum dispersant concentrations (0.001 M NaOH, 0.01 M SDS and 0.01 v/v Tween 20) is shown in Fig. 4-12. Coatings made from P25 dispersed by either Tween 20 or SDS were significantly (α=0.05) less active than coating made from P25 containing either no dispersant or NaOH. Coating made from P25 dispersed by NaOH performed equivalently to coating made from P25 with no dispersant.

4.2.3 Performance Comparison of Coatings prepared from P25 versus a 1:1 Mixture of Rutile and Anatase

The results presented in chapter 3 indicated that rutile with crystallite size of 22 nm or anatase with crystallite size of 7 nm are more photocatalytically active under the light spectrum of fluorescent bulbs than P25. It was also found that the rutile and anatase used different portions of the visible light spectrum. Thus, it is expected that a mixture of rutile and anatase would exhibit superior performance to either anatase or rutile alone. This was confirmed by a comparison of a 1:1 rutile/anatase mixture to P25. As shown in Figure 4-13, the rutile/anatase mixture was five times more active than P25. Therefore, in the present study,

optimization of NaOH concentration for dispersion and photocatalytic performance of a 1:1 rutile/anatase mixture was carried out.

4.2.4 Optimization of the NaOH Dispersant System for 1:1 Rutile/anatase Mixture

The NaOH dispersant system was further optimized using a 1:1 mixture of rutile and anatase as a model photocatalyst. The rutile/anatase photocatalyst was suspended in NaOH solutions ranging from 100 to 10^{-7} M NaOH, which gave a pH range from 6.8 to 13.4 (Fig. 4-14). The rutile/anatase particles were unstable at pH of 12.7 or higher and at pH of 6.9 or lower, settling within 12 hours. The stable range of pH was determined to between 7.5 and 11.8. The aqueous aggregate size of rutile/anatase particles at the stable pH values is shown in Fig. 4-15. At pH of 10.6 or 11.8, the aggregate size was in the range of 69 to 78 nm, which was significantly smaller than the aggregate size of 176 nm at pH 7.5. The zeta potential of rutile and anatase are -46.9 and -45.1 mV, respectively (Fig. 4-16).

Figure 4-17 relates dye degradation by a coating of rutile/anatase particles to the pH of the suspension from which the coating was prepared. The maximum rate of dye degradation was achieved by coating prepared from suspensions with pH in the range of 10.6 to 11.8. Performance dropped sharply with coating prepared from a suspension with pH of 12.7. Decrease in performance of coatings prepared from suspensions with pH lower than the optimum was more modest. A secondary minimum in dye degradation was obtained with coating prepared from a suspension with pH 7.5.

4.3 Discussion

4.3.1 The Effect of Dispersant

Surfactants mediated stabilization of TiO_2 suspension is through electrostatic repulsion or steric hindrance. The zeta potential of P25 in deionized water containing no dispersant (pH 6–7) was -0.5 mV. This is consistent with a reported IEP of 6.5 for P25.[91] The suspension was unstable, settling within 24 hours. Adding NaOH made the zeta potential more electronegative, consistent with equation 4-1. At 10^{-3} M NaOH (pH 9.2), the zeta potential was sufficiently electronegative (-38 mV) to stabilize the suspension for 24 hours. Interestingly, the zeta potential at which SDS stabilized the P25 (-42 mV) was very close to the zeta potential at which NaOH stabilized P25 (-38 mV). This suggests that the mechanism of stabilization by both SDS and NaOH is decrease of zeta potential away from IEP, leading to increased electrostatic repulsion between TiO_2 particles. Tween 20 had only a slight effect on the P25 zeta potential; not sufficient to stabilize the TiO_2 suspension through electrostatic forces. The optimum dosed concentration of Tween 20 for dispersion was 100 times higher than its CMC (0.0001 v/v, ref), suggesting that stabilization of TiO_2 was mediated by micelles creating steric hindrance to aggregation.

The presence of surfactants impaired the performance of P25 coating. Surfactants, physically adsorbed to the P25 particle surface, serve as radical sinks, diminishing the availability of hydroxyl radicals for dye degradation.[107, 108] The EDS analysis also indicated there is a high weight percentage of carbon (55.6 ± 0.2% for Tween 20, 54.9 ± 0.3% for SDS) on the P25 coating prepared using SDS or Tween 20 as dispersant, while carbon is absent from the P25

coating (prepared without dispersant or using NaOH as dispersant). Thus, the observed degradation of photocatalysis upon addition of surfactant is most likely due to reaction of photocatalytically generated free radicals with the surfactant molecules. Additionally, the continuity of the P25 coating was disturbed with the presence of SDS, giving a lower surface coverage of P25. This may also contribute to lower photocatalytic performance.

4.3.2 The Effect of pH on Coating Performance

The performance of photocatalyst coatings was found to depend on the pH of the suspensions from which they are prepared. Possible explanations for this effect are pH-dependent adsorption of dye on photocatalyst or pH-dependent aggregation of photocatalyst. Many studies suggest that photocatalytic degradation depends on the pH-dependent charge of dye molecules, which affects adsorption of dye on photocatalst.[109, 110] In this case, the effect of adsorption, however, may not be relevant because dye was allowed to dry on the coating. As suggested from the aqueous stability study, excessive or insufficient of NaOH caused instability and larger aggregate size. At constant surface loading, surface coverage of photocatalyst decreases as photocatalyst particle size increases (Figure 4-18). This seemingly obvious observation has not been reported in the literature. This observation was also confirmed from the scanning electron micrographs. Figure 4-19 and 4-20 indicated that larger aggregated size of photocatalyst gave rise to a lower surface coverage, while smaller aggregated size contribute to a uniform coating with high surface coverage photocatalyst.

4.4 Summary

- Sodium dodecyl sulfate and Tween 20 are effective in stabilizing aqueous suspension of TiO_2. However, they inhibit photocatalytic activity. NaOH effectively stabilizes aqueous TiO_2 suspensions and does not inhibit photocatalysis at concentrations of 10^{-2} M or less.

- Aggregate size influences surface coverage and consequently performance of TiO_2 coatings. Maintaining TiO_2 aqueous formulations within a pH range that stabilizes the formulations thus improves photocatalytic activity of coatings prepared from the formulations.

Table 4-1. Properties of photocatalysts employed in present research, as given by manufacturers

Photocatalyst	Component	Manufacturer	Product Name	Primary Particle Size (nm)	Mass Density (g/cm^3)
P25	Mixed phase particles	Evonik Industries AG	P25	N/A	4.26
1:1 rutile/anatase mixture	Rutile particles	MKnano	MKN-TiO2-R050P	50	4.23
	Anatase particles	MKnano	MKN-TiO2-C7	7	3.9

Table 4-2. X-ray diffraction parameters used for calculation of mean crystallite size of P25, anatase and rutile

	P25	Anatase	Rutile
K: shape factor	0.9	0.9	0.9
λ: x-ray wavelength (Å)	1.54	1.54	1.54
B: line broadening in FWHM intensity (°)	0.391	1.210	0.45
b: line broadening in FWHM intensity caused by instrument (°)	0.07	0.07	0.07
2θ: 2×Bragg angle (°)	25.402	25.401	27.598
L: mean crystallite size (nm)	25.4	7.1	21.5

Table 4-3. BET specific surface area and calculated specific surface area based on mean crystallite size

	P25	Anatase	Rutile
BET specific surface are (m^2/g)	44	231	35
Calculated specific surface area (m^2/g)	56	200	66

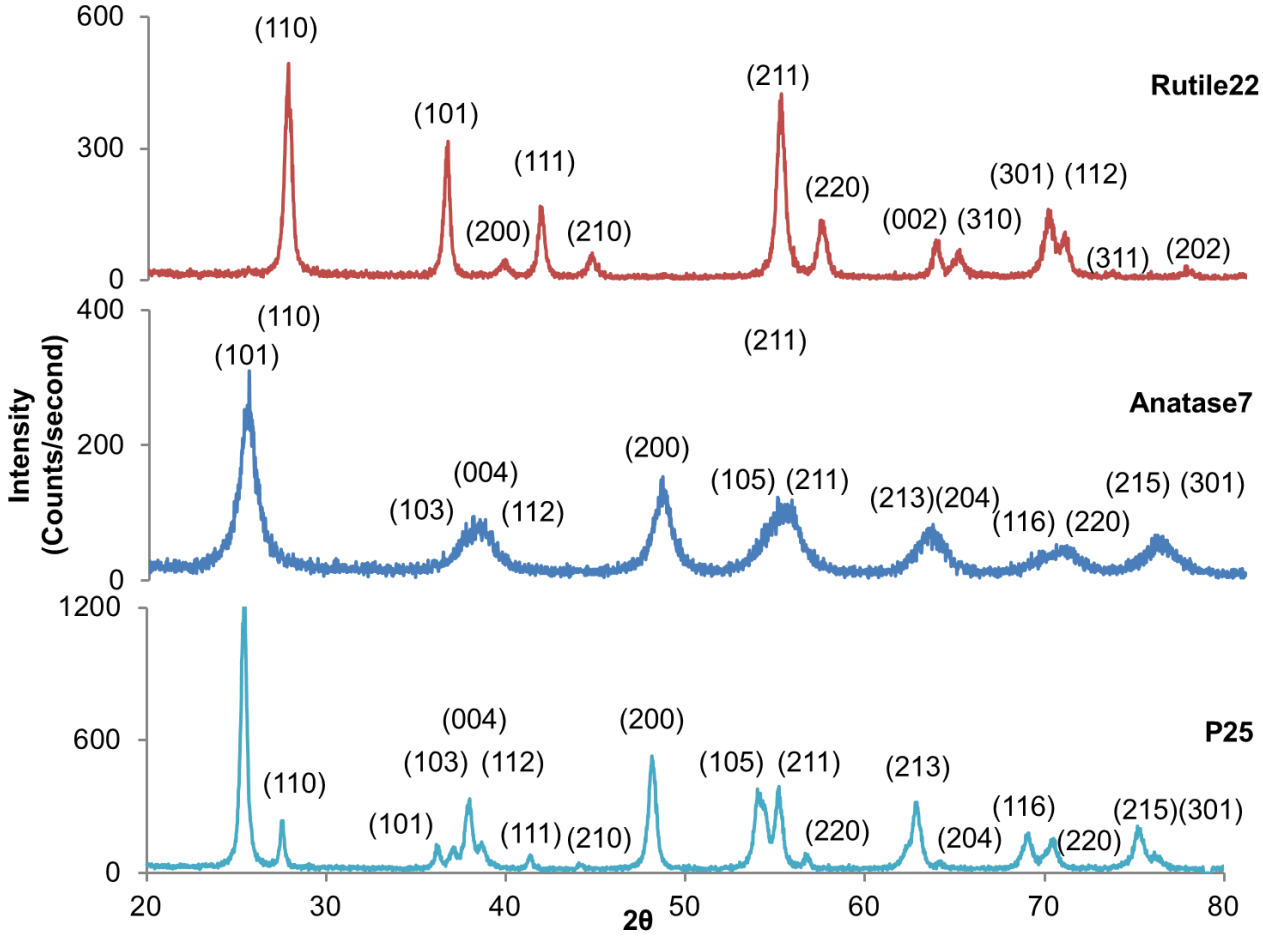

Figure 4-1. X-ray diffraction pattern of TiO_2

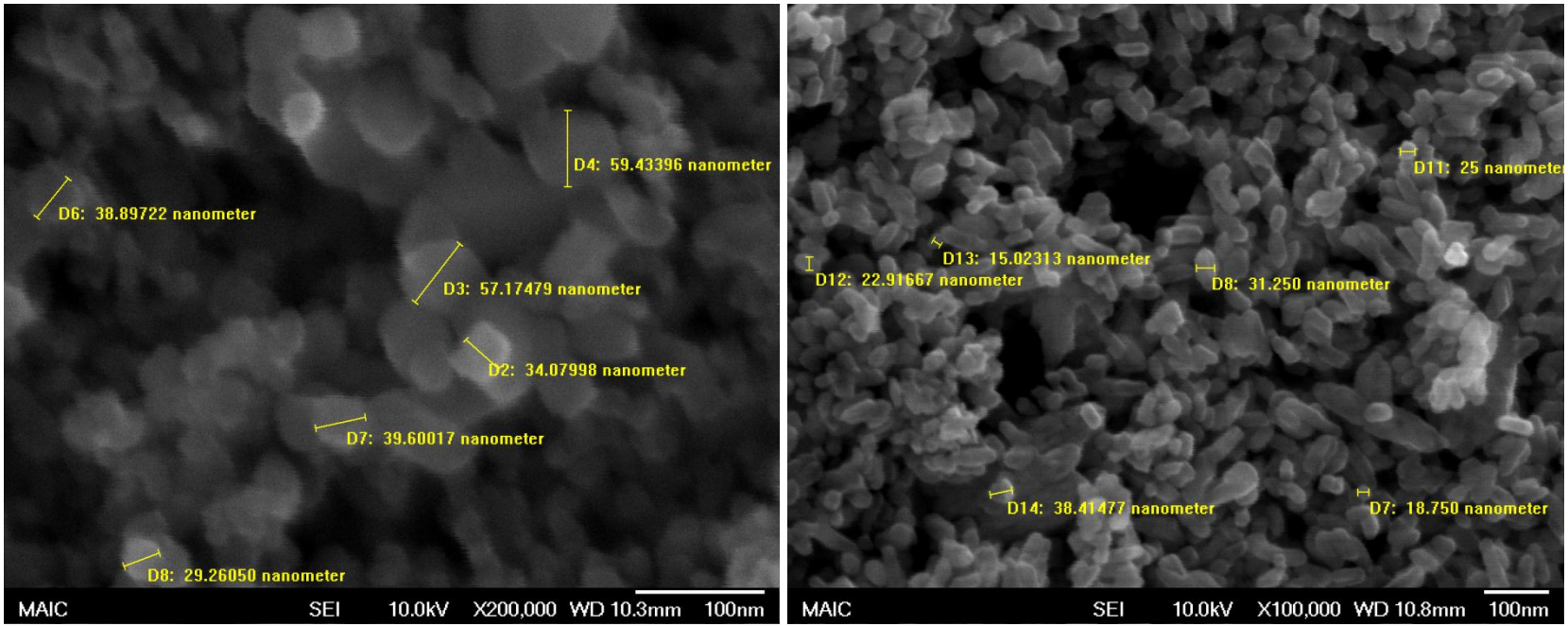

A B

Figure 4-2. Scanning electron micrograph of TiO_2 coating. A) P25 coating. B) Rutile/anatase coating

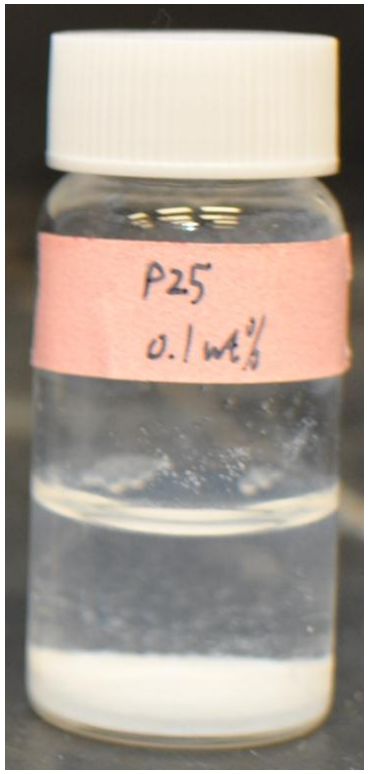

Figure 4-3. P25 suspended in DI water after 24 hours

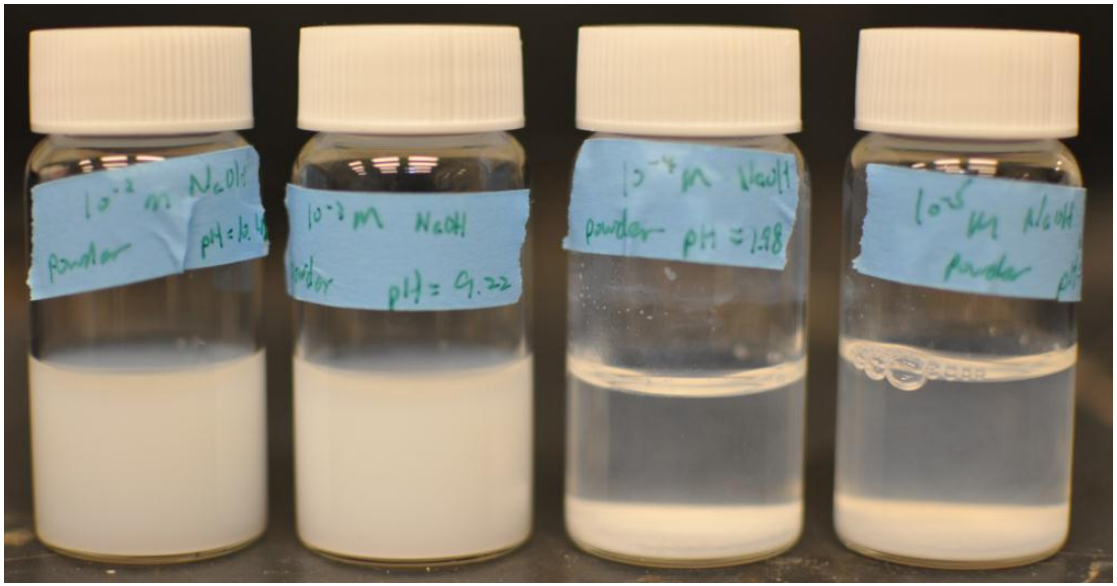

Figure 4-4. P25 suspended in NaOH solutions at various concentrations (10^{-2}–10^{-5} M) after 24 hours

A

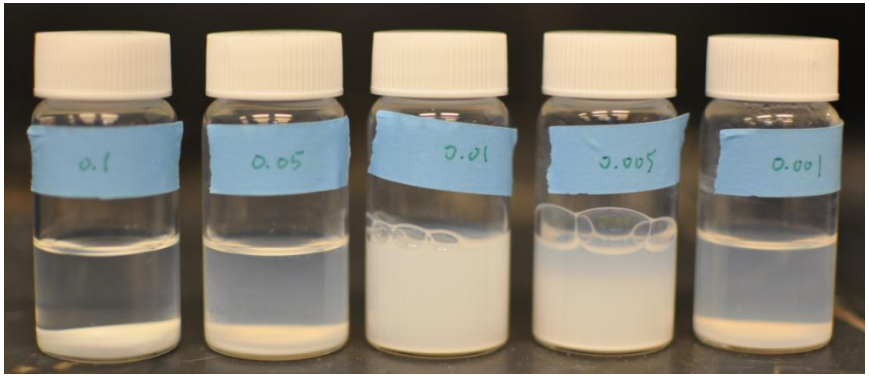

B

Figure 4-5. P25 suspended in Tween 20 solutions at various concentrations (volume fraction). A) 10^{-6}–10^{-2} v/v. B) 10^{-3}–10^{-1} v/v after 24 hours

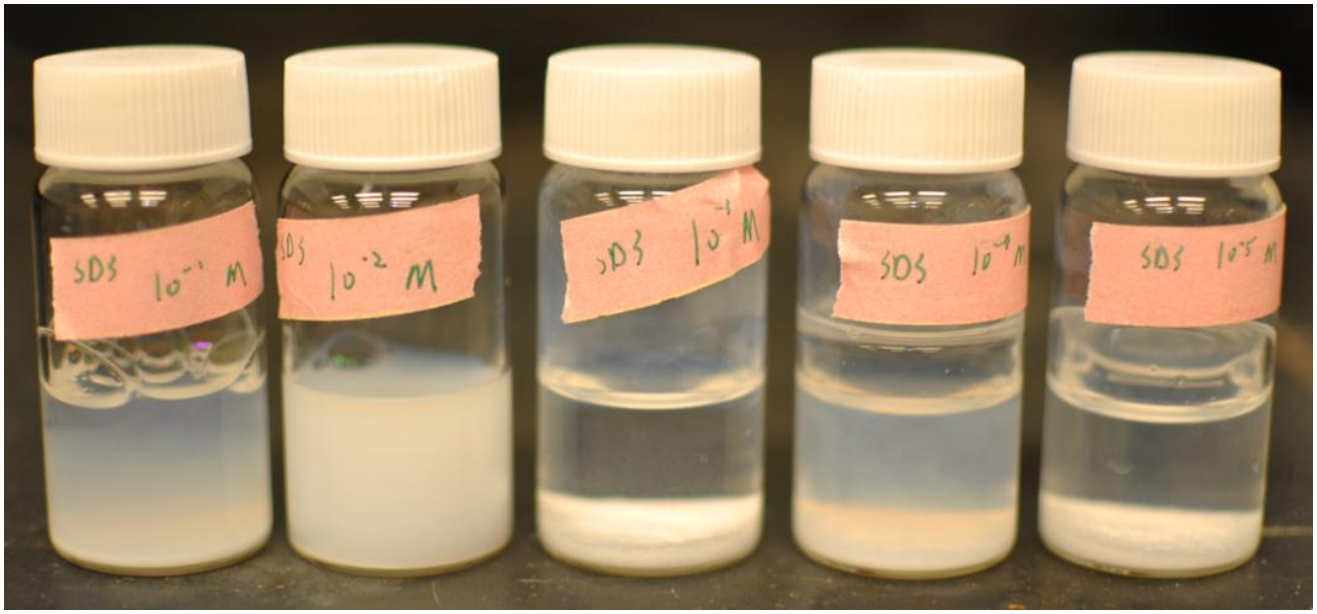

Figure 4-6. P25 suspended in SDS solutions at various dosed concentrations (10^{-5}–10^{-1} M) after 24 hours

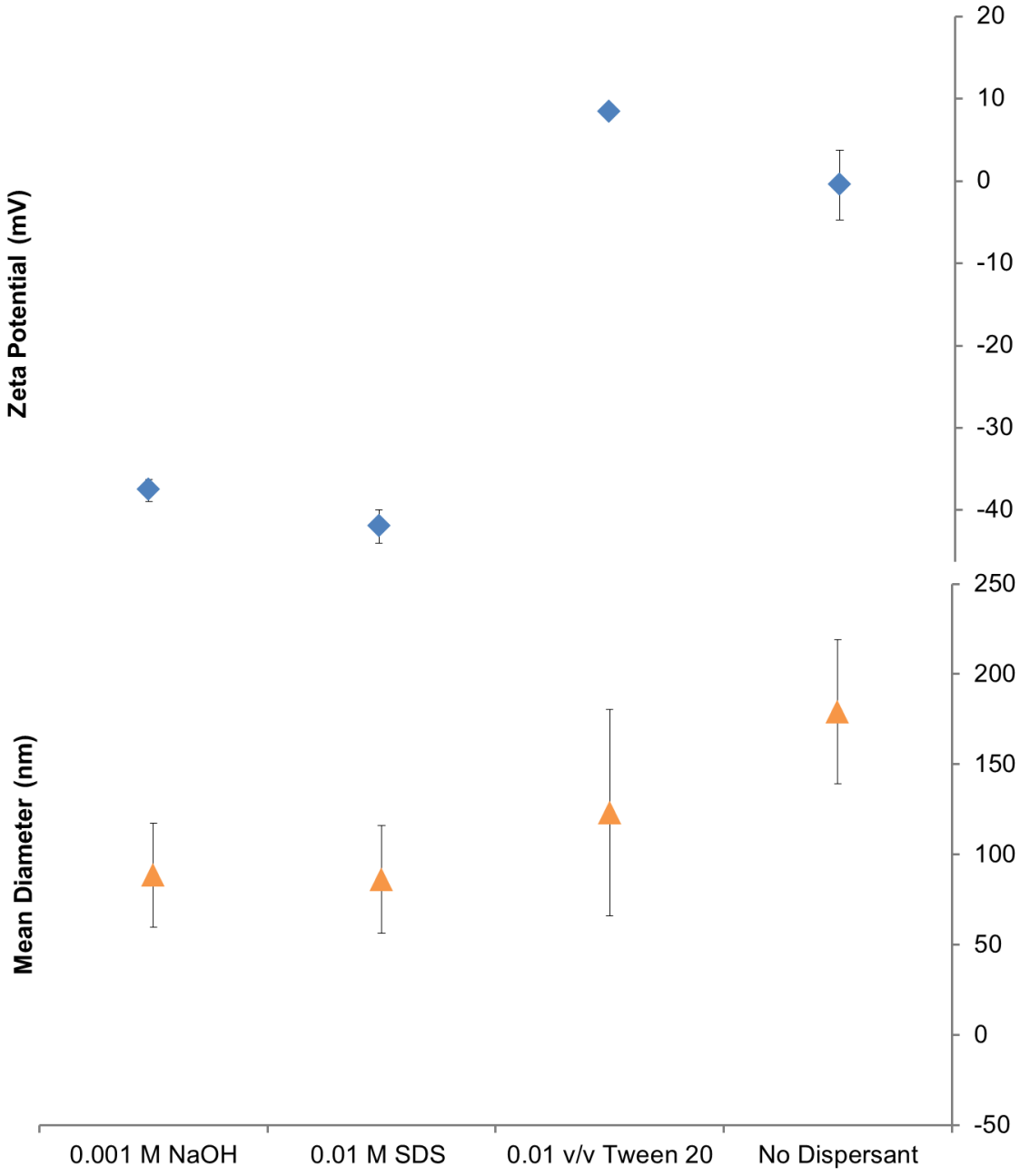

Figure 4-7. Mean diameter and zeta potential of P25 suspension with and without dispersant

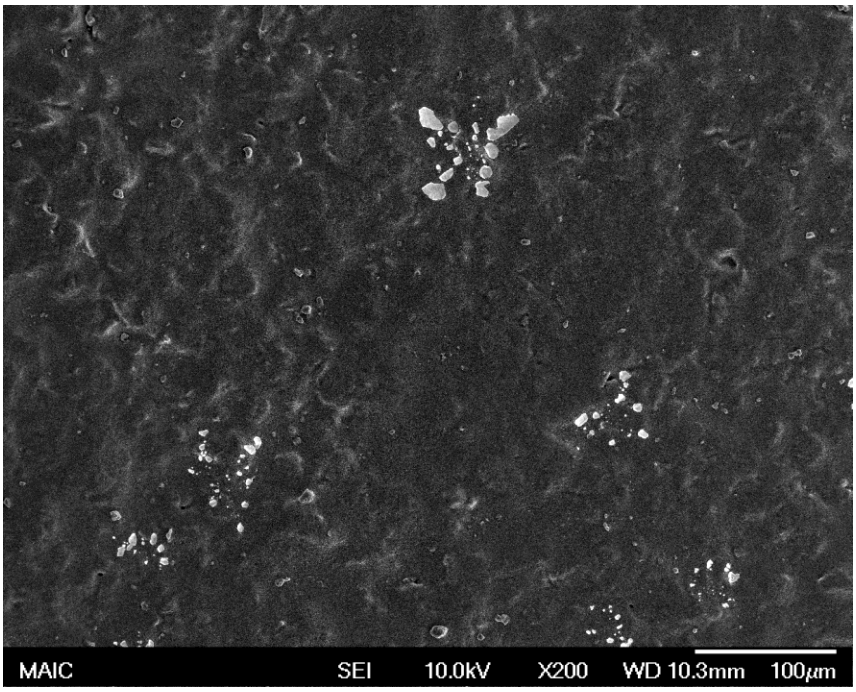

A

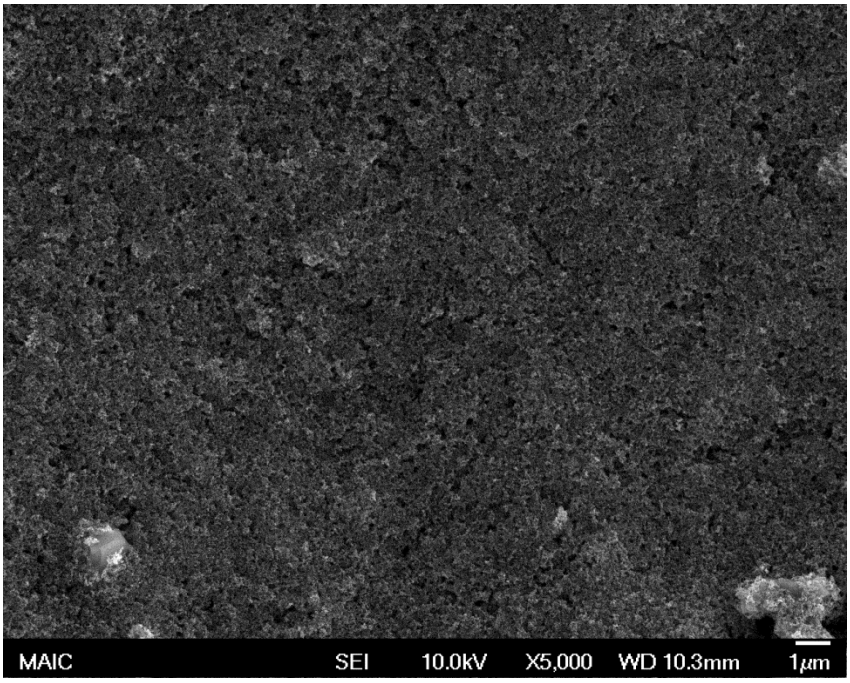

B

Figure 4-8. Scanning electron micrographs of P25 coating prepared using DI water containing no dispersant. A) 200-time magnification. B) 5000-time magnification

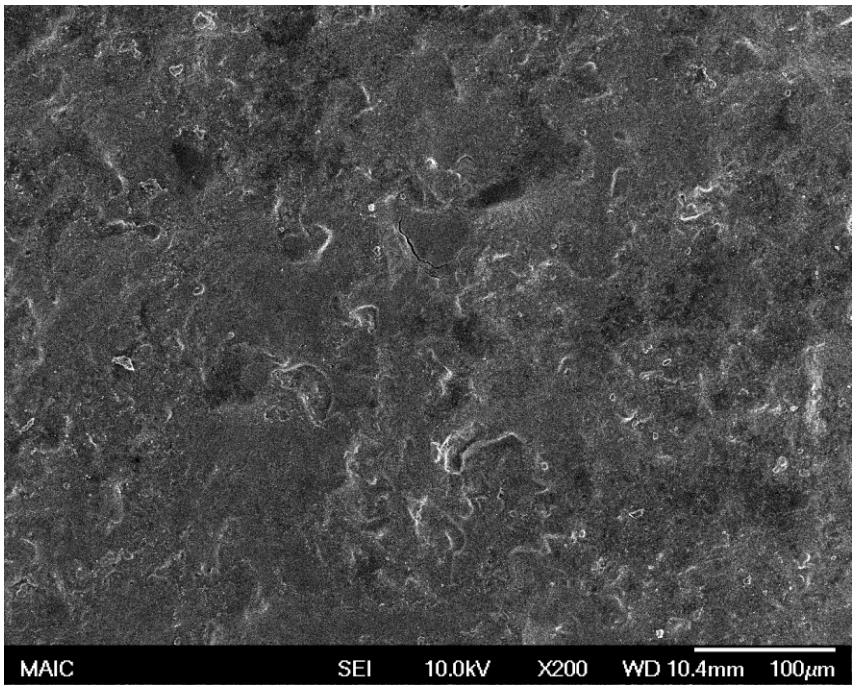

A

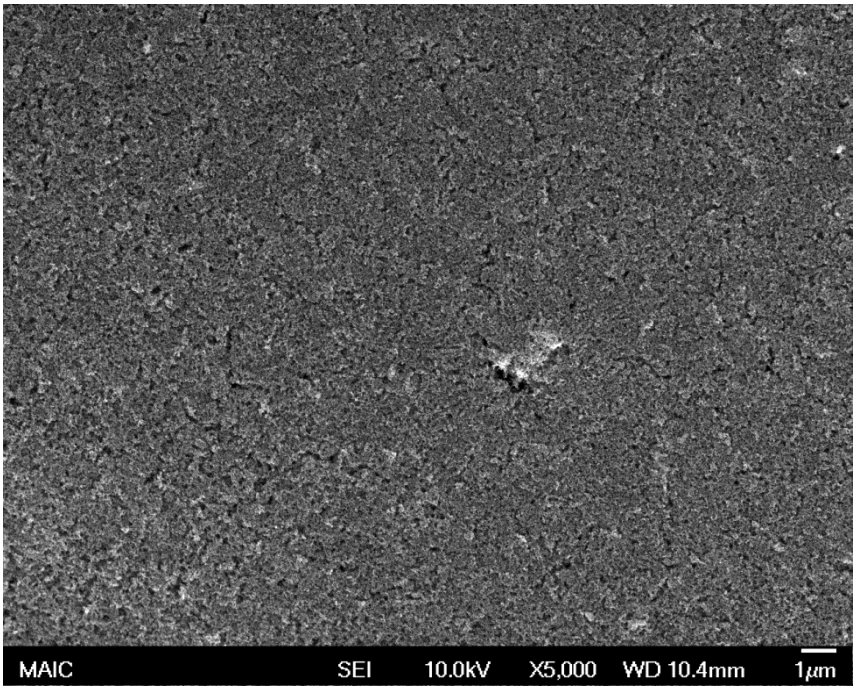

B

Figure 4-9. Scanning electron micrographs of P25 coating prepared using 0.001 M of NaOH. A) 200-time magnification. B) 5000-time magnification

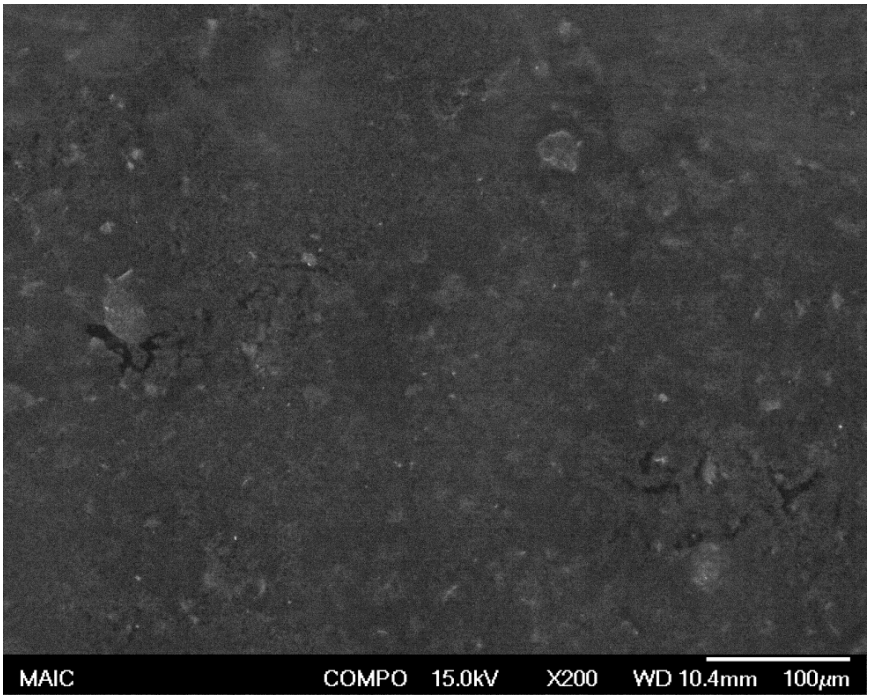

A

B C

Figure 4-10. Scanning electron micrographs of P25 coating prepared using Tween 20 as dispersant. A) 200-time magnification (secondary electron imaging mode). B) 5000-time magnification (secondary electron imaging mode). C) 5000-time magnification (backscattering electron mode)

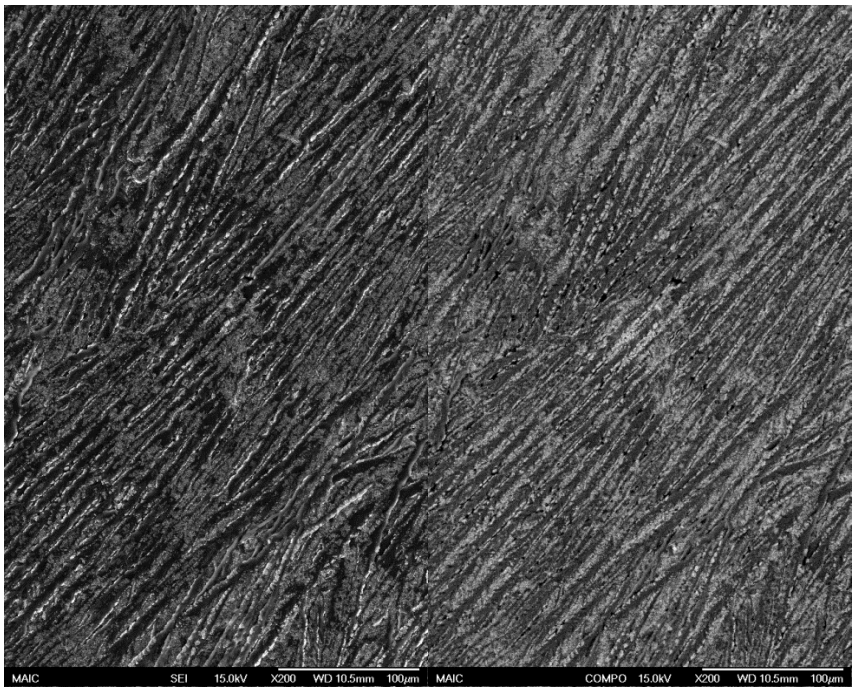

A B

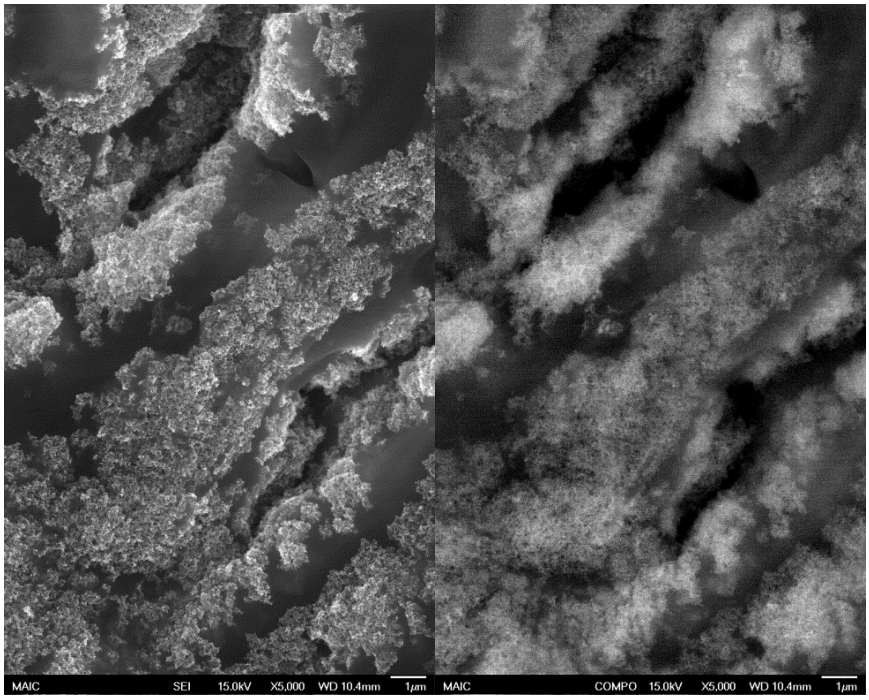

C D

Figure 4-11. Scanning electron micrographs of P25 coating prepared using SDS as dispersant. A) 200-time magnification (secondary electron imaging mode). B) 200-time magnification (backscattering electron mode). C) 5000-time magnification (secondary electron imaging mode). D) 5000-time magnification (backscattering electron mode)

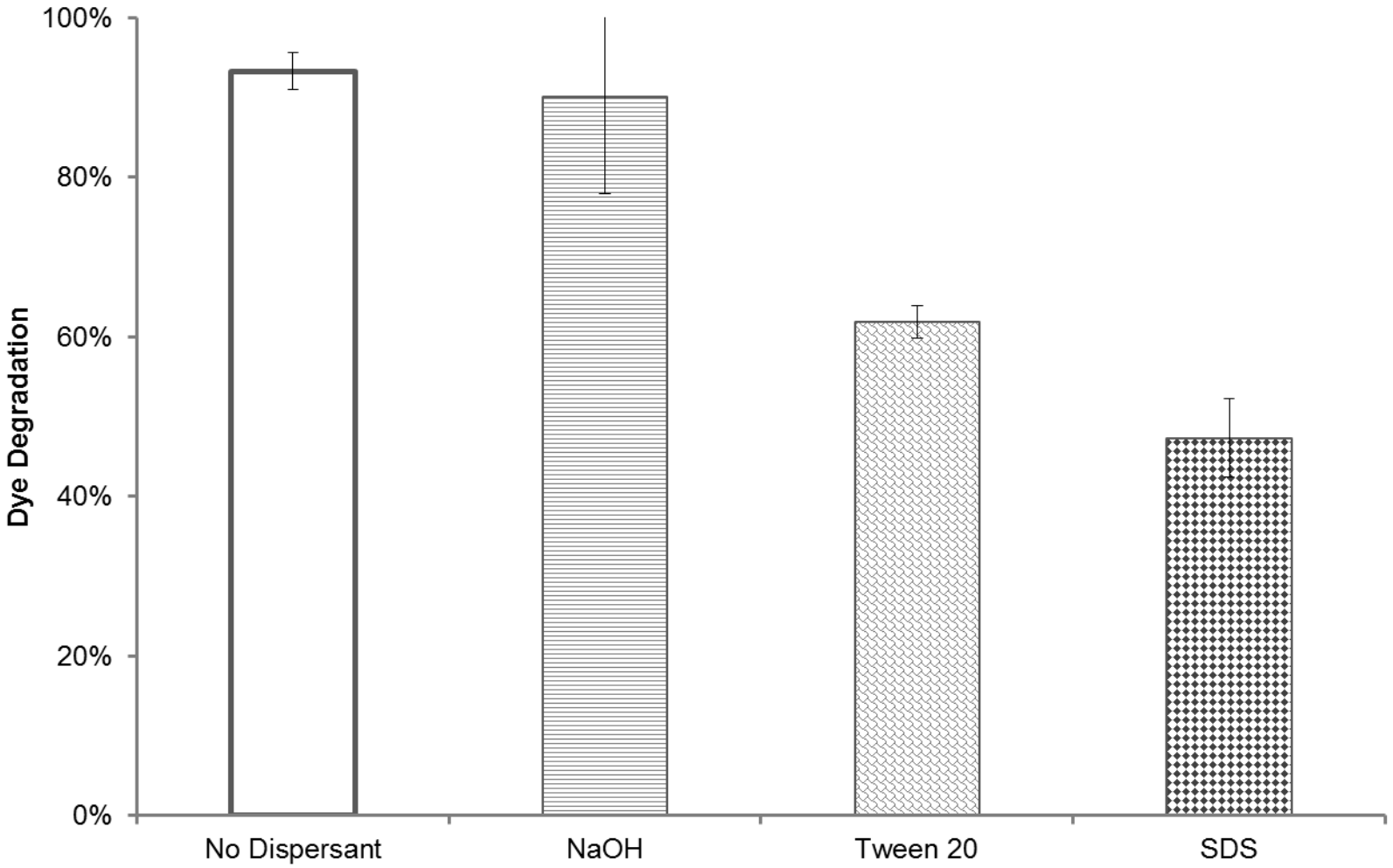

Figure 4-12. Dye degradation performance of P25 coating made from the suspensions with different dispersants. The coatings were exposed to visible light at 2 W/m^2

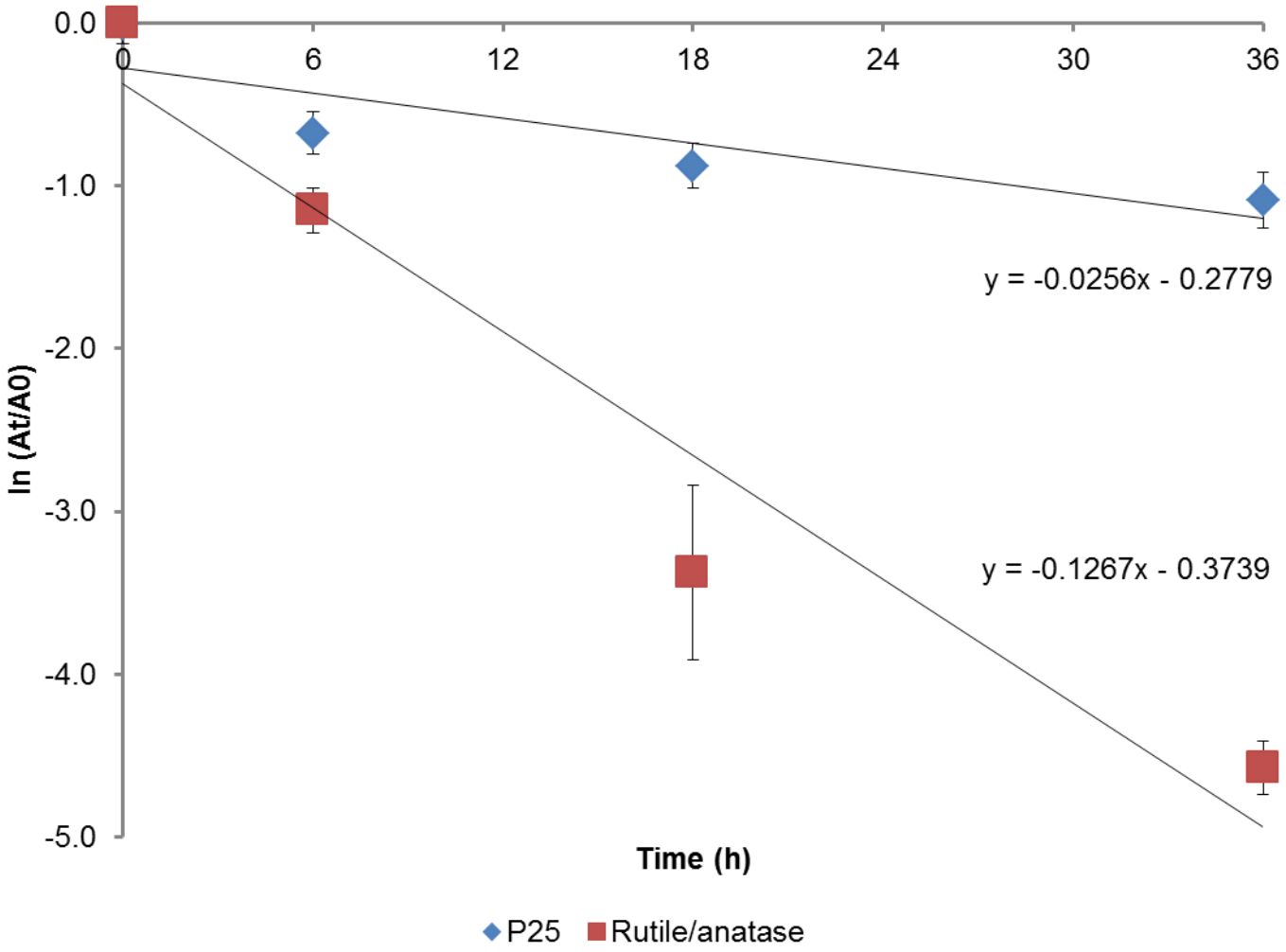

Figure 4-13. Dye degradation kinetics of P25 and anatase coating after exposed to visible light at 2 W/m^2

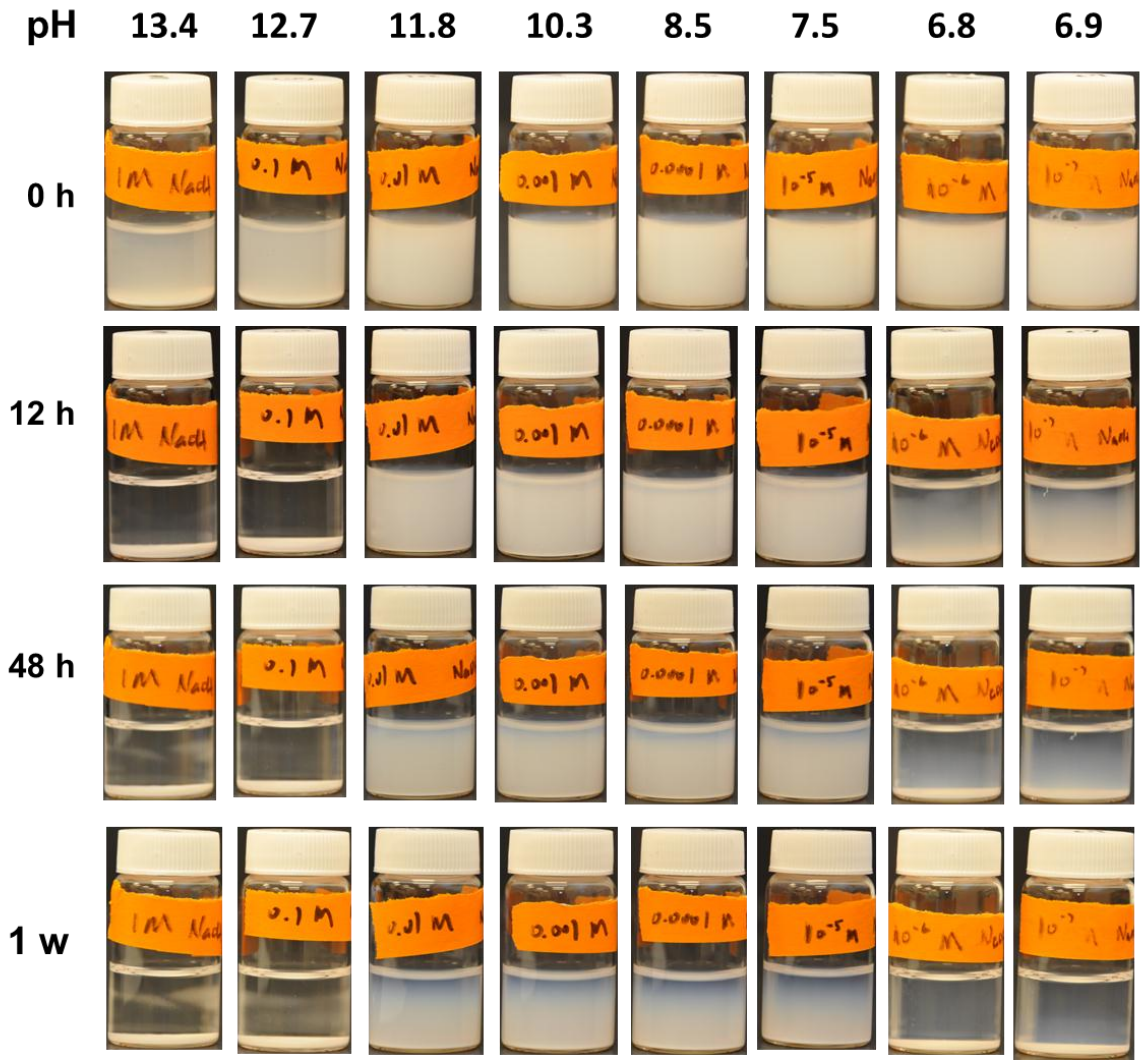

Figure 4-14. Temporal stability of TiO_2 suspension at different pH

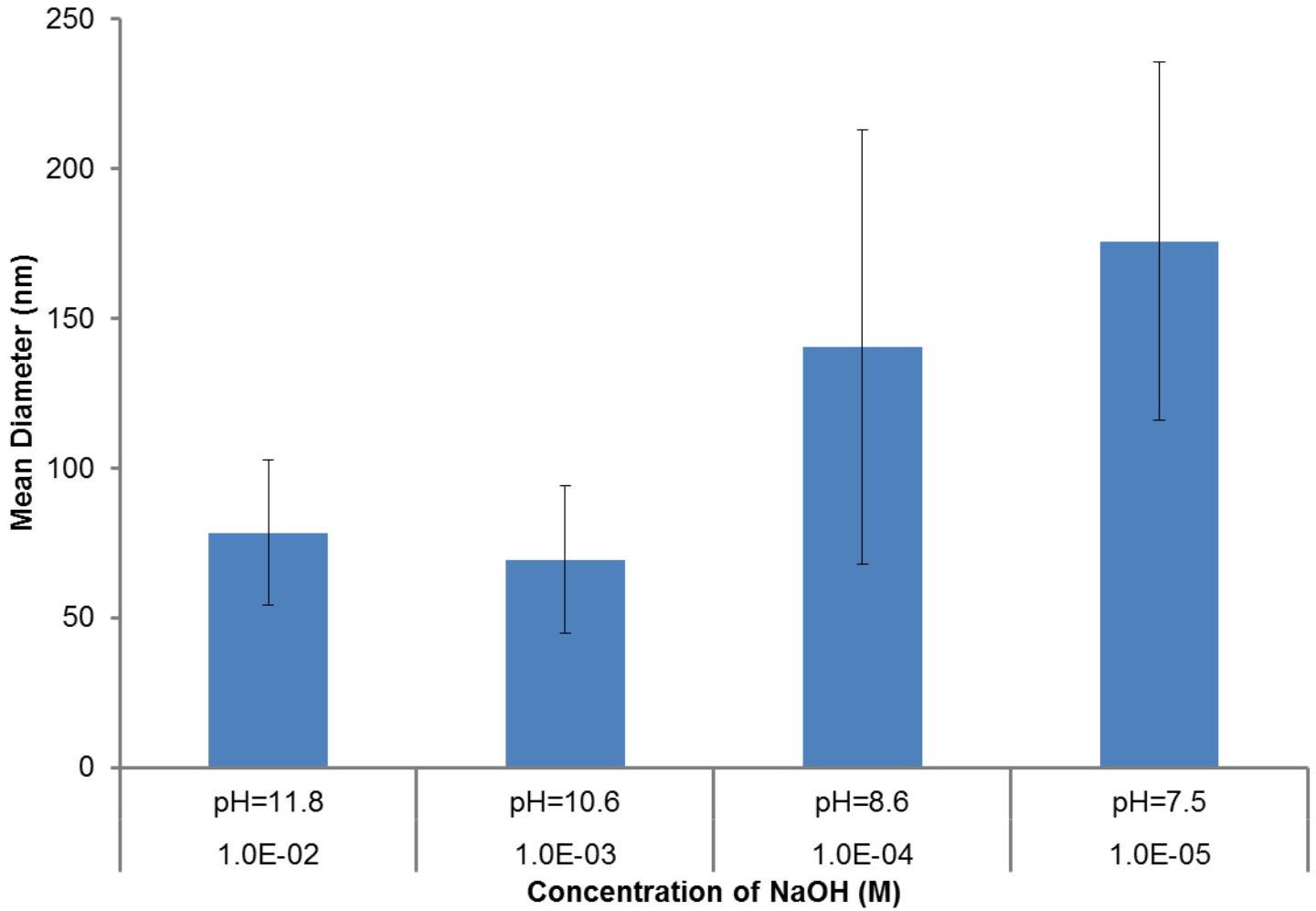

Figure 4-15. Aqueous aggregate size of anatase/rutile at various pH conditions

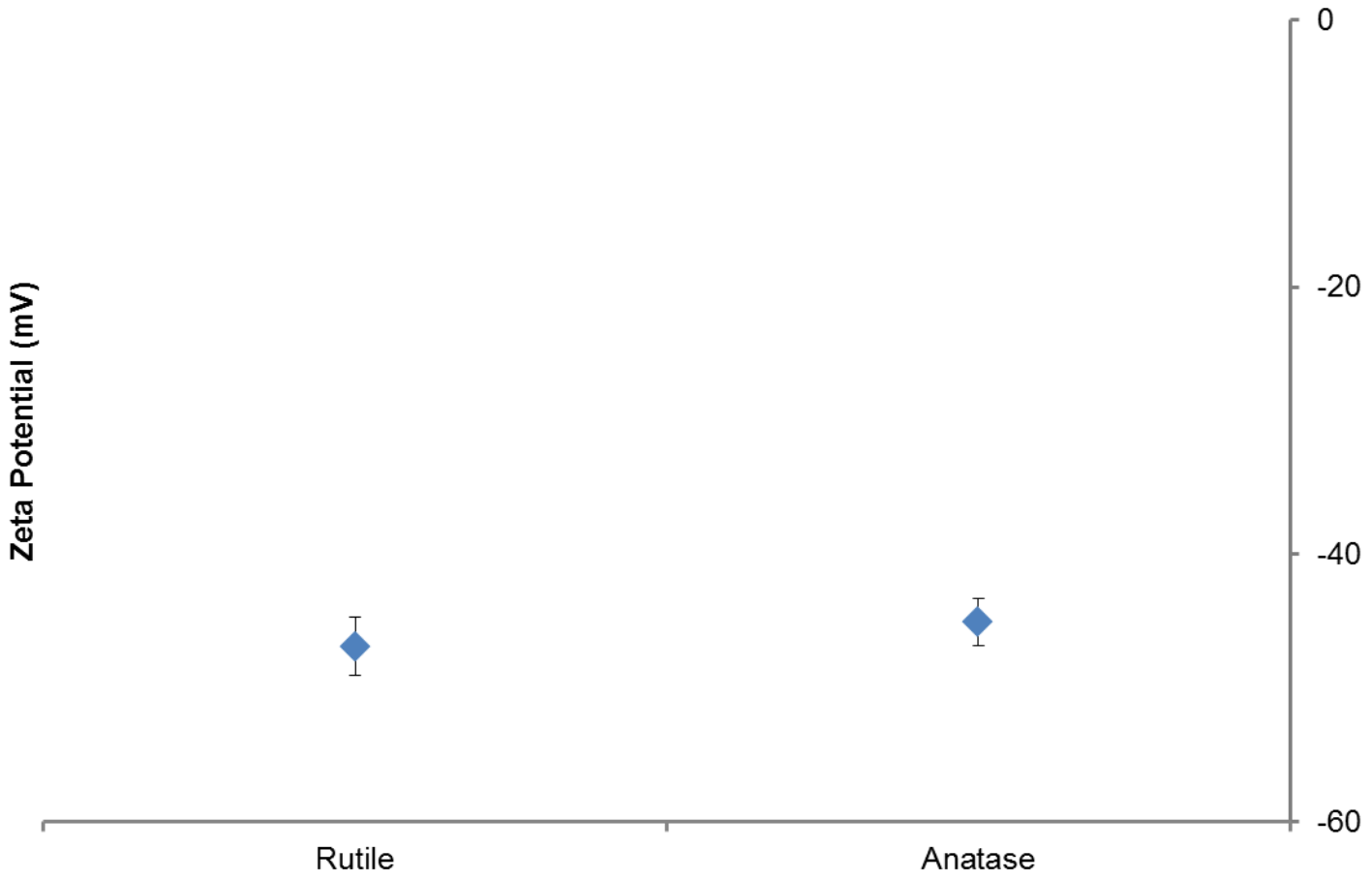

Figure 4-16. Zeta potential of rutile and anatase at pH 9

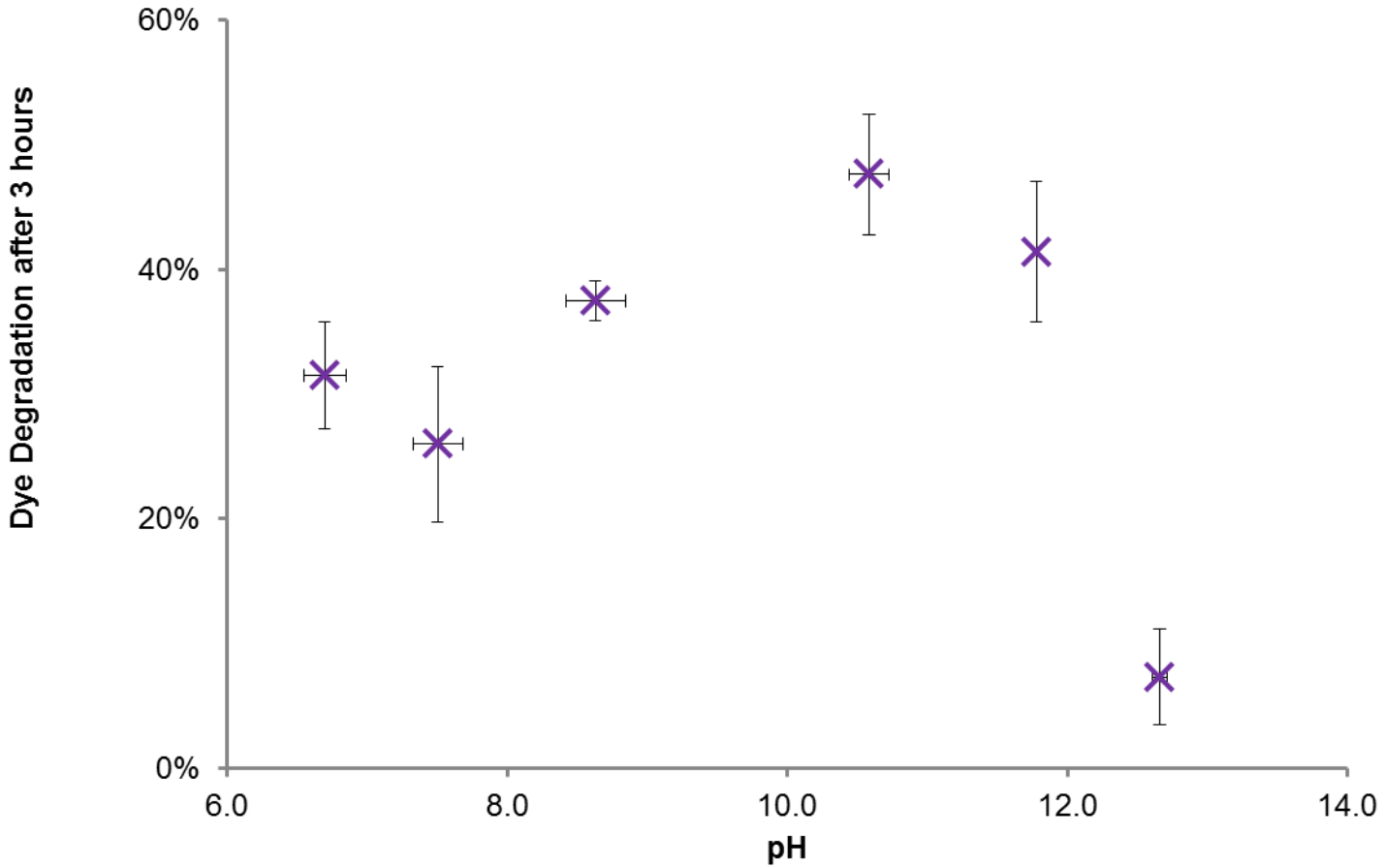

Figure 4-17. Relationship of dye degradation of rutile/anatase coating made from the suspensions adjusted at different pH after exposure to visible light irradiance of 2 W/m^2.

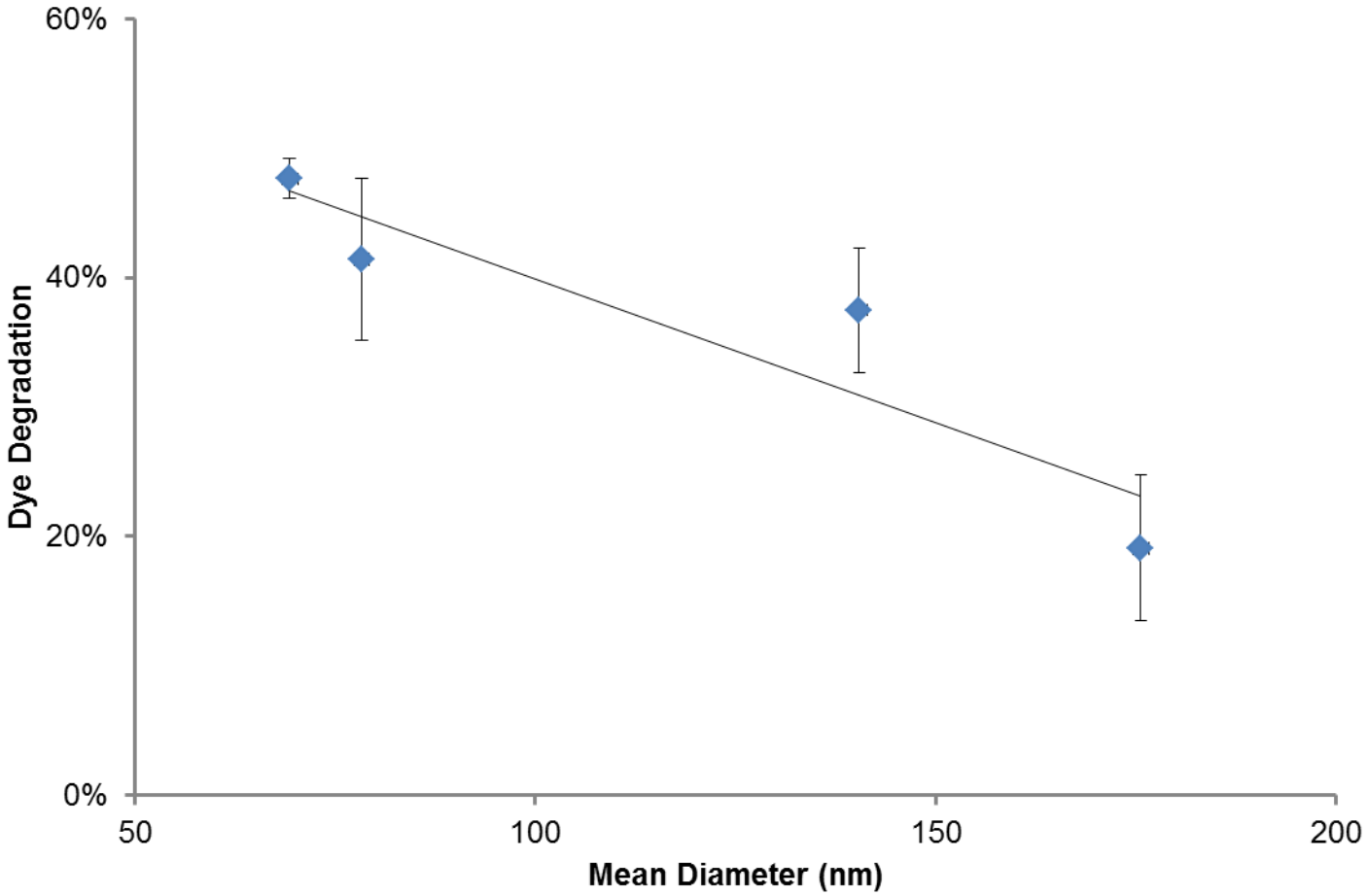

Figure 4-18. Relationship of dye degradation of rutile/anatase coating and the aqueous mean diameter of the suspension used to make the coating after exposure to visible light irradiance of 2 W/m^2.

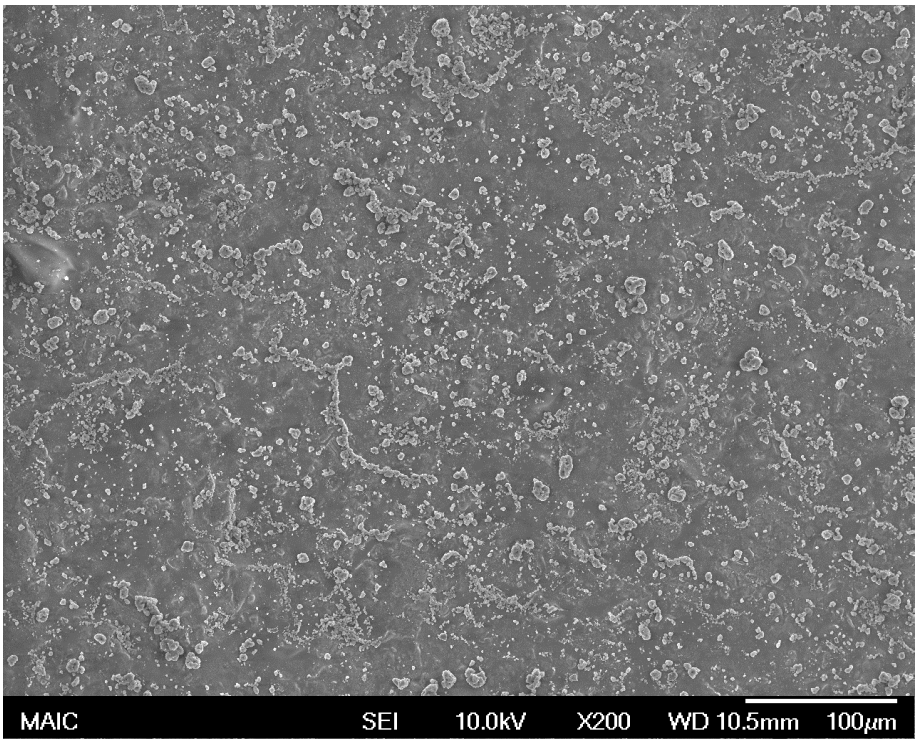

A

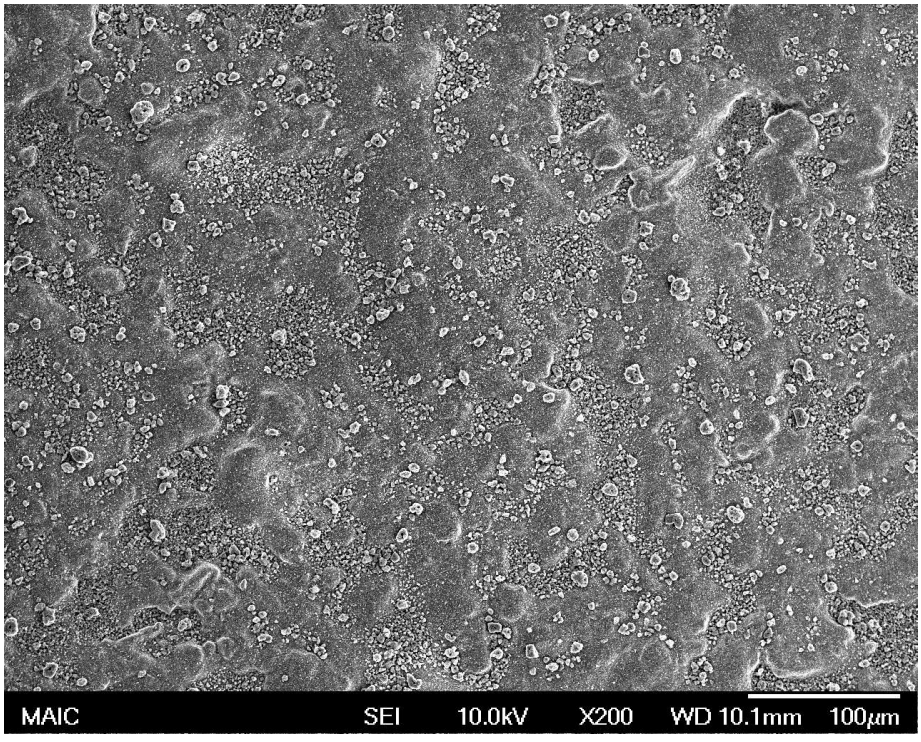

B

Figure 4-19. Scanning electron micrographs of rutile/anatase coating. A) deionized water (pH 6–7). B) 0.01 M of NaOH (pH 11.7)

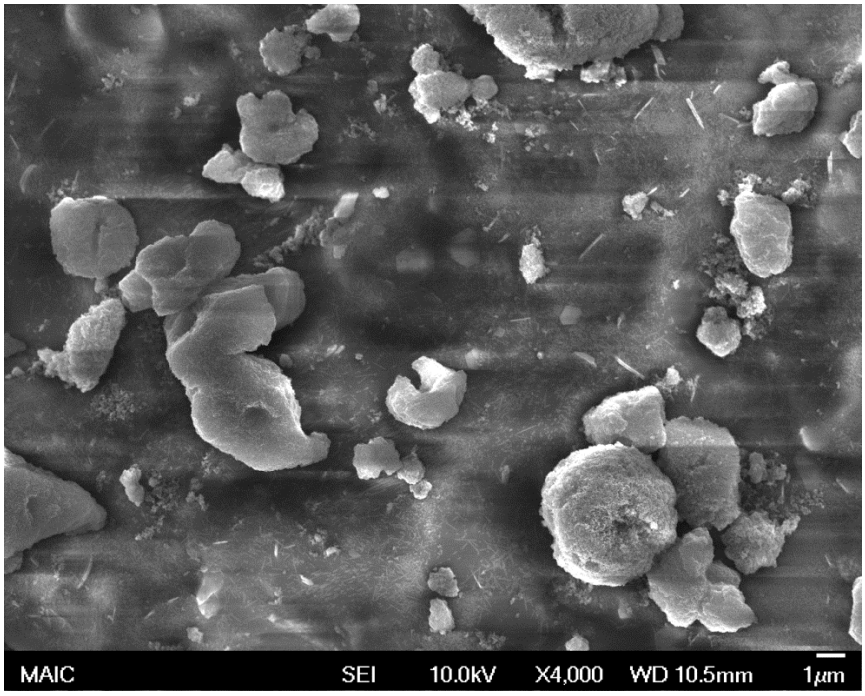

A

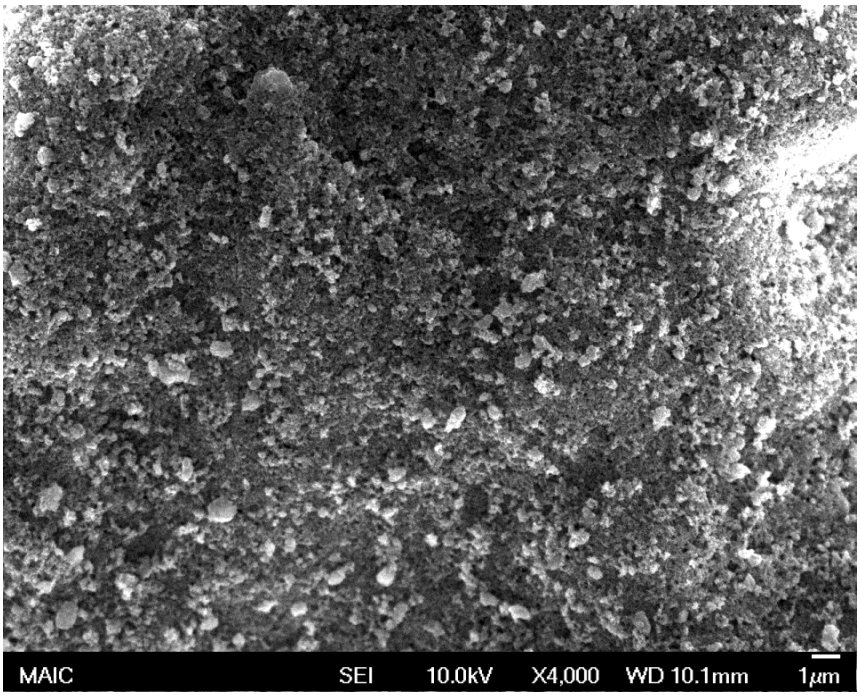

B

Figure 4-20. Scanning electron micrographs of rutile/anatase coating. A) deionized water (pH 6–7). B) 0.01 M of NaOH (pH 11.7). The feature in the images did not necessary represent the entire coating. However, larger aggregate with lower surface coverage of photocatalyst was more frequently observed for A

CHAPTER 5
PROTOTYPE TESTING OF TITANIUM DIOXIDE COATED ANTIMICROBIAL SURFACES

The effectiveness of PHF/TiO_2 nanocomposite in inactivating microbes on surface under both UVA and visible light irradiance was discussed in Chapters 2 and 3. Nanohygienix, a start-up company using TiO_2 based coatings to control indoor infections, expressed strong interest in applying PHF/TiO_2 nanocomposite as a photocatalyst for use in indoor facility with heavy human traffic.

Commercial sources of photocatalyst formulations that are claimed to have activity in the visible range include Showa Denko, Marusyo Sangyo and Sumitomo Chemicals from Japan, and Advanced Surface Treatments, BioShield, Inc. and EcoActive Surfaces, Inc. from the US. The Particle Engineering Research Center has tested visible light active photocatalysts from Japanese companies in our lab and found them to be incapable of microbial inactivation (unpublished data). Advanced Surface Treatments advertises their coatings for odor removal and organic degradation, but not for destruction of microbes. EcoActive Surfaces, Inc. has a visible light active product, OxiTitan™, which is reported to destroy 90% of virus and 66% of MRSA in 24 hours, respectively. It can be concluded that visible light photocatalysts that are capable of rapidly destroying harmful microbes (90% reduction of bacteria within few hours) are not commercially available.

The objective of the research reported in this chapter was to evaluate the effectiveness of coating indoor surfaces at three beta facilities with rutile/anatase and PHF/anatase formulations for photocatalytic inactivation of microbes. The beta facilities were Saint Stephen's Episcopal School (Bradenton, FL), Venice Regional Medical Center (VRMC) (Venice, FL) and Village on the Isle Retirement Facility (Venice, FL).

Surfaces at the beta facilities that were coated with a commercial product (Bioshield Primer and NuTiO) were monitored for comparison.

5.1 Experimental

5.1.1 Beta Facilities

Three beta facilities in Florida were chosen for testing prototype photocatalytic manufactured by the University of Florida, as described below.

Saint Stephen's Episcopal School (Bradenton, FL). Saint Stephen's Episcopal School is a private school (from PK3 to grade 12) located in Bradenton, Florida with 650 students enrollment. Three rooms (a dressing room in a gym and second grade classrooms #2 and #3) were selected for microbial sampling. Samples were taken from three different locations on the wall adjacent to the entrance; at one location on three different lockers; and at two locations on one bench and one location on a second bench in the dressing room (Fig. 5-1a and b). The dressing room had a fluorescent light that was left on continuously and no window. The visible irradiance measured at the sampled surfaces ranged from 0.04 to 0.07 W/m^2. In classrooms #2 and #3, three locations were tested on the wall adjacent to the window, the table and the counter top (Fig. 5-1c). Classrooms #2 and #3, which were across the hallway from each other, had windows and fluorescent lights that were turned off at night and on weekends. The visible irradiance at the sampled surfaces during the day ranged from 0.3 to 3.4 W/m^2, while the UVA irradiance ranged from 0.01 to 0.33 W/m^2.

Venice Regional Medical Center (Venice, FL). The Venice Regional Medical Center (VRMC) is a 312 bed regional healthcare system located in Venice, FL. Intensive care unit (ICU) stations 2, 3 and 4 were selected to collect microbial samples. Each ICU station contained a bed, counter top and closet (Fig. 5-2). Light was provided

by fluorescent lamps and windows. The visible irradiance measured at the sampled surfaces (wall, counter top, bed rail and knob) ranged from 0.5 to 2.02 W/m^2 (0.11 to 1.08 W/m^2 when the blind was closed). The UVA irradiance at the sampled surfaces ranged from 0 to 0.11 W/m^2 (0 W/m^2 when the blind was closed). Samples were taken in three different locations on each of the selected surfaces.

Village on the Isle retirement facility (Venice, FL). Village on the Isle is the licensed continuing care retirement community located in Venice, Florida. The facility provides independent living (Matthew Hall and Trinity Hall), assisted living (Mark Manor) and skilled nursing (Luke Haven). Microbial sampling was conducted at the Luke Haven Skilled Nursing Facility. Two patient rooms and a staff break room were selected for sampling. Each patient room contained two beds, a bathroom, chairs and cabinets. Light was provided by fluorescent lamps and windows. The visible irradiance measured at the sampled surfaces (wall, bathroom rail, soap dispenser, bed rail and thermostat) ranged from 0.16 to 1.87 W/m^2. The UVA irradiance at the sampled surfaces ranged from 0 to 0.01 W/m^2. The staff break room contained a table, counter top, chairs, lockers and two bathrooms. Light was provided by fluorescent lamps. The visible irradiance measured at the sampled surfaces (counter top, door knob and lockers) ranged from 0.32 to 0.6 W/m^2. The UVA irradiance at the sampled surfaces ranged from 0 to 0.01 W/m^2. Samples were taken in three different locations on each of the selected surfaces.

Visible and UVA irradiance was measured using a light detector (PMA2110, Solar Light Co., Glenside, PA) with UVA and visible light probes.

5.1.2 Chemicals and Reagents

Titanium dioxide (anatase, 7 nm; rutile, 20 nm) was obtained from MKnano (Williamsville, NY). Polyhydroxy fullerene (PHF) was synthesized in our laboratory according to the protocol of Gao et al. [22]. A 50% sodium hydroxide (NaOH) solution was obtained from Acros Organics (NJ, USA) and diluted to desired concentrations in deionized water. Commercial TiO_2 formulations (NuTiO Primer and NuTiO TiO_2) were obtained from Bioshield, Inc. (Fort Lauderdale, FL).

Tryptic soy agar (Becton, Dickinson and Company, Sparks, MD) was used to culture microbes. A mass of 40 g Tryptic soy agar powder was suspended in 1 L of deionized water and mixed thoroughly with heating to the boiling point. The solution was then autoclaved at 120 ºC and 16 bar for 15 minutes. Plates were made by pouring the autoclaved agar into 100×15 mm sterile plastic Petri dishes (Fisher Scientific) and air dried in a laminar flow hood (LABCONCO purifier class 2 safe cabinet) for 24 hours. The dried agar plates were used immediately or stored in inverted position in a refrigerator at 4°C.

5.1.3 Coating Preparation

Three different TiO_2 based, photocatalyst systems were used at the beta facilities. Photocatalyst system 1 consisted of Bioshield NuTiOTM TiO_2 formulation for use as top coat and Bioshield Primer formulation for use as bottom coat. Photocatalyst system 2 consisted of rutile/anatase formulation for use as top coat and Bioshield Primer formulation for use as bottom coat. Photocatalyst system 3 consisted of PHF/TiO_2 nanocomposite formulation for use as top coat and Bioshield Primer formulation for use as bottom coat.

The Bioshield NuTiOTM TiO2 and Bioshield Primer formulations were applied directly from the manufacturer's containers. The rutile/anatase formulation was prepared by adding 100 mg of rutile and 100 mg of anatase to 200 mL of diluted NaOH solution (pH = 9–9.5). The rutile/anatase suspension was sonicated (Misonix Sonicator 3000, Farmingdale, NY) at the highest power level (providing 180–200 W) for 30 minutes total (10 min on/2 min off × 3). This procedure was repeated to accumulate a total volume of 5 L. The PHF/TiO_2 nanocomposite formulation was prepared by adding 200 mg of anatase to 180 mL of diluted NaOH solution (pH = 9–9.5). The anatase suspension was sonicated (Misonix Sonicator 3000, Farmingdale, NY) at the highest power level (providing 180–200 W) for 30 minutes total (10 min on/2 min off × 3). A volume of 20 mL of PHF solution, containing 1000 mg/L of PHF, was then added and the suspension was mixed with magnetic stirrer for 10 minutes. This procedure was repeated to accumulate a total volume of 5 L.

All surfaces (walls, ceilings, furniture, attached fixtures, etc.) were steamed prior to coating to remove contaminants and ensure adhesion of the coating. After 15 minutes of drying, Bioshield NuTiOTM primer was applied using an electric sprayer (Model 2600, American Air & Water®, Inc. Hilton Head Island, SC). After 15 minutes of drying time, the top coat formulation was applied to all surfaces.

5.1.4 Microbial Sampling Procedures

After coatings were applied on surface, sterile cotton swabs were used to collect microbes from selected surfaces. A swab was immersed in sterile DI water, followed by wiping on selected surfaces (10×10 cm) back and forward 5 times. Microbes adhered to the wetted cotton were streaked on Tryptic soy agar plates. The plates were inverted

and then placed in a 37°C incubator for 48 hours. Colony forming units (CFUs) were counted.

5.2 Results

5.2.1 Saint Stephen's Episcopal School

Figure 5-3 shows the variation of microbe counts on a wall, lockers and benches coated with photocatalyst system 1 in the dressing room at Saint Stephens's Episcopal School. The microbial population on benches was much higher than those on the walls or lockers. A consistent decreasing trend (from 537 to 64 CFU/swab; almost a 90% reduction) in microbial counts was observed on the benches over a period of 8 months (Table 5-1). The walls and lockers were much less contaminated at the beginning. There were no consistent changes in counts on walls or lockers over an 8-month period.

Figure 5-4 shows the variation of microbe counts on a counter top, wall and table coated with photocatalyst system 1 in classroom #2. There was no consistent trend in microbe counts for any of the surfaces (Table 5-1)

Figure 5-5 shows the variation of microbe populations on uncoated counter top, wall and table in classroom #3. There was no consistent change on any of the surfaces (Table 5-1). A high spike in microbe counts for the table was observed at month 4.

It appears that marginal effect of photocatalyst system 1 in terms of reducing microbe populations

5.2.2 Venice Regional Medical Center

Figure 5-6 shows the variation of microbe populations on a wall, counter and bed rail in three different ICU stations at the Venice Regional Medical Center. A closet door knob was also sampled in two of the ICU stations.

The surfaces in station 2 were uncoated. In station 4, the surfaces were coated with photocatalyst system 1. In station 3, the surfaces were coated with photocatalyst system 2. As shown in Figure 5-6, the microbe counts of the selected surfaces in the VRMC were low at the initial sampling, ranging from 1 to 16 CFU/swab. Microbe counts on the bed rail in the ICU station coated with photocatalyst system 2 exhibited a decreasing trend, whereas counts on the wall and counter exhibited no consistent trend. (Table 5-2). At the ICU station coated with photocatalyst system 1, microbe counts were generally higher and more variable. No consistent trends in microbe counts were exhibited on any of the surfaces. Microbe counts in the uncoated ICU station exhibited very high numbers and variability between locations. There was an increasing trend in microbe counts on counter top and no consistent trends on the other surfaces (Table 5-2).

5.2.3 Luke Haven Skilled Nursing Facility

Figure 5-7 shows the variation of microbe counts on a wall, bathroom rail, soap dispenser, bed rail and thermostat among two patient rooms and door knob, lockers and counter top in a staff break room at the Luke Haven Skilled Nursing Facility. As can be seen from the microbe counts before treatment and after treatment, the effectiveness of steam cleaning was variable. Two months after coated with photocatalyst system 3, significant decreases in microbe counts were found six of the eight surfaces we sampled. Four of the eight surfaces showed more than 90% decrease in microbe counts. There was no significant change in microbe counts on two surfaces (wall in patient room and bathroom rail). In the case of walls, the initial count of microbes is very low, which made it difficult to quantify the effect. Minimal microbe reduction on the bathroom rails may be due to intermittent lighting in the bathroom.

5.3 Discussion

The variation of microbe count on all selected surfaces of the beta testing facilities was generally large, which may be due to the spatial random distribution of microbes in the built environment. The spatial distribution of microbe is affected by building attributes, such as the source of ventilation air, airflow rates, relative humidity and temperature.[111]

Photocatalyst system 1 failed to kill microbes effectively, but seemed to have an effect on preventing microbe reproduction. A consistent decrease in microbe counts on the benches coated with photocatalyst system 1 in the dressing room of Saint Stephen's Episcopal School was observed. This may be due to constant lighting condition, making the coating more efficient. The microbial counts at all the ICU stations were low because the units were subject to frequent cleaning with chemical disinfectants. Low microbial counts made it harder to quantify microbial reduction. However, photocatalyst system 2 still manifested an inactivation effect on one of the coated surfaces. Steam cleaning was inconsistent in killing all the microbes on surfaces at the Luke Haven Skilled Nursing Facility. Extended steaming may be required for more effective inactivation of microbes on surfaces prior to coating. Photocatalyst system 3 has only been monitored at one time (2 months) after coating. The preliminary indication is that this photocatalyst system is superior to the other photocatalyst systems. This suggests that polyhydroxy fullerene has an extended beneficial effect on photocatalysis. However, additional testing in the Luke Haven facility is required to confirm this conclusion.

5.4 Summary

- Without photocatalyst coating, microbe counts in indoor facilities subject to heavy human traffic are typically variable and, in some cases, trend upwards with time.
- A commercial photocatalyst and a rutile/anatase based photocatalyst were marginally effective in reducing microbe counts in the facilities.
- A PHF/anatase nanocomposite based system is still in testing phase, but has exhibited promising capability for reducing microbe counts at a beta facility.
- Steam cleaning procedure currently used by NanoHygienix is inconsistent at reducing initial microbe counts prior to coating.

Table 5-1. Identification of trends in microbe counts at Saint Stephen's Episcopal School

	Dressing room (coated with PS 1)			Classroom #2 (coated with PS 1)			Classroom #3 (uncoated)		
	wall	lockers	benches	counter top	wall	table	counter top	wall	table
r	-0.098	0.522	-0.745	-0.207	-0.228	-0.187	0.508	-0.248	0.002
P	0.763	0.081	0.005	0.519	0.476	0.561	0.1107	0.437	0.995
Trend*	No change	No change	Decrease	No change	No change	No change	No change	No change	No change

r: Pearson correlation coefficient
*Based on P ≤ 0.05

Table 5-2. Identification of trends in microbe counts at Venice Regional Medical Center

	Station 3 (coated with PS 2)			Station 4 (coated with PS 1)				Station 2 (uncoated)			
	wall	counter	bed rail	wall	counter	knob	bed rail	wall	counter	knob	bed rail
r	-0.120	-0.315	-0.736	0.000	0.603	-0.438	-0.035	-0.294	0.662	-0.082	0.712
P	0.742	0.375	0.024	1.000	0.065	0.205	0.923	0.409	0.037	0.821	0.113
Trend*	No change	No change	Decrease	No change	No change	No change	No change	No change	Increase	No change	No change

r: Pearson correlation coefficient
*Based on P ≤ 0.05

A B

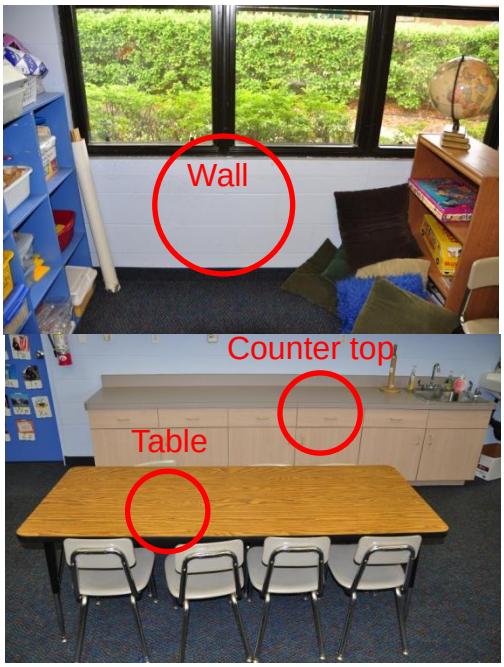

C

Figure 5-1. Microbial sampling locations at Saint Stephen's Episcopal School. A) Wall in the dressing room. B) Benches and lockers in the dressing room. C) Wall, counter top and table in one of the classrooms

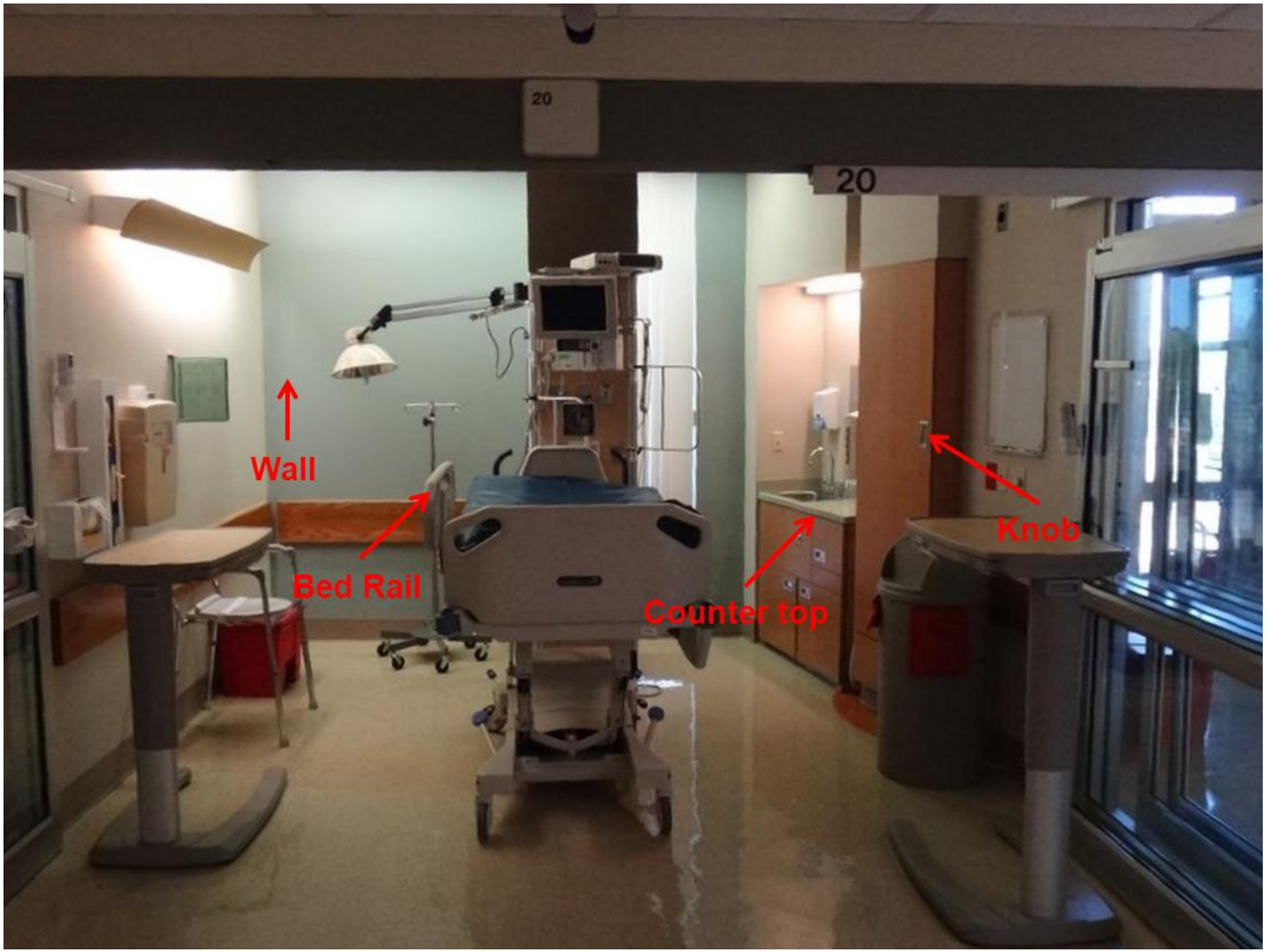

Figure 5-2. Microbial sampling locations of an ICU station at Venice Regional Medical Center: wall, bed rail, counter top and (door) knob

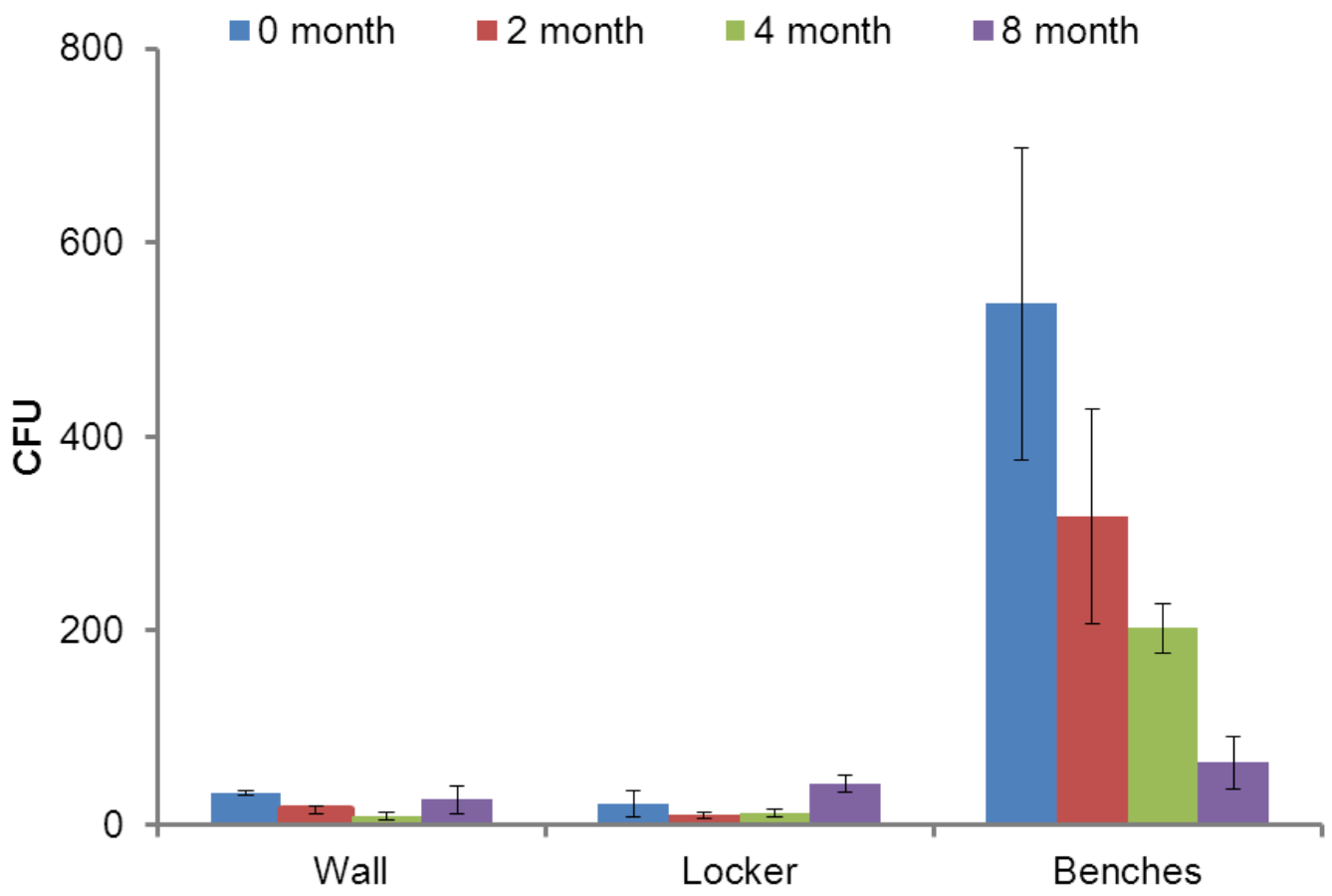

Figure 5-3. Time-dependent change in microbe counts on surfaces coated with photocatalyst system 1 in the dressing room of Saint Stephen's Episcopal School

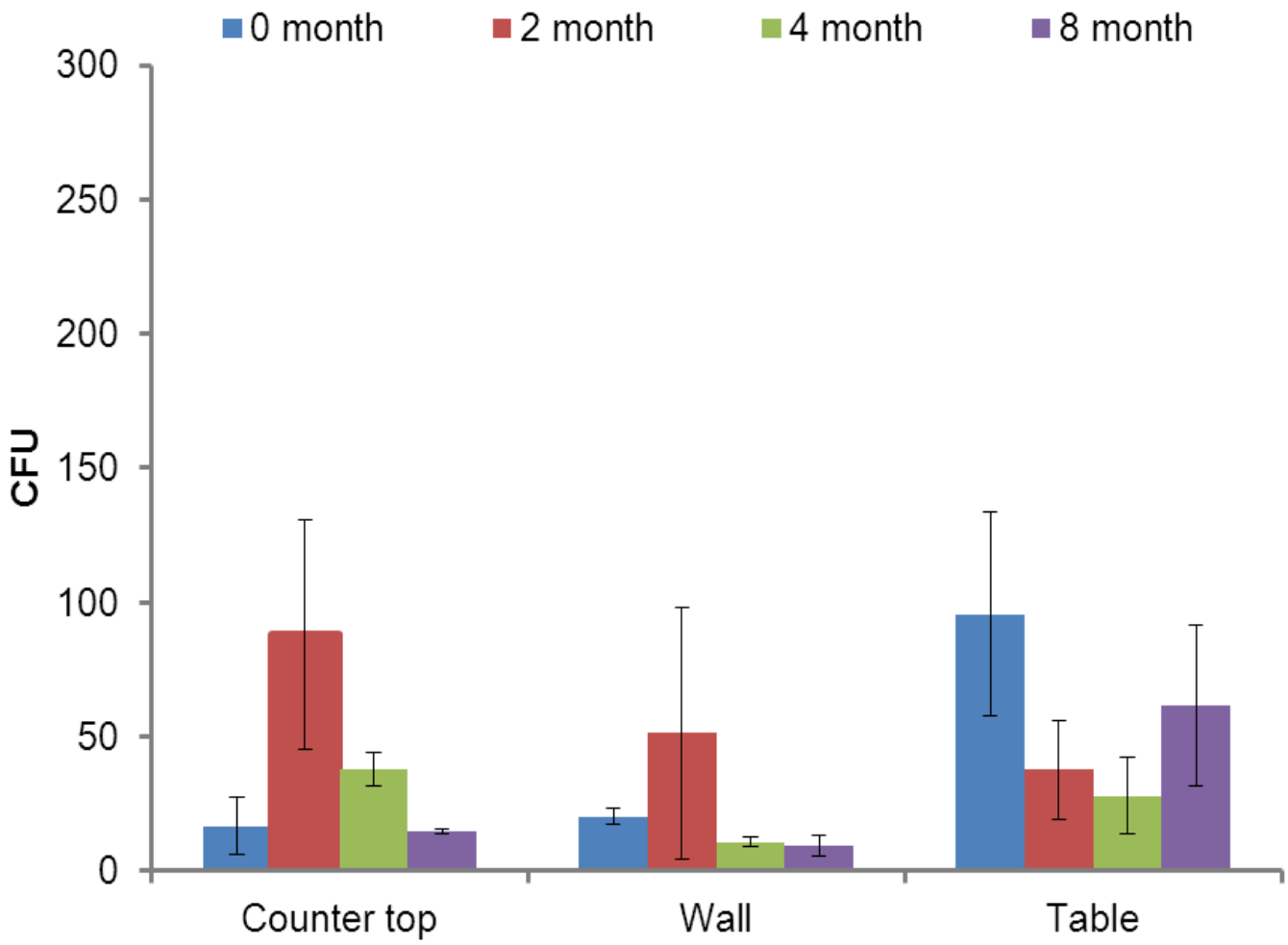

Figure 5-4. Time-dependent change in microbe counts on surfaces coated with photocatalyst system 1 in classroom #2 of Saint Stephen's Episcopal School

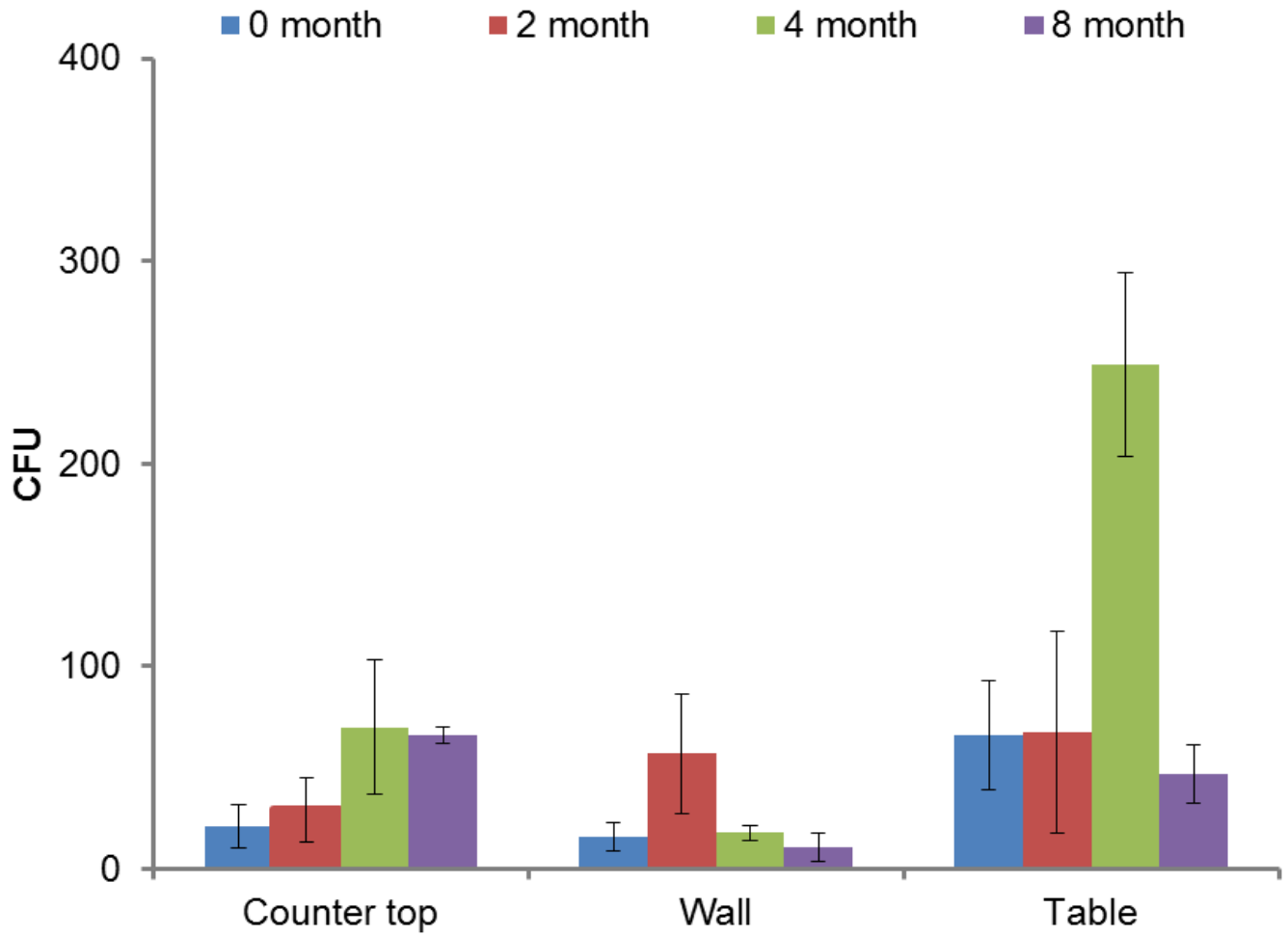

Figure 5-5. Time-dependent change in CFU on uncoated surfaces in Classroom 3 of Saint Stephen's Episcopal School

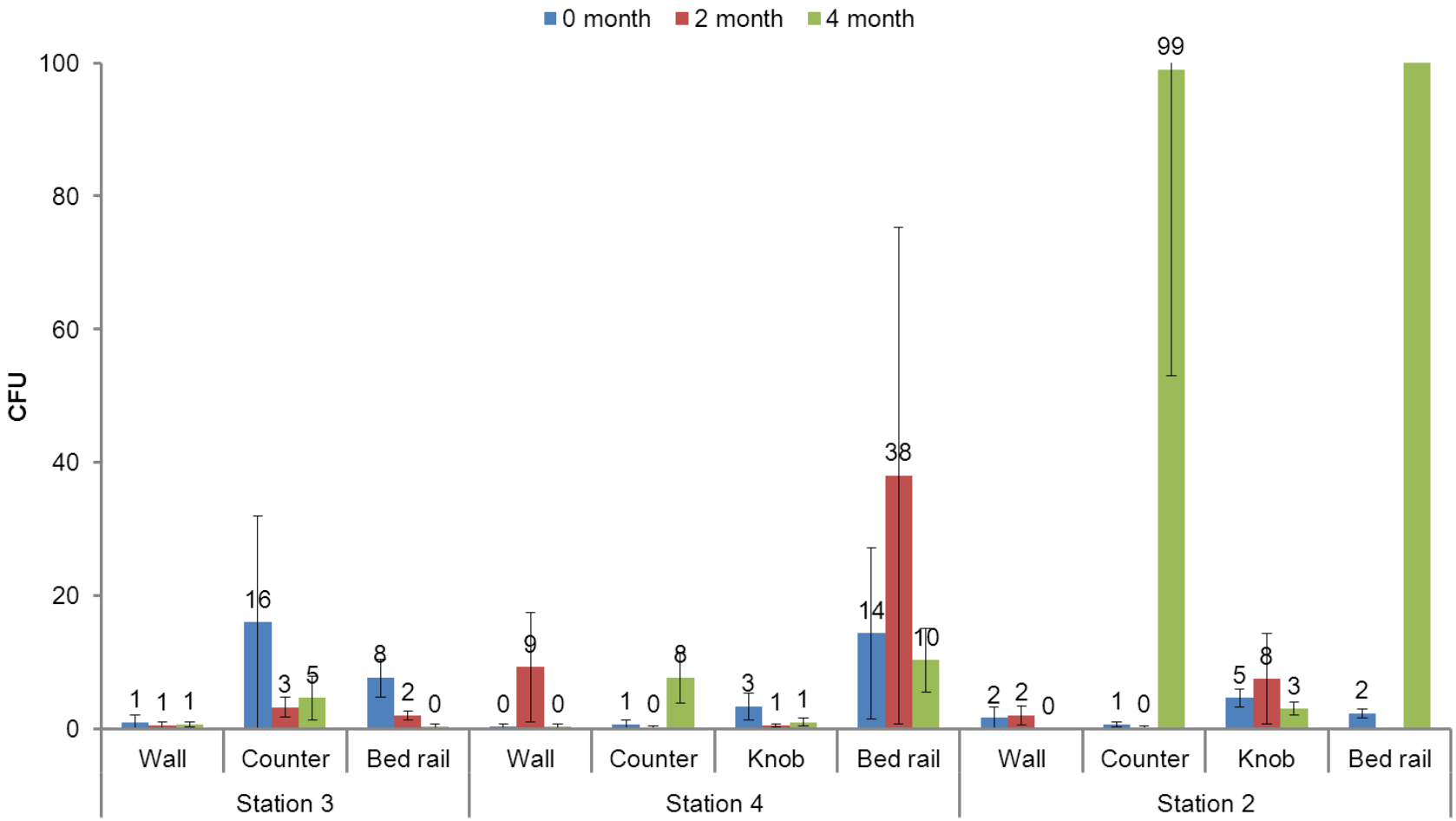

Figure 5-6. Time-dependent changes in microbe counts on surfaces in the ICU stations of Venice Regional Medical Center. Surfaces in station 2 were not coated; surfaces in station 4 were previously coated with photocatalyst system 1; surfaces in station 3 were coated with photocatalyst system 2

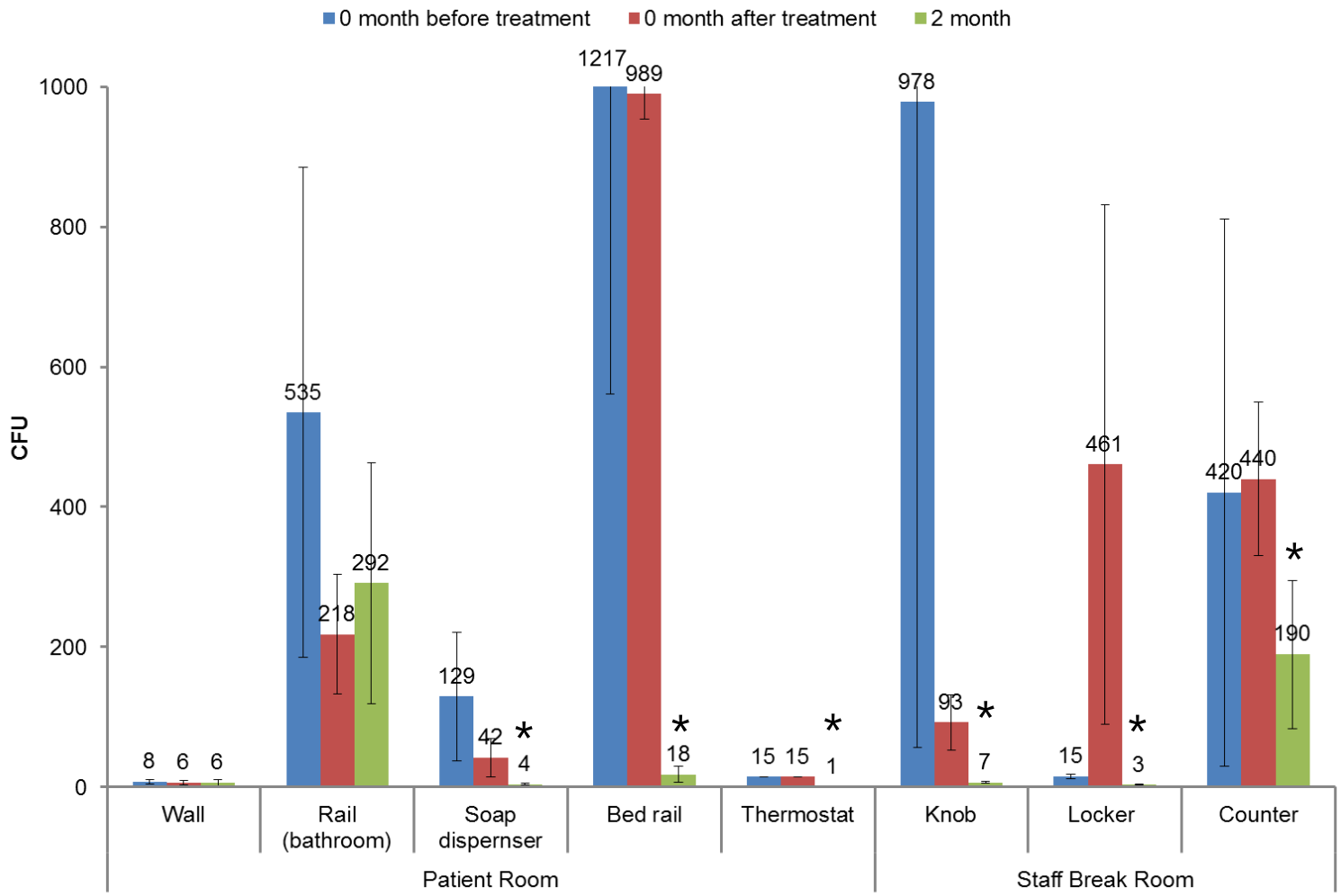

Figure 5-7. Time-dependent changes in microbe counts on surfaces coated with photocatalyst system 3 in the Luke Haven Skilled Nursing Facility of Village on the Isle Retirement Facility. Sampling locations where a significant decrease ($P < 0.05$) in microbe counts between the treatment date and the latest sampling date are marked by an asterisk

CHAPTER 6
CONCLUSIONS AND RECOMMENDATIONS FOR FURTHER RESEARCH

In the present study, thin, transparent coatings of anatase and rutile were found to be capable of inactivating microorganisms under UVA or visible light. Polyhydroxy fullerene was found to adsorb to anatase and enhance the rate at which photocatalytic inactivation takes place by a factor of two to three. Photocatalysis on both anatase and PHF/anatase coatings under UVA is capable of inactivating highly resistant spores of a common household fungus, *Asperigillus niger*. Under visible light, photocatalysis on both anatase and PHF/anatase coatings is capable of inactivating a bacterium commonly used as a surrogate of MRSA, *Staphylococcus aureus*. The degree to which both UVA and visible light photocatalysis is enhanced by PHF is controlled by the percentage of the anatase surface that is covered by this molecule.

The ability of nano TiO_2 coatings to catalyze dye degradation and microbe inactivation under visible light is unexpected, considering the measured band gaps of these materials. Utilization of visible spectrum by rutile and anatase has been confirmed with optical filter studies. While both rutile and anatase are capable of utilizing sub-400 nm light, only rutile can use light in the 400 nm to 500 range, and most of its activity is from light in this range. Anatase cannot use light in the 400-500 nm range, indicating that most of its photocatalytic activity is from light in the supra-500 nm portion of the spectrum. The confirmed purity of the TiO_2 powders used rule out aluminum or silicon as inadvertent dopants. Recent literature that raises the possibility that surface band gap can differ from bulk band gap and may explain this studies' findings.

Stabilization of aqueous TiO_2 suspensions prior to application to coat surfaces is important from the point of view of compatibility with spray application equipment and,

furthermore, has a strong influence on coating performance. Despite their effectiveness in stabilizing aqueous TiO_2 suspensions, surfactants are not practical as dispersants because they act as free radical sinks in the coating and thus impair coating performance. Sodium hydroxide at is also effective as a dispersant and at concentrations of 1E-2 M or less, does not impair coating performance. Aggregate size influences surface coverage and consequently performance of TiO_2 coatings. Maintaining TiO_2 aqueous formulations within a pH range that stabilizes the formulations thus improves photocatalytic activity of coatings prepared from the formulations.

The well dispersed, photocatalytic active rutile/anatase and PHF/anatase nanocomposite formulations developed in the present study were applied and evaluated in the beta testing facilities, as compared to the commercial photocatalyst formulation (NuTiO TiO_2) and uncoated surfaces. Without photocatalyst coating, microbe counts in indoor facilities subject to heavy human traffic are typically variable and, in some cases, trend upwards with time. The commercial photocatalyst and a rutile/anatase based photocatalyst were marginally effective in reducing microbe counts in the testing facilities. The PHF/anatase nanocomposite based system is still in testing phase, but has exhibited promising capability for reducing microbe counts at a beta facility.

Based on the findings of the present research, the first proposed task for future research is to investigate the mechanism on differential visible light spectrum utilization by rutile22 and anatase7. Rutile22 was found to utilize visible light mainly between 400 and 495 nm in this study. This result is consistent with the findings of Ariga *et al.*[30], in which he proposed that the surface band gap (2.3 eV) of rutile differed from its bulk

band gap (3.0 eV). Anatase7 was found to be active under visible light irradiance beyond 495 nm, but not active between 400 and 495 nm. This surprising finding has not been reported in the literature yet. Experiments with additional optical filters at the cut-off wavelength of 590 nm (provides zero transmission below 570 nm) and at the cut-off wavelength of 665 nm (provides zero transmission below 640 nm) are required to identify the specific visible light spectrum of the fluorescent lamp that anatase7 can use. Further studies are needed to identify whether surface aberrations in the crystal lattice of TiO_2 contributed to visible light activity.

PHF/TiO_2 nanocomposite is subject to mechanical abrasion in indoor facilities with heavy human traffic. Thus, the second proposed task is to evaluate the adhesion property of PHF/TiO_2 nanocomposite to common surfaces. Commercial wipe can be used to test the removal of PHF/TiO_2 deposited on some common surfaces such as ceramics, glasses or metal surfaces. SEM-EDS can provide qualitative and quantitative analysis of the remaining of PHF/TiO_2 coating after wiping. Alternatively, developing a chemical binder for PHF/TiO_2 nanocomposite can extend the lifetime usage of the coating applied in indoor facilities. Binder selected or developed for the PHF/TiO_2 nanocomposite should have the following characteristics: high adherence, minimum effect on PHF/TiO_2 performance, non-toxic and low cost.

The third proposed task is to conduct prototype testing of PHF/TiO_2 nanocomposite coating with more controlled parameters. Light sensors can be employed to record the total exposure time. Temperature and relative humidity should be monitored. The infection rate in the testing facilities should be recorded as well. All

these parameters should be taken into account to identify the effectiveness of PHF/TiO_2 nanocomposite coating.

LIST OF REFERENCES

(1) Chauhan, N.; Latge, J.P.; Calderone, R. Signalling and oxidant adaptation in *Candida Albicans* and *Aspergillus Fumigatus*. *Nature Reviews Microbiology* **2006,** *4,* (6), 435-444.

(2) Paterson, D.L. Resistance in gram-negative bacteria: enterobacteriaceae. *American Journal of Infection Control* **2006,** *34,* (5 Suppl 1), S20-8; discussion S64-73.

(3) Rice, L.B. Antimicrobial resistance in gram-positive bacteria. *American Journal of Infection Control* **2006,** *34,* (5 Suppl 1), S11-9; discussion S64-73.

(4) Schwab, C.J. and Straus, D.C. The roles of *Penicillium* and *Aspergillus* in sick building syndrome. *Advances in Applied Microbiology* **2004,** *55,* 215-238.

(5) Utrup, L.J.; Werner, K.; Frey, A.H. Minimizing pathogenic bacteria, including spores, in indoor air. *Journal of Environmental Health* **2003,** *66,* (5), 19-26, 29.

(6) Influenza *2012,* (06/20)

(7) BusinessInsider *2012,* (6/20)

(8) Klein, E.; Smith, D.L.; Laxminarayan, R. Hospitalizations and deaths caused by methicillin-resistant *Staphylococcus Aureus*, United States, 1999–2005. *Emerging Infectious Diseases* **2007,** *13,* (12), 1840-1846.

(9) NHLBI Morbidity & mortality: 2007 chartbook on cardiovascular, lung, and blood diseases, L. national heart, and blood institute. **2007**.

(10) Cummins, S.K. and Jackson, R.J. The built environment and children's health. *Pediatric Clinics of North America* **2001,** *48,* (5), 1241-1252.

(11) Friedman, M.S. Impact of changes in transportation and commuting behaviors during the 1996 summer olympic games in Atlanta on air quality and childhood asthma *JAMA: The Journal of the American Medical Association* **2001,** *285,* (7), 897-905.

(12) Lanphear, B.P.; Aligne, C.A.; Auinger, P.; Weitzman, M.; Byrd, R.S. Residential exposures associated with asthma in US children *Pediatrics* **2001,** *107,* (3), 505-511.

(13) Krishna, V.B. Enhancement of titanium dioxide photocatalysis with polyhydroxy fullerenes. *University of Florida* **2007** c

(14) Block, S.S. *Disinfection, sterilization and preservation.* Philadelphia, PA: Lippincott Williams & Wilkins: **2001**.

(15) Page, K.; Wilson, M.; Parkin, I.P. Antimicrobial surfaces and their potential in reducing the role of the inanimate environment in the incidence of hospital-acquired infections. *Journal of Materials Chemistry* **2009,** *19,* (23), 3819-3831.

(16) Hoffmann, M.R.; Martin, S.T.; Choi, W.; Bahnemann, W. Environmental applications of semiconductor photocatalysis. *Chemical Review* **1995,** *95,* 69-96.

(17) Rochette, P.J. UVA-induced cyclobutane pyrimidine dimers form predominantly at thymine-thymine dipyrimidines and correlate with the mutation spectrum in rodent cells. *Nucleic Acids Research.* **2003,** *31,* (11), 2786-2794.

(18) Asahi, R.; Morikawa, T.; Ohwaki, T.; Aoki, K.; Taga, Y. Visible-light photocatalysis in nitrogen-doped titanium oxides. *Science* **2001,** *293,* (5528), 269-271.

(19) In, S.; Orlov, A.; Berg, R.; García, F.; Pedrosa-Jimenez, S.; Tikhov, M.S.; Wright, D.S.; Lambert, R.M. Effective visible light-activated B-doped and B, N-codoped TiO_2 photocatalysts. *Journal of the American Chemical Society* **2007,** *129,* (45), 13790-13791.

(20) Zhu, L.; Cui, X.; Shen, J.; Yang, X.; Zhang, Z. Visible light photoelectrochemical response of carbon- doped TiO_2 thin films prepared by DC reactive magnetron sputtering. *Acta Physico-Chimica Sinica* **2007,** *23,* (11), 1662-1666.

(21) Ksibi, M.; Rossignol, S.; Tatibouët, J.; Trapalis, C. Synthesis and solid characterization of nitrogen and sulfur-doped TiO_2 photocatalysts active under near visible light. *Materials Letters* **2008,** *62,* (26), 4204-4206.

(22) Iwasaki, M.; Hara, M.; Kawada, H.; Tada, H.; Ito, S. Cobalt ion-doped TiO_2 photocatalyst response to visible light. *Journal of Colloid and Interface Science* **2000,** *224,* (1), 202-204.

(23) Borgarello, E.; Kiwi, J.; Graetzel, M.; Pelizzetti, E.; Visca, M. Visible light induced water cleavage in colloidal solutions of chromium-doped titanium dioxide particles. *Journal of the American Chemical Society* **1982,** *104,* (11), 2996-3002.

(24) Klosek, S. and Raftery, D. Visible light driven V-doped TiO_2 photocatalyst and its photooxidation of ethanol. *The Journal of Physical Chemistry B* **2001,** *105,* (14), 2815-2819.

(25) Zhu, J.; Chen, F.; Zhang, J.; Chen, H.; Anpo, M. Fe^{3+}-TiO_2 photocatalysts prepared by combining sol–gel method with hydrothermal treatment and their characterization. *Journal of Photochemistry and Photobiology A: Chemistry* **2006,** *180,* (1-2), 196-204.

(26) Choi, W.; Termin, A.; Hoffmann, M.R. The role of metal ion dopants in quantum-sized TiO_2: Correlation between photoreactivity and charge carrier recombination dynamics. *The Journal of Physical Chemistry* **1994,** *98,* (51), 13669-13679.

(27) Chen, X.; Liu, L.; Yu, P.Y.; Mao, S.S. Increasing solar absorption for photocatalysis with black hydrogenated titanium dioxide nanocrystals. *Science* **2011,** *331,* 746-750.

(28) Tao, J.; Luttrell, T.; Batzill, M. A two-dimensional phase of TiO_2 with a reduced bandgap. *Nature Chemistry* **2011,** *3,* 296-300.

(29) Zuo, F.; Wang, L.; Wu, T.; Zhang, Z.; Borchardt, D.; Feng, P. Self-doped Ti^{3+} enhanced photocatalyst for hydrogen production under visible light. *Journal of the American Chemical Society* **2010,** *132,* (34), 11856-11857.

(30) Ariga, H.; Taniike, T.; Morikawa, H.; Tada, M.; Min, B.K.; Watanabe, K.; Matsumoto, Y.; Ikeda, S.; Saiki, K.; Iwasawa, Y. Surface-mediated visible-light photo-oxidation on pure TiO_2(001). *Journal of the American Chemical Society* **2009,** *131,* (41), 14670-14672.

(31) Wu, T.; Liu, G.; Zhao, J.; Hidaka, H.; Serpone, N. Photoassisted degradation of dye pollutants. V. self-photosensitized oxidative transformation of rhodamine bunder visible light irradiation in aqueous TiO_2 dispersions. *The Journal of Physical Chemistry B* **1998,** *102,* (30), 5845-5851.

(32) Wu, T.; Lin, T.; Zhao, J.; Hidaka, H.; Serpone, N. TiO_2-assisted photodegradation of dyes. 9. photooxidation of a squarylium cyanine dye in aqueous dispersions under visible light irradiation. *Environmental Science & Technology* **1999,** *33,* (9), 1379-1387.

(33) Xu, Y. and Langford, C.H. UV- or visible-light-induced degradation of X3B on TiO_2 nanoparticles: The influence of adsorption. *Langmuir* **2001,** *17,* (3), 897-902.

(34) Cho, Y.; Choi, W.; Lee, C.; Hyeon, T.; Lee, H. Visible light-induced degradation of carbon tetrachloride on dye-sensitized TiO_2. *Environmental Science & Technology* **2001,** *35,* (5), 966-970.

(35) Hara, K.; Miyamoto, K.; Abe, Y.; Yanagida, M. Electron transport in coumarin-dye-sensitized nanocrystalline TiO_2 electrodes. *The Journal of Physical Chemistry B* **2005,** *109,* (50), 23776-23778.

(36) Vinodgopal, K.; Hua, X.; Dahlgren, R.L.; Lappin, A.G.; Patterson, L.K.; Kamat, P.V. Photochemistry of ru(bpy)$_2$(dcbpy)$^{2+}$ on Al_2O_3 and TiO_2 surfaces. an insight into the mechanism of photosensitization. *The Journal of Physical Chemistry* **1995,** *99,* (27), 10883-10889.

(37) Abe, R.; Hara, K.; Sayama, K.; Domen, K.; Arakawa, H. Steady hydrogen evolution from water on eosin Y-fixed TiO_2 photocatalyst using a silane-coupling reagent under visible light irradiation. *Journal of Photochemistry and Photobiology A: Chemistry* **2000,** *137,* (1), 63-69.

(38) Skotheim, T. Photovoltaic properties of Au–merocyanine–TiO_2 sandwich cells. I. dark electrical properties and transient effects. *The Journal of Chemical Physics* **1982,** *77,* (12), 6144.

(39) Chatterjee, D.; Patnam, V.R.; Sikdar, A.; Joshi, P.; Misra, R.; Rao, N.N. Kinetics of the decoloration of reactive dyes over visible light-irradiated TiO_2 semiconductor photocatalyst. *Journal of Hazardous Materials* **2008,** *156,* (1-3), 435-441.

(40) Vinodgopal, K.; Stafford, U.; Gray, K.A.; Kamat, P.V. Electrochemically assisted photocatalysis. 2. the role of oxygen and reaction intermediates in the degradation of 4-chlorophenol on immobilized TiO_2 particulate films. *The Journal of Physical Chemistry* **1994,** *98,* (27), 6797-6803.

(41) Vinodgopal, K.; Bedja, I.; Kamat, P.V. Nanostructured semiconductor films for photocatalysis. photoelectrochemical behavior of SnO_2/TiO_2 composite systems and its role in photocatalytic degradation of a textile azo dye. *Chemistry of Materials* **1996,** *8,* (8), 2180-2187.

(42) Hoffman, A.J.; Mills, G.; Yee, H.; Hoffmann, M.R. Q-sized cadmium sulfide: Synthesis, characterization, and efficiency of photoinitiation of polymerization of several vinylic monomers *The Journal of Physical Chemistry* **1992,** *96,* (13), 5546-5552.

(43) Howe, R.F. Recent developments in photocatalysis. *Developments in Chemical Engineering and Mineral Processing* **1998,** *6,* (1-2), 55-84.

(44) Martin, S.T.; Herrmann, H.; Choi, W.; Hoffmann, M.R. Photochemical destruction of chemical contaminants on quantum-sized semiconductor particles. *Solar Engineering* **1995,** *1,* 409.

(45) Beydoun, D.; Amal, R.; Low, G.; McEvoy, S. Role of nanoparticles in photocatalysis. *Journal of Nanoparticle Research* **1999,** *1,* (4), 439-458.

(46) Kormann, C.; Bahnemann, D.W.; Hoffmann, M.R. Preparation and characterization of quantum-size titanium dioxide. *The Journal of Physical Chemistry* **1988,** *92,* (18), 5196-5201.

(47) Wang, C.; Zhang, Z.; Ying, J.Y. Photocatalytic decomposition of halogenated organics over nanocrystalline titania. *Nanostructured Materials* **1997,** *9,* (1-8), 583-586.

(48) Zhang, Z.; Wang, C.; Zakaria, R.; Ying, J.Y. Role of particle size in nanocrystalline TiO_2-based photocatalysts. *The Journal of Physical Chemistry B* **1998,** *102,* (52), 10871-10878.

(49) Satoh, N.; Nakashima, T.; Kamikura, K.; Yamamoto, K. Quantum size effect in TiO_2 nanoparticles prepared by finely controlled metal assembly on dendrimer templates. *Nature Nanotechnology* **2008,** *3,* (2), 106-111.

(50) Yan, M.; Chen, F.; Zhang, J.; Anpo, M. Preparation of controllable crystalline titania and study on the photocatalytic properties. *The Journal of Physical Chemistry B.* **2005,** *109,* (18), 8673-8678.

(51) Arabatzis, I.M.; Stergiopoulosa, T.; Bernardc, M.C.; Laboud, D.; Neophytidesd, S.G.; Falaras, P.M. Silver-modified titanium dioxide thin films for efficient photodegradation of methyl orange. *Applied Catalysis B: Environmental* **2003,** *42,* (2), 187-201.

(52) Arabatzis, I.M.; Stergiopoulosa, T.; Andreevab, D.; Kitovac, S.; Neophytidesd, S.G.; Falaras, P. Characterization and photocatalytic activity of Au/TiO_2 thin films for azo-dye degradation. *Journal of Catalysis* **2003,** *220,* (1), 127-135.

(53) Sun, B.; Vorontsov, A.; Smirniotis, P. Role of platinum deposited on TiO_2 in phenol photocatalytic oxidation. *Langmuir* **2003,** *19,* (8), 3151-3156.

(54) Ghows, N. and Entezari, M.H. Fast and easy synthesis of core-shell nanocrystal (CdS/TiO_2) at low temperature by micro-emulsion under ultrasound. *Ultrasonics Sonochemistry* **2010,** *18,* (2), 629-634.

(55) Marcì, G.; Augugliaro, V.; López-Muñoz, M.J.; Martín, C.; Palmisano, L.; Rives, V.; Schiavello, M.; Tilley, R.J.D.; Venezia, A.M. Preparation characterization and photocatalytic activity of polycrystalline ZnO/TiO_2 systems. 1. surface and bulk characterization. *The Journal of Physical Chemistry B* **2001,** *105,* (5), 1026-1032.

(56) Brahimi, R.; Bessekhouad, Y.; Bouguelia, A.; Trari, M. Visible light induced hydrogen evolution over the heterosystem Bi_2S_3/TiO_2. *Catalysis Today* **2007,** *122,* (1-2), 62-65.

(57) Kroto, H.W.; Heath, J.R.; O'Brien, S.C.; Curl, R.F.; Smalley, R.E. C_{60}: Buckminsterfullerene. *Nature* **1985,** *318,* 162-163.

(58) Krishna, V.; Noguchi, N.; Koopman, B.; Moudgil, B. Enhancement of titanium dioxide photocatalysis by water-soluble fullerenes. *Journal of Colloid and Interface Science* **2006,** *304,* (1), 166-171.

(59) Bouras, P.; Stathatos, E.; Lianos, P. Pure versus metal-ion-doped nanocrystalline titania for photocatalysis. *Applied Catalysis B: Environmental* **2007,** *73,* (1-2), 51-59.

(60) Rampaul, A.; Parkin, I.P.; O'Neill, S.A.; DeSouza, J.; Mills, A.; Elliott, N. Titania and tungsten doped titania thin films on glass; active photocatalysts. *Polyhedron* **2003,** *22,* (1), 35-44.

(61) Krishna, V.; Pumprueg, S.; Lee, S.; Zhao, J.; Sigmund, W.; Koopman, B.; Moudgil, B. Photocatalytic disinfection with titanium dioxide coated multi-wall carbon nanotubes. *Process Safety and Environmental Protection* **2005,** *83,* (4), 393-397.

(62) Lee, S.H.; Pumprueg, S.; Moudgil, B.; Sigmund, W. Inactivation of bacterial endospores by photocatalytic nanocomposites. *Colloids and Surfaces.B, Biointerfaces* **2005,** *40,* (2), 93-98.

(63) Akhavan, O. and Ghaderi, E. Photocatalytic reduction of graphene oxide nanosheets on TiO_2 Thin film for photoinactivation of bacteria in solar light irradiation. *The Journal of Physical Chemistry C* **2009,** *113,* (47), 20214-20220.

(64) Oh, W.; Zhang, F.; Chen, M. Synthesis and characterization of V–C_{60}/TiO_2 photocatalysts designed for degradation of methylene blue. *Journal of Industrial and Engineering Chemistry* **2010,** *16,* (2), 299-304.

(65) Zhang, L.; Wang, Y.; Xu, T.; Zhu, S.; Zhu, Y. Surface hybridization effect of C_{60} molecules on TiO_2 and enhancement of the photocatalytic activity. *Journal of Molecular Catalysis A: Chemical* **2010,** *331,* (1-2), 7-14.

(66) Krishna, V.; Yanes, D.; Imaram, W.; Angerhofer, A.; Koopman, B.; Moudgil, B. Mechanism of enhanced photocatalysis with polyhydroxy fullerenes. *Applied Catalysis B: Environmental* **2008,** *79,* (4), 376-381.

(67) Djordjevic, A.; Canadanovic-Brunet, J.M.; Vojinovic-Miloradov, M.; Bogdanovic, G. Antioxidant properties and hypothetic radical mechanism of fullerenol $C_{60}(OH)_{24}$. *Oxidation Communications* **2004,** *27,* (4), 806-812.

(68) Ryan, J.J.; Bateman, H.R.; Stover, A.; Gomez, G.; Norton, S.K.; Zhao, W.; Schwartz, L.B.; Lenk, R.; Kepley, C.L. Fullerene nanomaterials inhibit the allergic respons. *Journal of Immunology (Baltimore, Md.: 1950)* **2007,** *179,* (1), 665-672.

(69) Trajkovic, S.; Dobric, S.; Jacevic, V.; Dragojevic-Simic, V.; Milovanovic, Z.; Dordevic, A. Tissue-protective effects of fullerenol $C_{60}(OH)_{24}$ and amifostine in irradiated rat. *Colloids and Surfaces.B, Biointerfaces* **2007,** *58,* (1), 39-43.

(70) Cai, X.; Jia, H.; Liu, Z.; Hou, B.; Luo, C.; Feng, Z.; Li, W.; Liu, J. Polyhydroxylated fullerene derivative $C_{60}(OH)_{24}$ prevents mitochondrial dysfunction and oxidative damage in an MPP+-induced cellular model of parkinson's disease. *Journal of Neuroscience Research* **2008,** *86,* (16), 3622-3634.

(71) Schreiner, K.M.; Filley, T.R.; Blanchette, R.A.; Bowen, B.B.; Bolskar, R.D.; Hockaday, W.C.; Masiello, C.A.; Raebiger, J.W. White-rot basidiomycete-mediated decomposition of C_{60} fullerol. *Environmental Science & Technology* **2009,** *43,* (9), 3162-3168.

(72) Sayes, C.M.; Fortner, J.D.; Guo, W.; Lyon, D.; Boyd, A.M.; Ausman, K.D.; Tao, Y.J.; Sitharaman, B.; Wilson, L.J.; Hughes, J.B.; West, J.L.; Colvin, V.L. The differential cytotoxicity of water-soluble fullerene. *Nano Letters* **2004,** *4,* (10), 1881-1887.

(73) Dales, R.E.; Cakmak, S.; Judek, S.; Dann, T.; Coates, F.; Brook, J.R.; Burnett, R.T. The role of fungal spores in thunderstorm asthma. *Chest* **2003,** *123,* (3), 745-750.

(74) Vohra, A.; Goswami, D.Y.; Deshpande, D.A.; Block, S.S. Enhanced photocatalytic disinfection of indoor air. *Applied Catalysis B: Environmental* **2006,** *64,* (1-2), 57-65.

(75) Gao, J.; Wang, Y.; Folta, K.M.; Krishna, V.; Bai, W.; Indeglia, P.; Georgieva, A.; Nakamura, H.; Koopman, B.; Moudgil, B. Polyhydroxy fullerenes (fullerols or fullerenols): Beneficial effects on growth and lifespan in diverse biological models. *PloS One* **2011,** *6,* (5), e19976.

(76) Song, C.; Wang, P.; Makse, H.A. A phase diagram for jammed matter. *Nature* **2008,** *453,* 629-632.

(77) Hwang, Y.S. and Li, Q. Characterizing photochemical transformation of aqueous nC(60) under environmentally relevant conditions. *Environmental Science & Technology.* **2010,** *44*, (8), 3008-3013

(78) Kong, L.; Tedrow, O.; Chan, Y.F.; Zepp, R.G. Light-initiated transformations of fullerenol in aqueous media. *Environmental Science & Technology* **2009,** *43,* (24), 9155-9160.

(79) Lowry, R. *Concenpts and Applications of Inferential Statistics.* Accessed on 21th January 2012 at http://faculty.vassar.edu/lowry/webtext.html.

(80) Hu, L.; Flanders, P.M.; Miller, P.L.; Strathmann, T.J. Oxidation of sulfamethoxazole and related antimicrobial agents by TiO_2 photocatalysis. *Water Research* **2007,** *41,* (12), 2612-2626.

(81) Hu, C.; Yu, J.C.; Hao, Z.; Wong, P.K. Photocatalytic degradation of triazine-containing azo dyes in aqueous TiO_2 suspension. *Applied Catalysis B: Environmental* **2003,** *42,* (1), 47-55.

(82) Arpac, E.; Sayilkan, F.; Asilturk, M.; Tatar, P.; Kiraz, N.; Sayilkan, H. Photocatalytic performance of sn-doped and undoped TiO_2 nanostructured thin films under UV and vis-lights. *Journal of Hazardous Materials* **2007,** *140,* 69-74.

(83) Herrmann, J.M.; Tahiri, H.; Ait-Ichou, Y.; Lassaletta, G.; Gonzalez-Elipe, A.R.; Fernandez, A. Characterization and photocatalytic activity in aqueous medium of TiO_2 and ag-TiO_2 coatings on quartz. *Applied Catalysis B: Environmental* **1997,** *13,* (3-4), 219-228.

(84) Somekawa, S.; Kusumoto, Y.; Ikeda, M.; Ahmmad, B.; Horie, Y. Fabrication of N-doped TiO_2 thin films by laser ablation method: Mechanism of N-doping and evaluation of the thin films. *Catalysis Communications* **2008,** *9,* (3), 437-440.

(85) Wu, Y.; Zhang, J.; Xiao, L.; Chen, F. Preparation and characterization of TiO_2 photocatalysts by Fe^{3+} doping together with au deposition for the degradation of organic pollutant. *Applied Catalysis B: Environmental* **2009,** *88,* (3-4), 525-532.

(86) Kumaresan, L.; Mahalakshmi, M.; Palanichamy, M.; Murugesan, V. Synthesis, characterization, and photocatalytic activity of Sr^{2+} doped TiO_2 nanoplates. *Industrial & Engineering Chemistry Research* **2010,** *49,* (4), 1480-1485.

(87) Ökte, A.N. and Yilmaz, Ö. Characteristics of lanthanum loaded TiO_2-ZSM-5 photocatalysts: Decolorization and degradation processes of methyl orange. *Applied Catalysis A: General* **2009,** *354,* (1-2), 132-142.

(88) Carvalho, H.W.; Batista, A.P.; Hammer, P.; Ramalho, T.C. Photocatalytic degradation of methylene blue by TiO_2-cu thin films: Theoretical and experimental study. *Journal of Hazardous Materials* **2010,** *184,* 273-280.

(89) Patterson, A. The scherrer formula for X-ray particle size determination. *Physical Review* **1939,** *56,* (10), 978-982.

(90) NIST X-ray Photoelectron Spectroscopy Database Http://srdata.nist.gov/xps/ *2012,* (05/10)

(91) Pelton, R.; Geng, X.; Brook, M. Photocatalytic paper from colloidal TiO_2–fact or fantasy. *Advances in Colloid and Interface Science* **2006,** *127,* (1), 43-53.

(92) International Centre for Diffraction Data Http://www.icdd.com. *2012,* (05/11)

(93) CARP, O.; Huismanb, C.L.; Rellerb, A. Photoinduced reactivity of titanium dioxide. *Progress in Solid State Chemistry* **2004,** *32,* (1-2), 33-177.

(94) Mor, G.K.; Varghese, O.K.; Paulose, M.; Shankar, K.; Grimes, C.A. A review on highly ordered, vertically oriented TiO_2 nanotube arrays: Fabrication, material properties, and solar energy applications. *Solar Energy Materials and Solar Cells* **2006,** *90,* (14), 2011-2075.

(95) Kim, S.K.; Choi, G.; Lee, S.Y.; Seo, M.; Lee, S.W.; Han, J.H.; Ahn, H.; Han, S.; Hwang, C.S. Al-doped TiO_2 films with ultralow leakage currents for next generation DRAM capacitors. *Advanced Materials* **2008,** *20,* (8), 1429-1435.

(96) Islam, M.; Bredow, T.; Gerson, A. Electronic properties of oxygen-deficient and aluminum-doped rutile TiO_2 from first principles. *Physical Review B* **2007,** *76,* (4),

(97) Yan, X.; He, J.; G. Evans, D.; Duan, X.; Zhu, Y. Preparation, characterization and photocatalytic activity of si-doped and rare earth-doped TiO_2 from mesoporous precursors. *Applied Catalysis B: Environmental* **2005,** *55,* (4), 243-252.

(98) Harada, H. and Ueda, T. Photocatalytic activity of ultra-fine rutile in methanol-water solution and dependence of activity on particle size. *Chemical Physics Letters* **1984,** *106,* (3), 229-231.

(99) Ohko, Y.; Hashimoto, K.; Fujishima, A. Kinetics of photocatalytic reactions under extremely low-intensity UV illumination on titanium dioxide thin films. *The Journal of Physical Chemistry A* **1997,** *101,* (43), 8057-8062.

(100) Ohko, Y.; Tryk, D.A.; Hashimoto, K.; Fujishima, A. Autoxidation of acetaldehyde initiated by TiO_2 photocatalysis under weak UV illumination. *The Journal of Physical Chemistry B* **1998,** *102,* (15), 2699-2704.

(101) Fujishima, A.; Rao, T.N.; Tryk, D.A. Titanium dioxide photocatalysis. *Journal of Photochemistry and Photobiology C: Photochemistry Reviews* **2000,** *1,* (1), 1-21.

(102) Levine, S. and Dube, G.P. Interaction between two hydrophobic colloidal particles, using the approximate debye-hückel theory. I. general properties. *Transactions of the Faraday Society* **1939,** *35,* 1125-1140.

(103) Landau, L. Theory of the stability of strongly charged lyophobic sols and of the adhesion of strongly charged particles in solutions of electrolytes. *Acta Physicochim URSS* **1941,** *14,* (6), 633-662.

(104) Macedo, E.A.; Skovborg, P.; Rasmussen, P. Calculation of phase equilibria for solutions of strong electrolytes in solvent—water mixtures *Chemical Engineering. Science* **1990,** *45,* (4), 875-882.

(105) Kosmulski, M. The pH-dependent surface charging and the points of zero charge. *Journal of Colloid and Interface Science* **2002,** *253,* (1), 77-87.

(106) Bullard, J.W. and Cima, M.J. Orientation dependence of the isoelectric point of TiO_2 (rutile) surfaces. *Langmuir* **2006,** *22,* (24), 10264-10271.

(107) Yoshikawa, N.; Kimura, T.; Kawase, Y. Oxidative degradation of nonionic surfactants with TiO_2 photocatalyst in a bubble column reactor. *The Canadian Journal of Chemical Engineering* **2008,** *81,* (3-4), 719-724.

(108) Kimura, T.; Yoshikawa, N.; Matsumura, N.; Kawase, Y. Photocatalytic degradation of nonionic surfactants with immobilized TiO_2 in an airlift reactor. *Journal of Environmental Science and Health, Part A- Toxic/Hazardous Substances & Environmental Engineering* **2004,** *39,* (11-12), 2867-2881.

(109) Zhang, F.; Zhao, J.; Shen, T.; Hidaka, H.; Pelizzetti, E.; Serpone, N. TiO_2-assisted photodegradation of dye pollutants II. adsorption and degradation kinetics of eosin in TiO_2 dispersions under visible light irradiation. *Applied Catalysis B: Environmental* **1998,** *15,* (1-2), 147-156.

(110) Houas, A. Photocatalytic degradation pathway of methylene blue in water. *Applied Catalysis B: Environmental* **2001,** *31,* (2), 145-157.

(111) Kembel, S.W.; Jones, E.; Kline, J.; Northcutt, D.; Stenson, J.; Womack, A.M.; Bohannan, B.J.; Brown, G.Z.; Green, J.L. Architectural design influences the diversity and structure of the built environment microbiome. *The ISME Journal* **2012,** 6, 1469-1479

(112) Linsebigler, A.; Lu, G.; Yates, J. Photocatalysis on TiO_2 surfaces: Principles, mechanisms, and selected results. *Chemical Reviews* **1995,** *95,* (3), 735-758.

BIOGRAPHICAL SKETCH

Wei Bai was born in Guangzhou, China. He received a bachelor's degree in environmental engineering from Jinan University in 2007. He received his master's degrees in environmental engineering sciences and materials science and engineering at the University of Florida in 2010. He was a Ph.D. student under the supervision of Dr. Ben Koopman and Dr. Brij Moudgil. He received his Ph.D. degree in environmental engineering sciences in the summer of 2012.